Molecular identification of the volume-regulated anion channel VRAC by a genome-wide siRNA screen

---

Inaugural-Dissertation to obtain the academic degree

Doctor rerum naturalium (Dr. rer. nat.)

Submitted to the Department of Biology, Chemistry and Pharmacy

of the Freie Universität Berlin

by

Felizia Katharina Voß

from Heidelberg

Berlin 2014

This work was prepared under the supervision of Prof. Dr. Dr. Thomas J. Jentsch at the Max-Delbrück-Centrum für Molekulare Medizin (MDC) and the Leibniz-Institut für molekulare Pharmakologie (FMP) in Berlin.

15.10.2010 – 21.10.2014

1. Gutachter: Prof. Dr. Dr. Thomas Jentsch

2. Gutachter: Prof. Dr. Volker Haucke

Tag der Disputation: 25.2.2015

Preface

Part of this work has been published in:

Voss F.K., Ullrich F., Münch J., Lazarow K., Lutter D., Mah N., Andrade-Navarro M.A., von Kries J.P., Stauber T., Jentsch T.J. (2014).
Identification of LRRC8 Heteromers as an Essential Component of the Volume-Regulated Anion Channel VRAC.
Science Vol. 344 no. 6184 pp. 634-638.

http://dx.doi.org/10.1126/science.1252826

Part of the experimental data shown in this work were produced by Dr. Tobias Stauber, Florian Ullrich and Jonas Münch.

Dr. Tobias Stauber performed the immunostainings and microscopy for the topology determination.

Florian Ullrich and Jonas Münch performed and evaluated the whole-cell patch-clamp measurements.

Dr. Katina Lazarow of the FMP Screening Unit assisted in the upscaling of the YFP-assay and siRNA transfection to the high-throughput format.

Dr. Nancy Mah performed the bioinformatics analysis of the primary screening data.

Table of Contents

List of Figures

List of Tables

List of Abbreviations

ATP	adenosine triphosphate
AVD	apoptotic volume decrease
bp	base pair
CaM	calmodulin
cAMP	cyclic adenosine monophosphate
CCD	charge-coupled device
cDNA	copy DNA, reverse-transcribed mRNA
CFTR	cystic fibrosis transmembrane conductance regulator
CRISPR	clustered regularly interspaced short palindromic repeats
C-terminal	carboxy-terminal
DCPIB	4-(2-butyl-6,7-dichloro-2-cyclopentylindan-1-on-5-yl)oxybutyric acid
DIDS	4, 4'-diisothiocyanatostilbene-2, 2'-disulfonic acid
DNA	deoxyribonucleic acid
DNase	deoxyribonuclease
dNTP	deoxyribonucleoside triphosphate
ER	endoplasmatic reticulum
EST	expressed sequence tag
FLIPR	fluorometric imaging plate reader
GFP	green fluorescent protein
h	hour(s)
HEK cells	human embryonic kidney cells
KCC	K^+Cl^--co-transporter
kDa	kilodalton
NHE	Na^+H^+-exchanger
min	minute(s)
NKCC	$Na^+K^+2Cl^-$-co-transporter
N-terminal	amino-terminal
PBS	phosphate-buffered saline
PCR	polymerase chain reaction
qRT-PCR	quantitative real-time PCR
RFP	red fluorescent protein
RNA	ribonucleic acid
RT-PCR	reverse transcriptase PCR
RVD	regulatory volume decrease
RVI	regulatory volume increase
s	second(s)
SDS	sodium dodecyl sulfate
SEM	standard error of the mean
siRNA	small interfering ribonucleic acid
VRAC	volume regulated anion channel
VSOAC	volume-sensitive organic osmolyte-anion channel
VSOR	volume-sensitive outwardly rectifying anion channel
YFP	yellow fluorescent protein

Abstract

The ability of a cell to adapt to changes in extracellular and intracellular osmolyte concentrations is crucial to its survival. During osmotic challenges, extensive swelling of the cell has to be prevented and is counteracted by a process called regulatory volume decrease. A key player in this process is the volume-regulated anion channel (VRAC), which has been extensively described and characterized by electrophysiological means but the protein(s) composing the channel could not be identified so far. We used a fluorescence-based assay in a genome-wide siRNA screen to identify the gene(s) underlying the ubiquitously observed VRAC current. Subsequent bioinformatics data analysis and manual hit assessment defined candidate genes for a secondary screen using independent siRNA pools. Of these the most prominent effect was yielded by the siRNA pool against *LRRC8A*. We subsequently confirmed this putative four-transmembrane-domain protein as an essential component of VRAC by electrophysiological measurements in combination with the generation of knockout cell lines for LRRC8A and the four other members of the LRRC8 protein family using the CRISPR/Cas technology. We furthermore investigated the transmembrane topology of LRRC8A and the subcellular localization of all LRRC8 family members. We could show that LRRC8A localizes to the plasma membrane where it forms heteromers with the other members of this protein family and that current kinetics depend on the subunit composition. Finally, we demonstrated that LRRC8A is indispensable for the process of regulatory volume decrease.

Zusammenfassung

Die Fähigkeit einer Zelle, sich an Schwankungen der intrazellulären und extrazellulären Osmolytkonzentration anzupassen, ist unabdingbar für ihr Überleben. Während dieser osmotischen Schwankungen wird dem übermäßigen Anschwellen der Zelle durch den Prozess der regulatorischen Volumenabnahme entgegen gewirkt. Eine Schlüsselfunktion in diesem Prozess nimmt der volumenregulierte Anionenkanal (VRAC) ein, der bereits eingehend anhand von elektrophysiologischen Methoden beschrieben wurde. Die molekulare Identifikation des/der Proteins(e), welches(e) den Kanal bildet(n), ist jedoch bisher nicht gelungen. Wir haben einen fluoreszenzbasierten Assay in einem genomweiten siRNA-Screen verwendet um Gene zu identifizieren, die dem ubiquitär vorhandenen VRAC-Strom zugrunde liegen. Die anschließende bioinformatische Datenanalyse und manuelle Trefferbeurteilung ergab eine Kandidatenliste für den Sekundärscreen, welcher mit unabhängigen siRNA-Pools durchgeführt wurde. Von diesen Kandidaten konnte der deutlichste Effekt mit dem siRNA-Pool für das *LRRC8A* Gen erzielt werden. Das kodierte Protein LRRC8A, welches vier vorausgesagte Transmembrandomänen besitzt, konnte daraufhin in elektrophysiologischen Messungen sowie anhand von Experimenten in Knockout-Zelllinien, welche mit Hilfe der CRISPR/Cas-Technologie hergestellt wurden, als essentieller Bestandteil von VRAC bestätigt werden. Des Weiteren wurde die Transmembrantopologie von LRRC8A sowie die subzelluläre Lokalisation aller LRRC8-Proteine untersucht. So konnte gezeigt werden, dass LRRC8A in der Plasmamembran vorliegt, wo es mit den anderen Mitgliedern der Proteinfamilie Heteromere bildet, deren Zusammensetzung die Kinetik des VRAC-Stroms beeinflusst. Abschließend konnte gezeigt werden, dass der Prozess der regulatorischen Volumenabnahme von LRRC8A abhängt.

1. Introduction

1.1 Cell volume regulation

A fundamental property of animal cells is their selectively permeable membrane that keeps large molecules like proteins and sugars but also very small particles like ions from freely entering or leaving the cell following their concentration gradient. Water on the other hand can mostly unimpededly cross this barrier, which it will do according to the osmotic pressure conveyed by the osmotically active particles that are present on either side of the selective membrane. Whenever the osmotic equilibrium from the outside to the inside of a cell is perturbed, this will result in cell volume changes that have to be counteracted in order to prevent excessive swelling or shrinking which could harm the integrity of the cell and its surrounding tissue. These challenges in cell volume can be the result of general physiological processes like the accumulation of metabolites, epithelial absorption and secretion or apoptotic induction. Thus, under physiological conditions, osmolarity changes more frequently occur on the intracellular side. Nevertheless, there are cells that are commonly exposed to changes in the extracellular osmolarity due to their specialized function and localization, for example epithelial cells of the intestine, blood cells or kidney medulla cells. On the other hand pathological conditions like hypoxia, ischemia or intracellular acidosis can also result in critical volume changes (Do and Civan, 2006; Lambert et al., 2008).

Besides being a pure reaction to the mentioned osmotic challenges, cell volume changes are also thought to serve a role as signals in the regulation of essential physiological processes like trans-epithelial transport, cell migration, proliferation and programmed cell death (Hoffmann et al., 2009).

The entity of regulatory measures counteracting cell swelling or shrinking are called regulatory volume decrease (RVD) and regulatory volume increase (RVI), respectively. There are various ion channels and transporters involved in both processes (Fig.1).

During regulatory volume increase, the main transporters involver are the ubiquitously expressed Na^+/H^+-exchanger NHE1 in conjunction with the Na^+/Cl^--cotransporter NKCC1 and Cl^-/HCO_3^--antiporters of the anion exchanger (AE) family. They mediate a net uptake of NaCl, which provides the osmotic driving force for water inflow and thereby prevents further shrinkage of the cell (Hoffmann et al., 2009). Other members of

the Na^+/H^+-exchanger family like NHE2 and NHE4 as well as the Na^+/Cl^- cotransporter NKCC2 have also been shown to be shrinkage-activated, but due to their restricted expression pattern these transporters are probably of less general importance during volume regulation. In many cell types, the involvement of hypertonicity-induced cation channels (HICCs) has been shown, but since their molecular identity is so far unknown, further studies on them have been limited to rather unspecific pharmacological approaches. Some of these analyses, however, suggest a relation of HICCs to the epithelial sodium channel ENaC, which exhibits a similar pharmacological profile (Wehner et al., 2006).

In addition to the adjustment of the ionic content of the cell upon osmotic perturbations, the concentration of organic osmolytes, in particular of the aminoethanesulfonic acid taurine, is influenced during RVI and RVD. The activity of the taurine carrier TauT, which mediates active taurine uptake into the cytosol, depends on the extracellular NaCl concentration. It was shown that taurine uptake activity is increased during RVI whereas it is inhibited during hypoosmotic cell swelling, where taurine release plays a major role during the RVD response (Lambert, 2004).

During regulatory volume decrease (RVD), mainly K^+, Cl^- and organic osmolytes are being transported out of the cytosol to be followed by water. This prevents further swelling of the cell and ideally leads to recovery of its original volume.

For K^+, a great variety of different channels and transporters have been described as being volume-regulated or at least partially activated by cell swelling or cell swelling-triggered events, like an increase in the intracellular Ca^{2+} concentration. Depending on the cell line investigated, different types of K^+ channels were reported to be involved in RVD. Among them are the large- , intermediate- , and small-conductance K^+ channels, as well as voltage-gated K^+ channels of the KCNK-family (KCNK2, KCNK5, KCNK4) and the KCNQ family (KCNQ1, KCNQ4 and KCNQ5) (Wehner, 2006). K^+/Cl^--cotransporters of the KCC family, in particular KCC1, also play an essential role during RVD, especially in red blood cells, but also in several other cell lines (Gamba, 2005).

K^+ release during RVD will hyperpolarize the membrane potential (V_m) and thus would prevent further K^+ efflux from the cell unless a parallel Cl^- conductance would provide an electrical shunt. The basal Cl^- conductance of most cell types under isoosmolar conditions is low and therefore a swelling-induced increase of this conductance can be utilized during RVD (Hoffmann et al., 2009). The current underlying this increase in Cl^-

conductance is termed $I_{Cl(swell)}$. It was first described electrophysiologically by Akihiro Hazama and Yasunobu Okada. (Hazama and Okada, 1988). Since then the underlying channel has been referred to by different terms including volume-regulated anion channel (VRAC), volume-sensitive outwardly rectifying channel (VSOR) and volume-sensitive organic osmolyte and anion channel (VSOAC). Since the VRAC is the major topic of this work, its biophysical properties, possible regulatory mechanisms and physiological importance will be discussed in detail in the following sections.

As described above for RVI, organic osmolytes like taurine contribute also to RVD. Upon cell swelling, taurine uptake via the transporter TauT is inhibited and an additional increase in taurine release has been observed in many cell types upon hypoosmotic stimulation (Lambert, 2004).

Both the molecular identity of VRAC and the swelling-activated taurine release pathway have not been discovered thus far. It has been discussed, however, whether the volume-regulated anion channel and the swelling-activated taurine release channel are the same entit, hence the term VSOAC. However, this hypothesis still remains controversial. Other transporters like the anion exchanger AE3 have also been implicated in taurine release during RVD (Shennan, 2008).

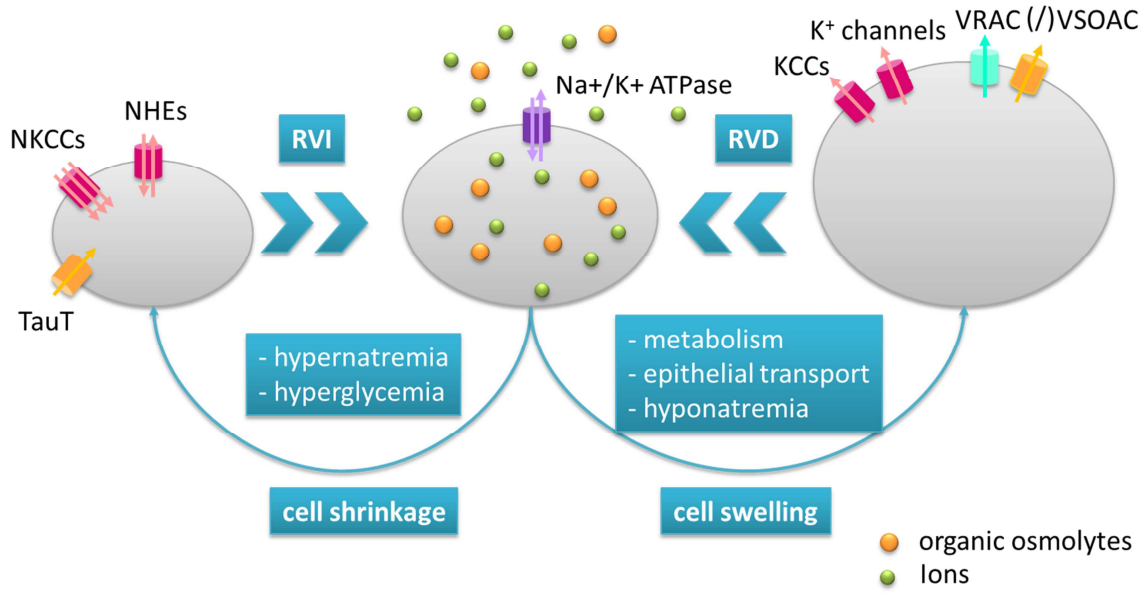

Figure 1: Schematic overview of influencing factors and transport processes in RVI and RVD

1.2 Biophysical and pharmacological properties of VRAC/ $I_{Cl(swell)}$

Despite the lack of knowledge about the molecular identity of the volume-regulated anion channel, it has been possible to describe its general biophysical properties by electrophysiological measurements upon the induction of cell swelling. To this end, cell swelling is usually induced by exposing cultured cells to a hypoosmolar extracellular solution, while recording the anion current over the plasma membrane through voltage-clamp experiments. To exclude the contribution of K^+ channels to this current, K^+ is usually replaced by Cs^+ in the intracellular pipette solution. Through these experiments several groups showed that the swelling-activated chloride current $I_{Cl(swell)}$ exhibits several characteristic features, that are well conserved among different cell types (Nilius et al., 1997a; Okada, 1997; Strange et al., 1996). It should also be stated explicitly that in every vertebrate cell line investigated hitherto $I_{Cl(swell)}$ is present upon hypotonic stimulation. It displays a slight outward rectification and shows a time-dependent inactivation at positive potential that varies in its extent among different cell types (Jackson and Strange, 1995; Leaney et al., 1997; Lepple-Wienhues et al., 1998). It has been discussed whether these differences in the inactivation kinetics of $I_{Cl(swell)}$ are based on different isoforms of the channel or rather depend on external conditions like the composition of the extracellular medium. In this regard, it has been shown for some cell lines that changes in extracellular pH or extracellular Mg^{2+} and Ca^{2+} concentrations can modulate the voltage- and time-dependence of $I_{Cl(swell)}$ inactivation (Nilius et al., 1997a). In contrast to this, current densities vary among different cell types only by a factor of 2-3 (Nilius et al., 1994b).

The permeability of VRAC corresponds to the Eisenman I sequence ($SCN^- > I^- > NO_3^- > Br^- > Cl^- > F^- > Glc^-$) and, as mentioned above, it has been suggested that larger molecules like the organic osmolytes taurine or *myo*-inositol might also permeate through VRAC (Jackson and Strange, 1993; Kirk et al., 1992). Additionally, HCO_3^- and lactate have been shown to be transported through VRAC (Nilius et al., 1998; Verdon et al., 1995) and might contribute to the RVD response in cells with low intracellular Cl^- concentrations like skeletal muscle and nerve cells (Hoffmann and Simonsen, 1989).

VRAC channel activity depends on the presence of intracellular ATP, but not on its hydrolysis (Oiki et al., 1994). This could suggest a modulatory effect of ATP and possible binding to a part of the channel or a regulatory subunit. Changes in the intracellular Ca^{2+} concentration, which have been demonstrated to occur upon volume perturbations, do not influence VRAC activation (Kubo and Okada, 1992; Nilius et al., 1994a; Strange et al.,

1996). It has, however, been shown that a permissive intracellular Ca^{2+} concentration of 50 nM is required for VRAC activity (Szucs et al., 1996b).

The recording of single-channel events has proven difficult, which resulted in reports that vary substantially in the determined single-channel conductances (Nilius and Droogmans, 2003; Okada, 2006). A major obstacle for these measurements is the technical difficulty of swelling the cells and simultaneously or subsequently applying a patch pipette to the cell surface for the recoding of single-channel events (Okada, 2006).

There have been great efforts for pharmacological studies on $I_{Cl(swell).}$ VRAC can be inhibited by classical Cl^- channel blockers such as DIDS and NPPB at micro- to millimolar concentrations. But since these compounds are known to affect many different channels and transporters, the effect on VRAC is rather unspecific (Jentsch et al., 2002). The estrogen receptor antagonists tamoxifen, cliphen, and nafoxidine have been shown to inhibit $I_{Cl(swell)}$ at micromolar concentrations but the effectiveness of these compounds varies among different cell types (Maertens et al., 2001). $I_{Cl(swell)}$ is to some extent also blocked by niflumic acid, flufenamic acid, arachidonic acid and glibenclamide, as well as by some antimalarials such as mefloquine (Jentsch et al., 2002; Nilius and Droogmans, 2003). Recently, it has also been shown that carbenoxolone, a known inhibitor of gap-junctions, also inhibits $I_{Cl(swell)}$ at similar concentrations (Benfenati et al., 2009).

The most specific known inhibitors of VRAC are the acidic di-aryl-urea NS3728 and the indanone compound DCPIB with IC_{50} values of 0.4 µM and 1.0 µM respectively (Decher et al., 2001; Helix et al., 2003). In case of DCPIB, however, it was shown subsequently that the glutamate receptor GLT-1 and connexin hemichannels were also blocked by this compound (Bowens et al., 2013). In general, the lack of high-affinity inhibitors of VRAC has been a substantial obstacle for the identification of the protein(s) underlying $I_{Cl(swell)}$ and the investigation of its physiological importance (see also section 2).

Interestingly, $I_{Cl(swell)}$ is also blocked by millimolar concentrations (again depending on the cell type) of extracellular nucleotides like ATP (Tsumura et al., 1996), which might be a clue towards the involvement of VRAC in ATP release during RVD (see also section 1.4).

1.3 (Postulated) regulatory mechanisms of VRAC activity

Although the mechanism of VRAC activation is unknown, a number of possible pathways and regulatory elements have been described and investigated.

In this regard, a general question is whether VRAC itself senses the changes in cell volume and how this sensing is achieved on the molecular level, or if other proteins are involved in the detection of volume perturbations and activate VRAC via signaling cascades. These could involve multiple players like secondary messengers, kinases, phosphatases and G-protein coupled receptors.

A change in cell volume could also be detected as a mechanical stimulus through bending or stretching of the plasma membrane or a disruption of its tethering to the cytoskeleton. A direct mechanical activation of VRAC currents, however, has been mostly discarded. Cl^- currents that could be elicited by mechanical stimulation usually differed from VRAC in their characteristics and typical VRAC currents were only observed upon application of an osmotic stimulus (Christensen and Hoffmann, 1992). A functional connection to the cytoskeleton, however, might very well play an important role in $I_{Cl(swell)}$ activation. In at least some cell types, disruption of the F-actin cytoskeleton potentiates VRAC currents (Levitan et al., 1995; Morishima et al., 2000; Schwiebert et al., 1994). One hypothesis as to how actin filament integrity could be linked to VRAC activity is via the unfolding of membrane invaginations that are prevented under isotonic conditions by tethering to the cytoskeleton. During cell swelling, these connections could break apart and membrane unfolding could then disrupt a protein-protein interaction silencing VRAC, in turn leading to the appearance of $I_{Cl(swell)}$ (Okada, 1997). Another possible link to the cytoskeleton could be provided by integrins, which also have been proposed to be involved in VRAC activation (Browe and Baumgarten, 2003, 2004, 2006). Besides this, the actin-binding protein annexin II and the scaffolding protein caveolin-1 have also been shown to modulate VRAC activity, pointing towards an involvement of filament- and membrane-structural changes in the volume-sensing cascade (Nilius et al., 1996; Trouet et al., 1999).

During cell swelling, also the lipid composition of the plasma membrane undergoes changes that could potentially trigger channel activation. It was shown that cholesterol depletion potentiates VRAC and can to some extent activate $I_{Cl(swell)}$ even in non-swollen cells (Klausen et al., 2006; Levitan et al., 2000; Romanenko et al., 2004). Cholesterol is known to alter the membrane deformation energy and can thereby influence channel opening. However, since the local cholesterol concentration is also tightly connected to the occurrence of lipid rafts and caveolae as well as F-actin organization at the membrane, the observed effects could actually support the functional link to the cytoskeleton as a major modulator of VRAC activity (Hoffmann et al., 2009).

A more indirect mode of activation could be through the sensing of changes in the intracellular ionic strength which occur upon cell swelling. It was shown in several cell lines that these changes induce $I_{Cl(swell),}$ possibly even without changes in the actual volume of the cell (Cannon et al., 1998; Sabirov et al., 2000; Voets et al., 1999). The mechanism how changes in the ionic strength could lead to channel activation are not yet understood but they could affect signaling molecules by changing their surface potential (Okada et al., 2009). Besides this, ATP binding to the channel has been suggested as a possible molecular mechanism to connect changes in intracellular ionic strength to VRAC activity since low intracellular ATP has an inhibitory effect (Nilius and Droogmans, 2003).

A similar hypothesis involves the concept of macromolecular crowding, which is also affected during cell swelling and could likewise influence the activity of kinases or phosphatases, which in turn could alter VRAC activity (Nilius et al., 1997a).

A further possible mechanism of osmosensing is through the generation of reactive oxygen species (ROS). This occurs upon cell swelling and has been shown to activate $I_{Cl(swell)}$ under isotonic conditions in several cell types (Browe and Baumgarten, 2004; Jiao et al., 2006; Shimizu et al., 2004; Varela et al., 2004). However, it is not clear whether ROS function as a volume signal or rather modulate VRAC function downstream of the osmosensing event, or if they even have an effect on protein phosphorylation in the signaling cascade regulating $I_{Cl(swell)}$ (Hoffmann et al., 2009) .

Not only the volume sensing mechanism and the molecular principle of swelling activation, but also the connecting elements of signal transduction have remained largely unknown. There have, however, been a number of studies that point towards the involvement of specific members of known signaling cascades. One line of evidence suggests that GTP-binding proteins contribute to VRAC activation. In many cell types the intracellular application of GTPγS leads to VRAC activation without hypotonic stimulation (Doroshenko, 1991; Mitchell et al., 1997; Nilius et al., 1994a), suggesting a role of G-protein signaling in the activation cascade. So far no specific G-protein could be identified to take part in this process. Yet, both an inhibitor of the small GTPase RhoA and an inhibitor of its downstream kinase ROCK inhibit VRAC activation, pointing towards an involvement of these proteins (Nilius et al., 1999). Accordingly, activation of the Rho pathway by expression of a constitutively active form of Rho in NIH3T3 cells increased the RVD response and VRAC activity when a rather weak swelling stimulus

was given (Pedersen et al., 2002). In contrast to this data, the transfection of constitutively active forms of $G_{\alpha,}$ Rho or ROCK did not lead to increased VRAC activity in CPAE cells, which might indicate a permissive role of the Rho pathway (Carton et al., 2002).

Protein phosphorylation in general has been investigated in relation to VRAC activity. Since the activation time of $I_{Cl(swell)}$ upon hypoosmotic stimulation is rather long (up to several minutes) it is possible that multiple phosphorylation steps are included in the signaling cascade for VRAC opening. Inhibition of the protein tyrosine kinase PTK prevents VRAC activation in lymphocytes and accordingly inhibitors of the protein tyrosine phosphatase PTP have a potentiating effect (Lepple-Wienhues et al., 1998). So far it is not clear whether VRAC itself or a regulatory protein is phosphorylated. Since the mentioned inhibitors are not very specific it is also still unclear which kinases and phosphatases play a role in VRAC regulation. There has been some evidence for the involvement of a member of the Src kinase family p56lck and the serine/threonine-specific myosin light-chain kinase MLCK, but the effects differ according to the cell type and are sometimes contradictory (Du et al., 2004; Lepple-Wienhues et al., 1998; Nilius et al., 2000). Furthermore, an antagonist of the angiotensin II type 1 receptor AT_1R suppressed VRAC activity whereas the downstream kinase EGFR was not required for VRAC activation. Downstream of EGFR the Ras-Raf-MEK-ERK pathway as well as the already mentioned Rho kinase could be involved in the signaling process since the inhibition of some of these components showed an effect on $I_{Cl(swell)}$ induction suggesting an at least permissive role on VRAC activity (Okada, 2006).

During volume regulation an increase in the intracellular Ca^{2+} concentration is an important element of the activation cascade for several cation channels and transporters as mentioned above. Thus, the Ca^{2+} dependence of $I_{Cl(swell)}$ has also been investigated. In most cell types, however, the activation of VRAC is independent of an increase in the intracellular Ca^{2+} concentration (Kubo and Okada, 1992; Nilius et al., 1994a; Strange et al., 1996). The molecular identification of the calcium-activated chloride channel ANO1 raised the questions whether one of the members of the anoctamin (*tmem16*) gene family might comprise VRAC (Almaca et al., 2009). This hypothesis could be discarded since the elicited currents are distinct from the typicial $I_{Cl(swell)}$ and neither overexpression nor knockout or knockdown of the ANO proteins investigated did abolish VRAC activity (Juul et al., 2014; Shimizu et al., 2013) (see also section 1.5). Nevertheless, VRAC

activity requires an intracellular free calcium concentration of about50 nM (see section 1.2) which suggests that Ca^{2+} may act as a second messenger during VRAC activation. In agreement with this hypothesis, the treatment of HeLa cells with calmodulin antagonists resulted also in VRAC inhibition (Kirk and Kirk, 1994; Szucs et al., 1996b).

1.4 Proposed (patho-) physiological importance of VRAC

Cell volume regulation and thereby also VRAC activity play an important role in many physiological and pathological processes, which will be addressed in more detail in this chapter. However, it has to be considered that the molecular identity of VRAC has remained elusive for the past decades and therefore many assumptions of an involvement of this channel in certain cellular events are largely based on (unspecific) pharmacological approaches. Nevertheless, the evidence for a possible role of VRAC is in many cases very intriguing and will be of great interest once the molecular identification of the channel facilitates further analysis.

The membrane potential of cells mainly depends on the basal K^+ conductances and thus is close to the K^+ equilibrium potential, but if an additional Cl^- conductance is present (or becomes activated) the membrane potential would shift towards the Cl^- equilibrium potential. Therefore, an activation of VRAC could in many cell types dramatically influence the membrane potential and the associated activity of other transporters and channels (Nilius et al., 1997a). Such an effect could be shown for cardiac cells, where the repolarization and thus the rhythmic cardiac activity are affected by $I_{Cl(swell)}$ (Vandenberg et al., 1994). Furthermore, it has been suggested that pancreatic β-cells could be depolarized by VRAC activation upon a glucose stimulus, which in turn would lead to insulin secretion (Best et al., 2010). It has to be noted, however, that in general there is very little to no basal VRAC activity and therefore the general maintenance of the membrane potential in most cell types does not depend on VRAC. Nevertheless, it is possible that VRAC can also be activated by other means than volume perturbations or osmotic stimuli and could thereby provide a mechanism to translate the metabolic state of a cell into an electric stimulus.

Under physiological conditions, the cells that most frequently face changes in extracellular and intracellular osmolarity are epithelial cells. Both secretory processes and absorption have an impact on osmolyte distribution and thus influence the cell volume. For instance, trans-epithelial Na^+-coupled uptake of glucose and amino acids leads to an intracellular accumulation of osmolytes, which would lead to cell swelling unless

counteracted by K^+ and Cl^- extrusion, mainly over the basolateral membrane. Here, VRAC is thought to assist in the recovery of the initial cell volume and thus the integrity of the epithelium (Pedersen et al., 2013). Since the activation of K^+ and Cl^- channels in the basolateral membrane not only prevents further swelling of the cell but also maintains the electrical driving force for the uptake process, it has also been discussed that epithelial transport relies more directly on volume-sensitive transport, which could mediate the cross-talk between apical and basolateral membranes (Hoffmann et al., 2007). On the apical side, a DIDS-sensitive Cl^- conductance has also been shown to play a role in the swelling response of epithelial cells. But since DIDS is a very unselective blocker of chloride channels and transporters, it is not clear whether this conductance is due to VRAC activity (Hoffmann et al., 2007).

Another physiological process that is tightly connected to changes in cell volume is cell proliferation. In general, proliferation is stimulated by cell swelling and inhibited by cell shrinkage (Lang et al., 2006). Accordingly, cell volume changes can be observed during the different stages of mitosis. These changes are mediated by several ion channels including VRAC. It has been shown that in Ehrlich Lettre ascites cells the maximal $I_{Cl(swell)}$ is reduced during the G1 and increased during the early S phase compared to the current during the G0 state (Klausen et al., 2007). Other studies also found differences in $I_{Cl(swell)}$ during different phases of the cell cycle (Doroshenko et al., 2001; Shen et al., 2000). Furthermore, inhibition of VRAC has been shown to affect proliferation in many different cell types (Klausen et al., 2007; Nilius et al., 1997b; Schlichter et al., 1996; Schumacher et al., 1995; Voets et al., 1995). Taken together, this evidence could suggest that an increase in VRAC activity or an increased potential for RVD is required for the entrance of cells into S phase and thus for cell division per se (Hoffmann, 2011). When it comes to cell proliferation control, cancer as a pathophysiological state is of great interest. It has indeed been shown that VRAC activity is increased in primary carcinoma cultures and in non-invasive cervical cancer cells (Chou et al., 1995).

Another process that links VRAC activity to cancer, especially cancer therapy, is apoptosis. During apoptotic induction, a significant shrinkage of the cell, called apoptotic volume decrease (AVD), can be observed and is thought to be necessary for a complete execution of apoptosis (Maeno et al., 2000; Poulsen et al., 2010). AVD is coupled to a cellular loss of ions, mainly K^+ and Cl^- and amino acids (Lang and Hoffmann, 2012; Orlov et al., 2013). Both chloride and amino acids like taurine may be released via VRAC

or VSOAC. When cells are treated with VRAC inhibitors like NS3728, this causes a reduced apoptotic response upon administration of the chemotherapeutic apoptosis inducer cisplatin (Poulsen et al., 2010). Furthermore, it was shown that multidrug resistant Ehrlich ascites tumor cells display a delayed and diminished AVD and VRAC activity in correlation with a decreased caspase-3 activation, indicating a lack of apoptotic activity (Poulsen et al., 2010). A decrease in Cl^- permeability could also be shown for several other multidrug resistance cell models (Gollapudi et al., 1992; Lee et al., 2007; Min et al., 2011). It is therefore very likely that a lack in VRAC activity contributes to the resistance of cancer cells to apoptosis-inducing reagents. However, it is still unclear how VRAC activity would be triggered during apoptotic induction without a swelling stimulus. In this regard, it is interesting to note that mitochondrion-mediated apoptosis inducers like staurosporin could trigger VRAC activity under isotonic conditions (Okada et al., 2004; Shimizu et al., 2013).

Another pathological process that could be linked to VRAC activity via its role in apoptotic induction is infection. When infected host cells are unable to undergo induced cell death upon pathogen entry, this can lead to a more severe course of the disease. Furthermore, volume regulation in general is known to play a role in immune defense mechanisms through volume-sensitive mechanisms like phagocytosis (Lang, 2007).

Besides the ability to escape apoptosis, another hallmark of cancer pathology is an increased migratory ability of malignant cells, leading to a critical progression of the disease via metastasis. Cell motility is thought to be regulated by the activity of different volume-sensitive ion channels at the leading and lagging edge of the cell. While shrinking-activated channels mediate ion uptake, followed by water influx at the leading part of the cell, swelling-activated channels like VRAC release ions at the rear end of the cell. The resulting osmotically driven water flow from one end of the cell to the other, leads to a forward movement of the cell (Jakab and Ritter, 2006; Schwab et al., 2007). Accordingly, it could indeed be shown that VRAC activity is linked to the migratory ability and invasion capacity of nasopharyngeal carcinoma and glioma cells (Mao et al., 2007; Soroceanu et al., 1999).

Pathological cell swelling is frequently observed upon ischemic events in the heart and in the brain. In the latter, they are extremely harmful, due to the very limited space for volume expansions inside the restricted dimensions of the skull. Very shortly after a stroke or trauma, swelling of astrocytes can be observed. The initial stimulus for this

swelling results from the activation of glutamate receptors (GluR) and $GABA_A$ receptors. This is probably caused by a hypoxia-induced lack of Na^+/K^+-ATPase activity. Cell swelling then activates VRAC. The specific role of VRAC in the following excitotoxic cascade is not clear yet and several possible scenarios have been proposed: It is possible that VRAC activation in swollen glia cells is followed by a further release of amino acids like glutamate through VRAC. This would contribute to the RVD response but potentiate the excitotoxic effect on the surrounding cells (Kimelberg, 2005). There is some evidence from studies in astrocytes and microglia that glutamate might be released through VRAC upon hypoosmotic stimulation but also when applying zymosan to induce ROS production or bradykinin, which is released after brain injury or stroke (Harrigan et al., 2008; Liu et al., 2009; Liu et al., 2006).

Another hypothesis is that the prominent depolarization induced by the GluR opening facilitates an increased Cl^- influx into neurons through VRAC. This would then lead to an even enhanced swelling resulting in necrotic death of these cells. After washout of glutamate, however, the cells would repolarize and VRAC could exert its regular role in RVD through the release of anions or organic osmolytes such as taurine (Okada et al., 2009). Nevertheless, inhibition of VRAC would likely be beneficial after an ischemic event, because it would decrease the glutamate release (if it occurs through VRAC) and possibly also reduce the potentiation of swelling through Cl^- influx. There is already some evidence that an inhibition of VRAC could have a neuroprotective effect. When tamoxifen, which inhibits VRAC in the micromolar range at least in some cell types, is administered to a rat stroke model after stroke induction, glutamate release is reduced by 50% (Feustel et al., 2004). It has to be noted, however, that tamoxifen is a rather unspecific VRAC inhibitor, which also inhibits estrogen receptors and possibly other ion channels.

Another effect of tamoxifen hints to a role of VRAC in the secretion of aqueous humour, which is the fluid responsible for the nutrition and moistening of the lens and the maintenance of the intraocular pressure. In breast cancer patients that have been treated with tamoxifen, a high incidence of cataract formation can be observed, which might be attributed to the (unintended) inhibition of VRAC activity (Zhang et al., 1994). In the ciliary epithelium, the tissue secreting aqueous homour in the eye, swelling-activated chloride channels are thought to be expressed on both epithelial surfaces. However, it has

not yet been determined whether these are distinct channels and/or if they are identical to VRAC.

As already mentioned at the beginning of this chapter, further experiments will have to reveal the actual role of the volume-regulated anion channel in the physiological context, once the molecular identity of the channel is ascertained. An already quite striking clue for the relevance of this channel for general physiological processes is the fact that the characteristic current $I_{Cl(swell)}$ can be observed in every vertebrate cell type investigated so far. This suggests that there has been a strong evolutionary pressure selecting against the loss of this channel and thus points to an essential role in cell survival, integrity or proliferation.

1.5 Former candidates for the molecular identity of VRAC

Since the early 1990s many efforts have been made to identify the protein underlying the volume-regulated anion channel, but so far none of the proposed candidates could be confirmed upon thorough experimental evaluation. Nevertheless, the suggested molecular identities of VRAC should be briefly reviewed here in order to show how each of them initially emerged and how they could be subsequently discarded. Furthermore, the number of publications on putative identities of VRAC during the past two decades impressively shows the considerable effort and interest invested in the discovery of this important channel.

The first protein suggested to comprise VRAC was the P-glycoprotein (P-gp), which is encoded by the multidrug resistance 1 (*MDR1*) gene in humans. It is a member of the ABC transporter family, which also contains the chloride channel CFTR. P-gp had already been shown to use the free energy from ATP-hydrolysis to extrude hydrophobic compounds from the cytosol, thus conferring multidrug resistance (Gottesman and Pastan, 1993). In 1992 Valverde et al. stated that overexpression of P-gp in NIH 3T3 fibroblasts or in the epithelial cell line S2 led to a volume-sensitive chloride current that was not present in untransfected control cells (Valverde et al., 1992). This already seemed doubtful since $I_{Cl(swell)}$ is ubiquitously present in all vertebrate cells and was indeed subsequently shown to be endogenously present in NIH 3T3 fibroblast as well (Gschwentner et al., 1995; Nilius et al., 1994b). Additionally, mutations in P-gp that abolished its transport activity did not affect $I_{Cl(swell)}$. This was, however, proposed to be the result of a bifunctional activity of P-gp (Gill et al., 1992). This hypothesis was again disputed by studies showing that neither locking P-gp in the transporter mode nor

activation of $I_{Cl(swell)}$ elicited an effect on the proposed opposite function (Tominaga et al., 1995; Viana et al., 1995). Moreover, heterologous expression of P-gp in *Xenopus laevis* oocytes failed to induce $I_{Cl(swell)}$, which was a strong indication that P-gp by itself does not form the channel (Morin et al., 1995). Finally, it was widely accepted that P-gp does not underlie $I_{Cl(swell)}$, although it still has been discussed whether P-gp might have a regulatory effect on VRAC activity (Hardy et al., 1995). Conversely it could be shown that neither P-gp knockdown by antisense oligonucleotides nor treatment with P-gp antibodies had an inhibitory effect on VRAC activity (Tominaga et al., 1995).

The second candidate in the hunt for the molecular identity of VRAC was the ubiquitously expressed protein pI_{Cln} which was identified in an expression-cloning approach. Overexpression of this protein in *Xenopus laevis* oocytes activated an outwardly rectifying anion current termed I_{Cln} with similar characteristics to $I_{Cl(swell)}$ (Paulmichl et al., 1992). A functional connection of pI_{Cln} to VRAC was supported by studies showing that treatment with antibodies or antisense oligonucleotides against pI_{Cln} reduced $I_{Cl(swell)}$ (Gschwentner et al., 1995; Krapivinsky et al., 1994). The putative secondary structure of the protein was, however, in conflict with the theory of it forming a plasma membrane localized ion channel, since it lacked hydrophobic stretches in its primary sequence sufficient to span the phospholipid bilayer. Accordingly, it could be observed that the protein mostly resides in the cytosol (Krapivinsky et al., 1994). Finally, pI_{Cln} was shown to be a spliceosome component (Pu et al., 1999). Additionally, further investigation of the I_{Cln} in *Xenopus laevis* oocytes and reconstituted liposomes could show substantial differences in ion-selectivity and current characteristics compared to $I_{Cl(swell)}$ (Fürst et al., 2000; Li et al., 1998; Voets et al., 1996).

Another candidate channel proposed to mediate $I_{Cl(swell)}$ was ClC-3, a member of the ClC-family of chloride channels and transporters. ClC-3 was cloned in 1994 from rat brain neuronal cells (Kawasaki et al., 1994). When heterologously expressed, it gave rise to outwardly rectifying anion currents, with much larger amplitudes than the $I_{Cl(swell)}$ from untransfected cells (Duan et al., 1997). In this study it was also shown that the current could be increased by cell swelling and that several characteristics of the ClC-3 current such as ion selectivity sequence and pharmacological profile conformed to $I_{Cl(swell)}$. Furthermore, the authors found a mutation that changed the ion selectivity sequence and abolished rectification of the channel, which indicated that ClC-3 was indeed the pore-forming protein conveying the current recorded from overexpressing cells. Nevertheless,

there were some notable differences between currents from ClC-3-transfected cells and endogenous $I_{Cl(swell)}$: Whereas VRAC shows virtually no basal activity, ClC-3 elicited large anion currents already under isotonic conditions, that are increased upon cell swelling. Furthermore, ClC-3 currents could be completely suppressed by activation of PKC, which is not the case for $I_{Cl(swell)}$ (Duan et al., 1999; Gosling et al., 1995; Szucs et al., 1996a). However, the ultimate proof against ClC-3 as a candidate for the VRAC identity is that $I_{Cl(swell)}$ is unchanged in cells from ClC-3 knockout mice, which could be shown by several groups in different cell types (Arreola et al., 2002; Gong et al., 2004; Stobrawa et al., 2001).

ClC-2 as another member of the CLC-family has been discussed as a candidate for the identity of VRAC (Nilius et al., 1997a), since it is to some extent also activated by osmotic swelling (Gründer et al., 1992; Jordt and Jentsch, 1997). Nevertheless, there are fundamental differences in current characteristic, including the direction of rectification, permeability sequence and inactivation kinetics that actually exclude ClC-2 from being VRAC (Thiemann et al., 1992).

Rather recently, a new family of chloride channels called bestrophins was identified in connection to a congenital form of retinal degeneration and was shown to be at least partially regulated by cell volume by the group of Criss Hartzell (Fischmeister and Hartzell, 2005). Following studies by the same group showed that in *Drosophila* S2 cells the endogenous volume-regulated chloride current is abolished upon knockdown of the *Drosophila* bestrophin dbest1 (Chien and Hartzell, 2007). This result was later confirmed by a genome-wide siRNA screening approach in which dbest1 was also identified as the volume-regulated anion channel of S2 cells (Stotz and Clapham, 2012). These results raised the question whether bestrophins also comprise VRAC in vertebrate cells. To test this hypothesis Hartzell and colleagues examined cells from bestrophin1 and 2 double knockout mice and found that $I_{Cl(swell)}$ was unchanged (Chien and Hartzell, 2008). Furthermore, endogenous bestrophin currents in S2 cells as well as heterologously expressed dbest1 currents in HEK cells show a different pharmacological profile than the vertebrate $I_{Cl(swell)}$ (Stotz and Clapham, 2012). According to these findings, bestrophins do not constitute the vertebrate form of VRAC but seem to be the main volume-regulated anion pathway in insect cells.

Finally, several members of the anoctamin protein family, which contains the calcium-activated chloride channels ANO1 and ANO2 (Pedemonte and Galietta, 2014), have been

suggested to be involved in volume-regulated chloride transport. The lab of Karl Kunzelmann reported that $I_{Cl(swell)}$ is reduced in cells from $ANO6^{-/-}$ mice as well as in cells treated with siRNAs against ANO1, ANO6, ANO8 or ANO 9 (Almaca et al., 2009). Furthermore, it was shown that overexpression of ANO1 and ANO2 increased $I_{Cl(swell)}$. However, these results were subsequently contradicted by two other publications showing that neither knockdown nor overexpression of ANO1, ANO6 or ANO10 had an significant effect on $I_{Cl(swell)}$ (Juul et al., 2014; Shimizu et al., 2013).

1.6 The LRRC8 protein family

Although the outcome of the genome-wide siRNA screen described in this work should not be anticipated, I would still like to give a general introduction to the protein family LRRC8 that became the focus of the post-screening experiments. Therefore, the information on the members of the LRRC8 gene family summarized here are a reflection of the *status quo* at the time when LRRC8A emerged as a candidate during the screen. All further information resulting from this work and the work by others will be discussed at the end of this thesis.

The name of the protein family LRRC8 stands for leucine-rich repeat containing family 8. The leucine-rich repeat (LRR) is a polypeptide motif comprised of 20-29 amino acids containing a conserved segment with the consensus sequence LxxLxLxxN/CxL, where x can be any amino acid and the "L" positions can also be occupied by valine, isoleucine and phenylalanine (Kobe and Kajava, 2001). LRRs have been identified in numerous proteins through sequence arrays, but the function of this domain is not completely understood yet. There is, however, evidence pointing to an important function of these domains in protein-protein interactions (Kobe and Deisenhofer, 1995; Papageorgiou et al., 1997).

The gene coding for LRRC8A was first discovered in a patient suffering from an immunodeficiency condition called agammaglobulinemia, where a mutation of it was identified as the likely underlying cause of the disease (Sawada et al., 2003). Subsequently, the complete gene family was identified and sequence analysis suggested a four-transmembrane topology for all family members and a strong conservation between the human and mouse homologues (Kubota et al., 2004). The LRRC8 family consists of 5 members, which are named LRRC8A, LRRC8B, LRRC8C, LRRC8D and LRRC8E (Fig. 2). Sequence analysis revealed that they originated from a common ancestor and that the paralogues B, C and D probably arose from tandem duplications whereas A and E

originated later by duplications of B and C, respectively. Accordingly, the paralogues B, C and D are located together in the human genome on chromosome 1 whereas A and E are located on chromosome 9 and 19, respectively (Abascal and Zardoya, 2012).

Each LRRC8 protein contains up to 17 leucine-rich repeats at the C-terminus while the putative transmembrane domains are located in the N-terminal part of the protein (Smits and Kajava, 2004). It was originally proposed that the LRR-containing C-terminus of the protein and thus also the N-terminus are located towards the extracellular medium (Sawada et al., 2003). However, Absascal and Zardoya proposed the opposite topology with both N- and C-terminus oriented towards the cytosol in their bioinformatics study (Abascal and Zardoya, 2012). They furthermore state that their analysis revealed an evolutionary relationship to pannexins. These four-transmembrane domain containing proteins can form hexameric channels in the plasma membrane, which have been implicated in a wide array of physiological functions (D'Hondt et al., 2009). Interestingly, pannexins are structurally related to connexins, which also form hexameric compelexes called connexons. These comprise gap-junctions and thereby connect the cytosol of neighboring cells for example in the CNS (Abascal and Zardoya, 2013). These similarities suggest that LRRC8 proteins might also be able to form hexameric complexes or even channels. In all four transmembrane domains and in the connecting loops, stretches of conserved amino acid sequences can be found when comparing the LRR8 family members with the pannexin family. Notably, four pairs of cysteine residues in the two extracellular loops are conserved between the two families. These cysteine residues might be involved in the formation of disulfide bonds between loops of the same protein or even between loops of adjacent proteins in a multimer, thereby stabilizing the complex. A similar role of extracellular cysteine pairs has been shown for connexins (Foote et al., 1998).

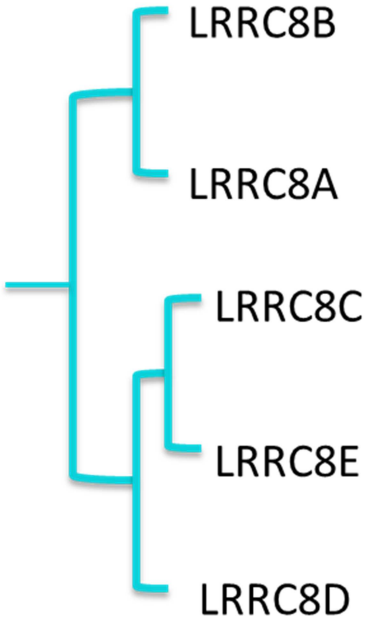

Figure 2: Schematic phylogenetic tree of the LRRC8 protein family (modified from Abscal and Zardoya, 2003)

The physiological role of LRRC8 proteins as remained largely unknown so far. As mentioned above, LRRC8A was identified in a patient suffering from agammaglobulinemia, which is characterized by a B-cell deficiency and is usually caused

by mutations in genes responsible for B-cell development (Sawada et al., 2003; Tsukada et al., 1993). It is therefore likely that LRRC8A also plays a role in the differentiation or proliferation of B-cells. Interestingly, the mutation in the patient was heterozygous and consisted of a chromosome translocation that leads to a truncated version of the protein. This truncated protein is apparently not functional anymore and furthermore seems to somehow also render the protein inactive that is being translated from the unaffected allele. This was also demonstrated by transplantation experiments with murine bone marrow cells heterologously expressing the mutant version of the protein, which resulted in inhibition of normal B-cell development (Sawada et al., 2003). This could be a further indication of a multimeric complex formation of LRRC8 proteins that would explain the dominant negative effect of this truncation (Abascal and Zardoya, 2012).

Besides these data on LRRC8A, there is a study on the gene encoding LRRC8C suggesting a connection to adipocyte differentiation and thus terming the gene “factor for adipocyte differentiation (fad) 158” (Tominaga et al., 2004). In this study the authors found that knockdown or LRRC8C prevented the differentiation of T3-L1 cells into adipocytes, while the overexpression resulted in the induction of adipocyte differentiation in a cell line that normally is not part of this lineage. Furthermore, the same group created a knockout mouse model for LRRC8C that showed a significantly reduced body mass as well as an improved insulin resistance under high-fat diet conditions (Hayashi et al., 2011). Concerning the intracellular localization of the protein it was stated that it resides in the ER when heterologously expressed in T3-L1 cells using a GFP tag for visualization (Tominaga et al., 2004).

2. Aim of the work

Despite the many physiological functions proposed to be connected to volume regulation in general and to the activity of the volume-regulated anion channel in particular, most of these could not be investigated in detail due to the lack of knowledge about the underlying molecular identity of this channel. Although VRAC is not the only ion channel, whose identification had kept scientists busy and puzzled for many years, it is a special case in respect to the obstacles that have impeded a successful discovery of the gene(s) encoding for the protein(s) that comprise VRAC.

Other channels have been identified using expression-cloning approaches, where a cell line is used that lacks the respective channel, which is then transfected with pools of cDNA. By subsequently dividing the pools that elicited currents upon transfection, one finally ends up with a single cDNA encoding the channel. This approach is however not applicable for VRAC since so far no cell line could be identified that lacked an endogenous volume-activated anion current and thus could provide a suitable expression system. A second possible strategy is to use a high affinity ligand for an affinity-purification approach in order to “fish” the protein comprising the channel. This is also not feasible for VRAC since no high-affinity ligands are known and many of the inhibitors that act on VRAC target several other ion channels as well. In the case of other ion channels, like for example CFTR, naturally occurring mutants lacking the current could be used to identify the gene connected to channel function, but as already mentioned above there is no cell line or individual reported that could be used for such a genetic screening approach.

Despite these difficulties, several candidate proteins have been proposed and were subsequently discarded. This and the many attempts to study the physiological role of VRAC using pharmacological tools show the great interest and need of the molecular identification of this channel.

Since the siRNA technology has become more accessible at large scale and genome-wide siRNA libraries are commercially available, this method became an attractive possibility for a new identification approach. The goal of this study was to set up and optimize a screening-assay for VRAC activity that could be adapted to a high-throughput scale to perform a genome-wide siRNA screen. Through this approach, candidate genes either encoding the channel itself and/or essential regulators or parts of the signaling cascade

leading to VRAC activation should be identified. Subsequently, the results of the screen should be assessed and validated through a secondary screen. The effect of siRNAs with a strong impact on the screening assay should be verified by electrophysiological measurements. Validated candidate genes should then be cloned and characterized in respect to their intracellular localization. Furthermore, the effect of their overexpression on VRAC activity has to be tested. In order to substantiate the identity of the channel it would be necessary to show that changes in protein sequence will reflect in intrinsic properties of the channel, such as current kinetics, ion selectivity or pharmacological profile.

The molecular identification of VRAC would be a major breakthrough for the field of volume regulation and ion homeostasis in general and would facilitate a plethora of further investigations concerning signal transduction, regulation and physiological as well as pathological importance that had not been possible thus far.

3. Materials and Methods

3.1 Materials

3.1.1 Chemicals

All chemicals were purchased from Sigma, Fluka or Roth, unless stated otherwise.

3.1.2 Cell lines

The cell lines shown in Table 1 were used for the experiments described in this work including the generation of knockout cell lines and the YFP-expressing HEK293 cell line.

Table 1: Cell lines

Cell line	Origin	Karyotype	References
HEK293	human embryonic kidney	hypo-triploid	(Graham et al., 1977) hpacultures.org.uk
HCT116	human colon carcinoma	diploid	(Brattain et al., 1981) (Thompson and Compton, 2008) hpacultures.org.uk
HeLa	human cervix epitheloid carcinoma	aneuploid	(Gey et al., 1952) hpacultures.org.uk
HL-60	human peripheral blood leukocytes	pseudodiploid	(Collins et al., 1977) hpacultures.org.uk

3.1.3 Cell culture reagents

For general cell culture, Dulbecco's Modified Eagle Medium (DMEM) or McCoy's 5A medium was used for HEK293 and HCT116 cells, respectively, supplemented with fetal calf serum (FCS) and 100 u/ml Penicillin and 0.1 mg/ml Streptomycin, unless stated otherwise. Phenol red-free DMEM was supplemented with 4 mM L-Glutamine.

In general, cells were cultured on tissue culture dishes (TPP Techno Plastic products or Greiner) at 37°C under a humidified atmosphere with 5% CO_2. Cell culture reagents were purchased from PAN biotech, unless stated otherwise.

3.1.4 Genome-wide siRNA library

The genome-wide siRNA screen was performed at the FMP Screening Unit using the Ambion Silencer® Human Genome siRNA Library V3 (Life Technologies). The library contains 189 384-well plates, with each gene being targeted by three independently placed siRNAs.

3.1.5 Expression constructs

The expression constructs generated for this study and/or used for electrophysiological measurements, immunocytochemistry, immunoprecipitation experiments, topology experiments and the generation of knockout cell lines are listed in Table 2.

Table 2: Expression constructs

Construct name*	backbone	no.**	comment
LRRC8A	pcDNA3.1/myc-His(-)B	5500	untagged
LRRC8B	pcDNA3.1/myc-His(-)B	5501	untagged
LRRC8C	pcDNA3.1/myc-His(-)B	5502	untagged
LRRC8D	pcDNA3.1/myc-His(-)B	5503	untagged
LRRC8E	pcDNA3.1/myc-His(-)B	5504	untagged
LRRC8A-myc	pcDNA3.1/myc-His(-)B	5651	no stop codon, C-term. myc-tag
LRRC8B-myc	pcDNA3.1/myc-His(-)B	5506	no stop codon, C-term. myc-tag
LRRC8C-myc	pcDNA3.1/myc-His(-)B	5507	no stop codon, C-term. myc-tag
LRRC8D-myc	pcDNA3.1/myc-His(-)B	5508	no stop codon, C-term. myc-tag
LRRC8E-myc	pcDNA3.1/myc-His(-)B	5509	no stop codon, C-term. myc-tag
LRRC8A-GFP	pEGFP-N1	5518	no stop codon, C-term. myc-tag
LRRC8B-GFP	pEGFP-N1	5519	no stop codon, C-term. myc-tag
LRRC8C-GFP	pEGFP-N1	5520	no stop codon, C-term. myc-tag
LRRC8D-GFP	pEGFP-N1	5521	no stop codon, C-term. myc-tag
LRRC8E-GFP	pEGFP-N1	5570	no stop codon, C-term. myc-tag
GFP-LRRC8A	pEGFP-C1	5514	N-term. GFP-tag
GFP-LRRC8B	pEGFP-C1	5568	N-term. GFP-tag
GFP-LRRC8C	pEGFP-C1	5569	N-term. GFP-tag
GFP-LRRC8D	pEGFP-C1	5515	N-term. GFP-tag
GFP-LRRC8E	pEGFP-C1	5516	N-term. GFP-tag
LRRC8A-RFP	pmRFP-N1	5524	no stop codon, C-term. RFP-tag
$LRRC8A_{trunc}$-GFP	pEGFP-N1	5526	truncated version, no stop codon, C-term. GFP-tag
GFP-LRRC8A-exHA	pEGFP-C1	5536	N-term. GFP-tag, HA-tag in extracellular loop
GFP-LRRC8A-ctHA	pEGFP-C1	5538	N-term. GFP-tag, C-term. HA-tag
LRRC8A-N66A-N83A-myc	pcDNA3.1/myc-His(-)B	5512	no stop codon, C-term. myc-tag, mutated glycosylation sites
GFP-ClC-1	pEGFP-C1	3135	N-term. GFP-tag

* Abbreviated version of the construct name not including the name of the backbone plasmid
** Number of construct in the internal plasmid database of the Jentsch laboratory

3.1.6 Commercial antibodies

The following commercial primary antibodies were used: rabbit anti-myc (A-14, Santa Cruz Biotechnology), rabbit anti-GFP (A-11122, Life Technologies) for IP and chicken anti-GFP (1020, Aves Lab) for Western blot, mouse anti-α-tubulin (DM1A, Sigma), mouse anti-HA (HA.11, Covance). Secondary antibodies were conjugated to AlexaFluor 488 or 546 (Molecular Probes) or to horseradish peroxidase (Jackson ImmunoResearch).

3.1.7 Lab-generated antibodies

Polyclonal antibodies against the different LRRC8 proteins were raised in rabbits and guinea-pigs against the peptides indicated in Table 3 that were coupled to KLH through an terminally added cysteine. The position of each peptide within the respective protein is

also indicated in Table 3. Peptide synthesis and animal immunization was performed by Pineda Antikörper-Service, Berlin, Germany.

Sera were affinity-purified using the immunizing peptide coupled to a Sulfolink coupling resin (Pierce). To this end, immunosera were incubated rotating at 4°C on the columns, then washed with high-salt TBS (TBS containing 500 mM NaCl) followed by additional washing steps with TBS and 0.1x TBS. Bound antibodies were eluted with 100 mM glycine pH 3.0 and 200-µl fractions were collected. Protein-containing fractions were identified in Ponceau S–stained dot blots, pooled, and the pH was adjusted to pH 7.5–8.0. After addition of 0.01% BSA and 0.02% NaN_3, antibodies were aliquoted and shock-frozen in liquid nitrogen. Long-term storage was at –80°C.

The specificity of the antibodies was assessed by Tobias Stauber in Western blots and for LRRC8A in immunofluorescence (Voss et al., 2014; unpublished data). The rabbit anti-KCC1 antibody was described previously (Rust et al., 2007).

Table 3: LRRC8 antibodies

Target protein	Target species*	Name	no**	immunizing peptide	peptide position
LRRC8A	**human/mouse**	mLRRC-8A-5a rb1	1339	QRTKSRIEQGIVDRSE	intra. loop
LRRC8B	human/**mouse**	mLRRC-8B-5b rb1	1345	QSLPYPQPGLESPGIESPT	intra. loop
LRRC8C	human/**mouse**	mLRRC-8C-ct rb2	1347	EDALFETLPSDVREQMKAD	C-term.
LRRC8D	human/**mouse**	mLRRC-8D-ct rb1	1348	LEVKEALNQDVNVPFANGI	C-term.
LRRC8E	human/**mouse**	mLRRC-8E-ct rb2	1351	LYEGLPAEVREKMEEE	C-term.

* The target species of the immunizing peptide are indicated in **bold**
****** Number of antibody in the internal antibody database of the Jentsch laboratory

3.2 Methods

3.2.1 Generation of the HEK293-YFP Cell Line

The T-REx® system (Life Technologies) was used to generate a stable HEK293 cell line inducibly expressing the halide-sensitive YFP(H148Q/I152L) (Galietta et al., 2001) as described in the manual. Clones were selected using 200 µg/ml hygromycine B and 10 µg/ml blasticidin. Monoclonal cell lines were subsequently tested for robust and homogenous expression of YFP after induction with 1.25 µg/ml doxycycline using live-cell imaging techniques. The clone 1:5-(6) was chosen for the genome-wide screening procedure. The cells were kept in DMEM with tetracycline-free Hyclone FCS and the above-mentioned antibiotics.

3.2.2 Plate layout and control siRNAs

The screen was performed in a 384-well format using Corning CellBIND® flat bottom assay plates. In total 189 plates were screened for one genome-wide screening round and two replicate screens were performed consecutively. On each screening plate (Fig.3) rows 23 and 24 were used for the placement of several control siRNAs: siRNA pools against YFP (Silencer GFP siRNA from Ambion) as well as a cell death-inducing siRNA mixture (AllStars Hs Cell Death Control siRNA from Qiagen) were used as transfection controls. A non-targeting siRNA (Silencer Negative Control from Ambion) was used as negative control and an siRNA pool against AE2 (ON-TARGETplus SMARTpool siRNA SLC4A2 from Thermo Scientific) was used as assay-specific positive control (see also section 4.2). In wells O23, P23, O24, and P24, hypotonic solution containing 1% Triton X was added to determine the background signal (see section 3.2.5). For detailed plate layout see Fig. 3.

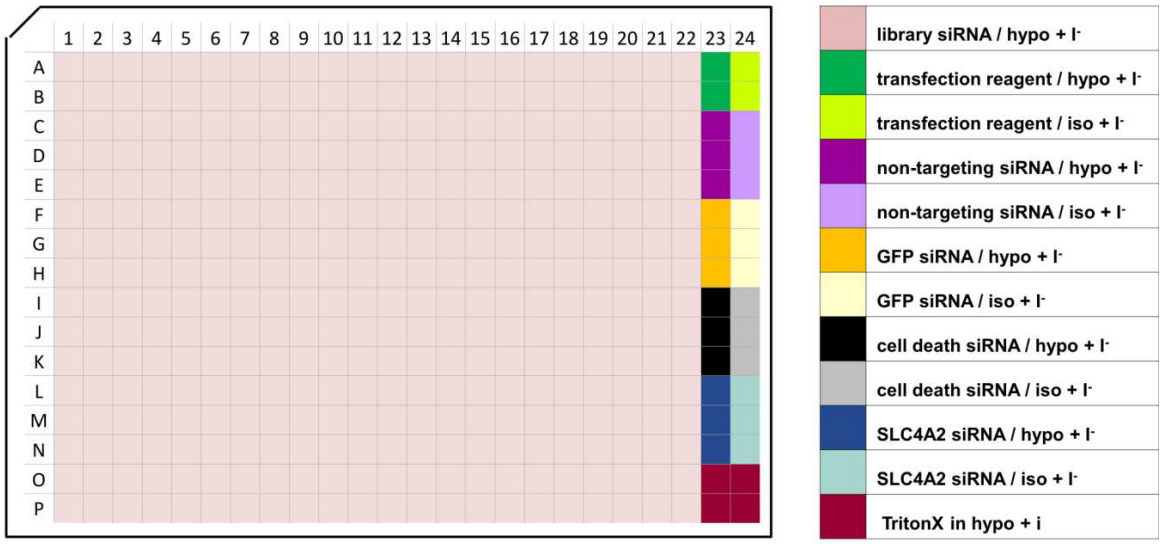

Figure 3: Plate layout including the position of control siRNAs
Cells in wells of rows 1-22 were transfected with individual siRNAs of the Ambion Silencer® Human Genome siRNA Library V3 and tested for hypotonicity-induced YFP-quenching (experimental wells). Rows 23 and 24 contained control wells that were treated as indicated.

3.2.3 High-throughput siRNA transfection

For siRNA transfection, 8 µl of a 500 nM library-siRNA-OptiMEM® solution was pipetted into each well of the 384-well assay plate using the Tecan Freedom EVO 200 workstation. Subsequently, 0.2 µl Lipofectamine® RNAimax transfection reagent (Life Technologies) previously diluted in 11.8 µl Opti-MEM® (Life Technologies) were added to yield the final transfection mixture. Then, 6000 cells/well in antibiotic-free DMEM were seeded onto the pre-dispensed transfection mixture using a BioTek EL406™

dispenser, resulting in a final concentration of 50 nM siRNA in a total volume of 80 µl per well. 24 h post-transfection, the cell culture medium was exchanged to phenol red-free DMEM containing 1.25 µg/ml doxycycline to induce YFP-expression.

For the prescreen and the secondary screen, the same transfection set-up was used to transfect ON-TARGETplus SMARTpool siRNAs against the candidate genes listed in Table 7 and Table 8, respectively . Parts of the pipetting steps for the transfection were performed manually using single or multiple-channel pipettes instead of the automated workstation due to the smaller sample number.

3.2.4 YFP-based screening-assay

The YFP-quenching assay was performed 72 h post-transfection. As a first step, the cell culture medium was exchanged in all wells of the plate with 10 µl of isotonic solution (in mM: 145 NaCl, 5 KCl, 1 $MgCl_2$, 2 $CaCl_2$, 10 glucose, 10 HEPES, pH 7.4, 329 mOsm) using the Tecan Freedom EVO 200 workstation. The plates were then transferred into the FLIPR^{TM} (Molecular Devices) High Throughput Cellular Screening Device and fluorescence measurements were initiated. All wells of the plate were simultaneously illuminated at λ=495-505 nm and YFP-fluorescence was measured at λ=526-585 nm using the FLIPR^{TM} Fluo3 LED/filter set. After 5 measurements in intervals of 5 s, parallel pipetting within the FLIPR^{TM} added 25 µl iodide-containing hypotonic (rows 1-23) (in mM: 70 NaI, 5 NaCl, 5 KCl; 1 $MgCl_2$, 2 $CaCl_2$, 10 glucose, 10 HEPES pH 7.4, 189 mOsm) or isotonic (row 24) (in mM: 70 NaI, 5 NaCl, 5 KCl; 1 $MgCl_2$, 2 $CaCl_2$, 10 glucose, 140 mannitol, 10 HEPES pH 7.4, 329 mOsm) solution into each well. The solution added to wells O23, P23, O24 and P24 was hypotonic and contained 1% Triton X in order to determine the background signal. The mixture of the pre-existing 10 µl isotonic solution and the newly added 25 µl hypotonic solution resulted in a final osmolarity of 229 mOsm, i.e. a ~30% decrease in osmolarity, and a final concentration of 50 mM iodide. All assay solutions were prepared freshly for each screening day and the osmolarity was monitored by using an Osmomat 030 freezing point osmometer (Gonotec). Fluorescence measurements were continued for 55 s in 5-s intervals, followed by 8 measurements in 30-s intervals to minimize bleaching, and finally 10 measurements in 1-s intervals. The total length of the measurement (500 s) was sufficient for YFP-quenching to nearly reach steady state. At time points 0 s and 5 s (before pipetting) and at 25, 30, 35, 40, 45, and 490 s (during/after pipetting) photographs of the entire plate were

taken to allow post-hoc control of the integrity of the cell layer of each well. The same assay set-up was used for the prescreen and the secondary screen.

For preliminary live-cell experiments, cells were seeded onto glass-bottom dishes (MatTek) and induced with doxycycline as described above. Fluorescence measurements were performed at an inverted microscope (Zeiss Axiovert 200 equipped with a 40x 1.30 NA oil immersion lens) connected to a Polychrom II monochromator (TILL photonics) at an excitation wavelength of 514 nm. The emitted light was filtered with a 535±30 nm filter and captured with a Sensicam CCD camera (PCO) using the 4x4 binning of the TillVision software package (TILL photonics). Pictures were taken every 2 s for 10 min total. After recording a baseline for ~60 s, the medium was exchanged by manual pipetting to iodide- containing isotonic (in mM: 70 NaI, 5 NaCl, 5 KCl; 1 $MgCl_2$, 2 $CaCl_2$, 10 glucose, 140 mannitol, 10 HEPES pH 7.4, 329 mOsm), hypotonic (in mM: 70 NaI, 5 NaCl, 5 KCl; 1 $MgCl_2$, 2 $CaCl_2$, 10 glucose, 10 HEPES pH 7.4, 189 mOsm) or iodide-free isotonic (in mM: 145 NaCl, 5 KCl, 1 $MgCl_2$, 2 $CaCl_2$, 10 glucose, 10 HEPES pH 7.4, 329 mOsm) saline. Fluorescence traces were then analyzed by subtracting the signal from a background ROI of the same image and normalizing to the time point t=120 s (after the pipetting artifact).

For preliminary experiments on 96-well plates (Corning), the Safire II plate reader (Tecan) was used. The medium was removed manually by using a 12-channel pipette, cells were washed once with isotonic saline and then 100 µl of the respective saline (as described for the live-cell experiments) was added to each well. The plate was immediately entered into the plate reader and YFP fluorescence was measured at 510 nm excitation wavelength and 540 nm emission wavelength with a gain of 120 in 60-s intervals with 8 reads per time point for a total measurement time of 10 min.

3.2.5 Bioinformatics analysis and hit assessment

The primary data generated from the FLIPR^{TM} measurements was subjected to subsequent data processing to extract several parameters for data evaluation and hit definition (Fig. 4). The averaged fluorescence before the pipetting step, F^{abs}_{ante}, was obtained by averaging values from measurements 1-3 and was used to set a warning 'low cell' flag when its value was less than 0.8 times of the mean F^{abs}_{ante} averaged over all experimental wells from the plate. After pipetting, the fluorescence acutely changed to new values (pipetting artifact) that remained stable for about 30 s before swelling-induced quenching of YFP set in. We averaged fluorescence values from measurements 9 to 12 to obtain

F^{abs}_{start} which was subsequently used for normalization. F^{abs}_{fin} was defined as averaged fluorescence from the four last measurements and was used to generate another 'warning flag' if fluorescence had not reached quasi-steady-state at the end of the measurement. The averaged fluorescence (over the last 300 s) of the four control wells from each assay plate, that had been exposed to Triton X to maximally quench YFP fluorescence were used to determine background fluorescence F_{BG}, which was then used for subtraction. Furthermore, the background-subtracted fluorescence value of each well was normalized to the corresponding F^{abs}_{start} value to yield F* (Fig. 4A).

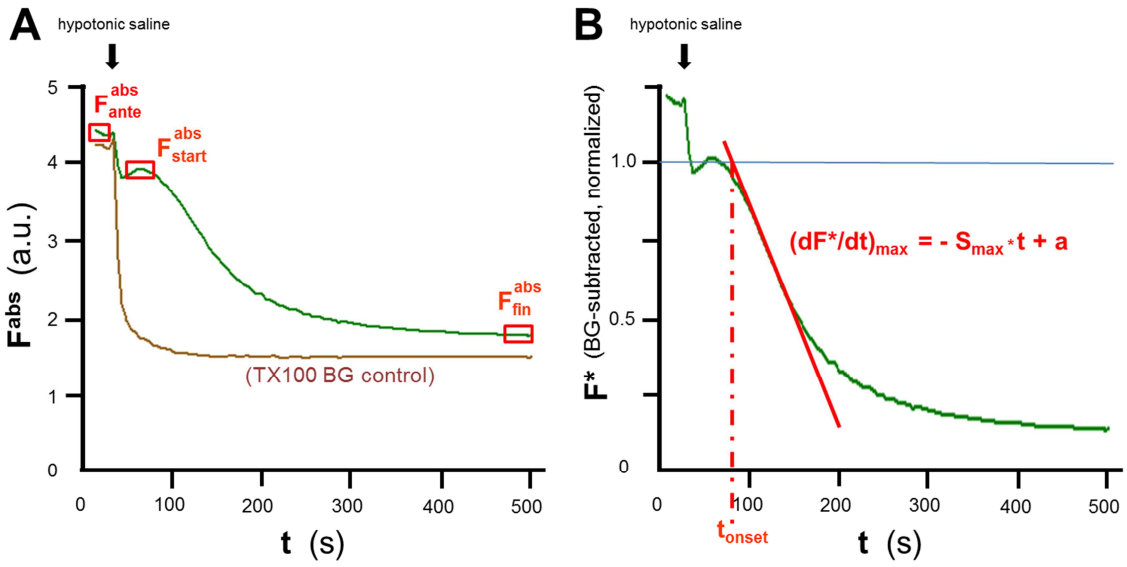

Figure 4: Parameters extracted from the primary data during bioinformatics analysis
Example traces, showing the absolute, non-corrected values of fluorescence (F^{abs}) measured at λ=526-585 nm as a function of time. The green curve shows a representative trace for cells that were exposed to hypotonic, iodide-containing solution at the time indicated by the arrow. The brown curve shows a control well to which hypotonic, iodide-containing solution with 1% Triton X was added. (B) Background-subtracted and normalized fluorescence F*. After subtracting the background determined in control wells treated with Triton X, the fluorescence of every experimental well was normalized to its individual F^{abs}_{start} value. The maximal slope of fluorescence decrease S_{max} was determined by linear regression to the curve between 35 and 300 seconds. t_{onset} was defined as indicated.

Since siRNA-mediated knockdown of VRAC might only reduce the speed of iodide quenching by impacting iodide current magnitude, but not necessarily the final intracellular iodide concentration (reflected in F^{abs}_{fin}), we also determined the slope of fluorescence change by linear regression of 11 points in a sliding window between 35 and 350 s. The maximum of these slopes was defined as S_{max}. The intersection of the corresponding linear regression line with F*=1 defined t_{onset} (Fig. 4B) as a measure for the speed of response to the hypotonic challenge, a delay that might be changed e.g. by interfering with the signal transduction cascade leading to VRAC opening. For each individual plate the mean maximal slope $S_{max,mean}$ of all experimental wells and the

standard deviation were calculated. For all essential parameters, Z-scores were calculated in order to express differences in terms of standard deviations, with e.g. Z=2 meaning that the slope is slower by two standard deviations compared to the average of the experimental wells of the plate.

The main parameter used for hit definition was S_{max}. In order to account for different efficiencies of siRNA knockdown within the three individual siRNAs against each gene, we calculated the mean Z-scores obtained with the two 'best' siRNAs (giving the largest values of Z) and primarily relied on this information for further hit assessment. For this the mean values from both replicate screens were taken into account.

Besides the evaluation of fluorescence values, the photographs taken during the measurements were also analyzed individually by eye to detect artifacts caused by dirt particles or disruption of the cell layer to exclude false positives/negatives from further analysis.

Additional to the data retrieved from the primary screen, an bioinformatics inquiry was performed to obtain information on "protein family belonging" from the UniProtKB database (Magrane and Consortium, 2011), the genes' tissue expression pattern (as determined by publicly available microarray data (Lopes et al., 2011)) as well as on the predicted number of transmembrane domains through the online-analysis tool TMHMM 2.0c (Krogh et al., 2001).

Candidate selection for the secondary screen was performed by revising hitlists from the above-mentioned mean "best of 2" Z-scores for S_{max} and subsequent assessment towards the following parameters: minimally one transmembrane domains, broad tissue expression or member of a gene-family with overall broad tissue expression, known function not incompatible with ion channel identity.

3.2.6 Cloning and mutagenesis of candidate constructs

For candidate genes, cDNA was cloned from HEK293 or HeLa cell total cDNA that was prepared as described in section 3.2.11 (qRT PCR) using specific primers. In cases where cloning from these cDNA libraries was not successful, cDNA clones were ordered from SourceBioscience and used as template for PCR. For PCRs, Phusion (Finnzymes) or OptiTaq (Roboklon) DNA polymerase was used. Oligonucleotides were ordered from eurofins genomics. Isolation of plasmid DNA from *E. coli* cultures or agarose gel fragments was performed using the Nucleo Spin® Plasmid QuickPure or the Nucleo Spin®

Gel and PCR Clean-up kit (Macherey & Nagel), respectively. Restriction enzymes were purchased from Fermentas or New England Biolabs and used according to the suppliers' protocol. Agarose gels were prepared using UltraPure agarose (Invitrogen) in TAE buffer (40 mM Tris, 40 mM acetic acid, 1 mM EDTA, pH 8.0) and samples were mixed with 6x DNA loading buffer (60 mM Tris-HCl (pH 8.0), 60% glycerol, 60 mM EDTA, 0.4% Orange G) before submitting them to agarose gelelectrophoresis. DNA concentrations were determined with a Nanodrop ND-1000 spectrophotometer (PeqLab). Vector ligation was performed using a T4 Ligase (Fermentas). Bacteria were transformed using electroporation and plated onto selective agar-media. Positive clones were identified using restriction digests or sequencing of plasmid DNA.

To generate expression constructs with a GFP fused to their N-termini or C-termini, cDNA encoding the respective human protein was cloned with stop codon into pEGFP-C1 or without stop codon into pEGFP-N1, respectively. For expression of C-terminally RFP-tagged constructs, the cDNA was cloned into pmRFP-N1. For untagged and C-terminally myc-tagged (deglycosylation experiment and co-immunoprecipitations upon heterologous expression) expression, cDNAs were cloned (with and without stop codon, respectively) into pcDNA3.1/myc-His(-)B (Invitrogen). HA-tags and point mutations were introduced by PCR. All constructs were confirmed by sequencing the complete ORF. For an overview of used constructs see Table 2.

3.2.7 Electrophysiology

HEK or HCT cells were plated onto gelatine-coated coverslips and transfected using Fugene HD (Promega) or Lipofectamine 2000 (Life Technologies) transfection reagents, respectively. One of the transfected LRRC8 isoforms was fused C-terminally to GFP. When LRRC8A was co-transfected with other LRRC8 isoforms only the latter carried GFP because plasma membrane fluorescence indicated co-expression with LRRC8A.

To measure cells with siRNA mediated knockdown of LRRC8A SMARTpool siRNAs were transfected in a 96-well plate format. For each 96-well 1.6 µl of a 5 µM SMARTpool siRNA stock solution were mixed with 8.4 µl Opti-MEM® (Life Technologies) and separately 0.4 µl Lipofectamine® RNAimax transfection reagent (Life Technologies) were diluted in 9.6 µl Opti-MEM® and then added to the siRNA-mixture and incubated for 20 min at room temperature. Then 12.000 cells/well were added in 140 µl antibiotic free medium, which resulted in a final siRNA concentration of 50 nM. 48 h post-transfection cells were splitted onto gelatine-coated coverslips and patch-clamp

experiments were then performed 72 h post-transfection. For rescue experiments cells were transfected 24-48 h after the siRNA transfection using 50 ng plasmid-DNA and 0.15 µl Fugene HD (Promega) transfection reagent.

Whole-cell voltage-clamp experiments were performed in isotonic extracellular solution containing (in mM) 150 NaCl, 6 KCl, 1 $MgCl_2$, 1.5 $CaCl_2$, 10 glucose, and 10 HEPES, pH 7.4 with NaOH (320 mOsm). $I_{Cl(swell)}$ was elicited by perfusing the cells with hypotonic solution containing (in mM) 105 NaCl, 6 CsCl, 1 $MgCl_2$, 1.5 $CaCl_2$, 10 glucose, 10 HEPES, pH 7.4 with NaOH (240 mOsm). For anion selectivity experiments, NaCl was replaced in this solution by an equimolar amount of NaI, $NaNO_3$, or Na-D-gluconate. The pipette solution contained (in mM) 40 CsCl, 100 Cs-methanesulfonate, 1 $MgCl_2$, 1.9 $CaCl_2$, 5 EGTA, 4 Na_2ATP, and 10 HEPES, pH 7.2 with CsOH (290 mOsm). Osmolarities of all solutions were assessed with an Osmomat 030 freezing point osmometer (Gonotec). All experiments were performed at constant temperature of 20–22°C. Currents were recorded with an EPC-10 USB patch-clamp amplifier and PatchMaster software (HEKA Elektronik) or a MultiClamp 700B patch-clamp amplifier/Digidata 1440A digitizer and pClamp 10 software (Molecular Devices). Patch pipettes had a resistance of 1–3 MΩ. Series resistance was compensated by 80–90% to minimize voltage errors. Currents were sampled at 5 kHz and low-pass filtered at 10 kHz. The holding potential was -30 mV. Cells with a membrane resistance below 800 MΩ or series resistance above 10 MΩ were discarded. The standard protocol for measuring the time course of $I_{Cl(swell)}$ activation, applied every 15 s after membrane rupture, consisted of a 0.6-s step to -80 mV followed by a 2.6-s ramp from -100 to 100 mV. The read-out for $I_{Cl(swell)}$ was the steady-state whole-cell current at -80 mV normalized to the cell capacitance (current density) subtracted by the baseline current density at -80 mV before perfusion with hypotonic solution. The voltage protocol, applied after complete activation of $I_{Cl(swell)}$, consisted of 1-s or 2-s steps starting from -120 mV to 120 mV in 20-mV intervals preceded and followed by a 0.5-s step to -80 mV every 5 s.

The inactivation kinetics of $I_{Cl(swell)}$ could not be fitted appropriately by a single-exponential function. We therefore calculated the fraction of remaining current by dividing the current amplitude at the end of the 2-s voltage step by the current amplitude 1.5 ms after the beginning of the voltage step (avoiding contamination by capacitive transients). The half inactivation time $t_{1/2}$ was determined by the time point where the inactivation reached half of the total inactivation after 2 s. Calculation of current densities

and inactivation characteristics was carried out with an automatic script written in MATLAB R2011a (MathWorks) and plotted with GraphPad Prism 5 (GraphPad Software). Boltzmann curve-fitting and calculation of $V_{1/2}$ was done with GraphPad Prism with the following fitting constraints: bottom value less than 0.2, top value greater than 0.9. Example current traces were lowpass-filtered at 2 kHz and reduced to a sampling rate of 1 kHz for clarity. Averaged data is presented as mean ± SEM. Significance was calculated by one-way ANOVA and Tukey's post-hoc test, where applicable. At least 4 cells per condition were measured on at least two different days; exact n-values are given in the figures. Where possible, measurements were done blinded. Electrophysiological measurements were performed by Florian Ullrich and Jonas Münch.

3.2.8 Deglycosylation experiments

To assess glycosylation of LRRC8A, HEK cells were transfected on 10-cm dishes using 17 µl of polyethylenimine (PEI) and 6 µg of plasmid encoding myc-tagged LRRC8A (wildtype or mutant). Cells were lysed in Ripa lysis buffer (150 mM NaCl, 1% NP-40, 0.5% sodium deoxycholate, 0.1% SDS, 50 mM Tris, pH 8.0, 4 mM Pefabloc (Roth), complete proteinase inhibitor cocktail (Roche)). After 10 min centrifugation at 14.000 rpm at 4°C, protein concentrations of cell lysates were determined by BCA assay. 60 µg of total protein were mixed with 2 µl of denaturing buffer (NEB) and 2 µl of 0.1 M Tris/HCl pH 7.4 in a reaction volume of 20 µl and denatured at 75°C for 10 min. Then 4 µl of 10xG7 Buffer (NEB), 4 µl of 10% NP-40 (NEB) and 4 µl of PNGase F (Roche) were added in a total volume of 40 µl. After 2 h incubation at 37°C, the reaction was terminated by adding 10 µl of 5xLämmli sample buffer. Samples were separated by SDS-PAGE and analyzed by Western blot using the LRRC8A antibody.

3.2.9 Co-immunoprecipitation, SDS-Page and Western blots

For co-immunoprecipitation, HEK cells were co-transfected with plasmids (6 µg total) encoding myc-tagged or untagged LRRC8A and N-terminal fusion constructs of LRRC8A-E or ClC-1 (or soluble GFP) on 10-cm dishes using PEI as described above. 48 h post-transfection cells were lysed in 300 µl lysis buffer (150 mM NaCl, 1% NP-40, 0.5% sodium deoxycholate, 50 mM Tris-HCl pH 7.5, 4 mM Pefabloc (Roth), complete proteinase inhibitor cocktail (Roche)) for 10 min on ice. The lysate was pre-cleared by centrifugation at 14.000 rpm for 10 min at 4°C and subsequently spun at 30.000 rpm for 30 min at 4°C. 150 µl of the supernatant were mixed with 5 µg of the respective antibody and IP buffer (150 mM NaCl, 0.1% NP-40; 0.05% sodium deoxycholate, 50 mM Tris-

HCl, pH 7.5, complete proteinase inhibitor cocktail (Roche)) was added to final volume of 800 µl. The sample was rotated for 1-2 h at 4°C before 10 µl of Protein A Dynabeads® (Life Technologies) were added and rotation continued overnight at 4°C. After four washes with 500 µl IP buffer, precipitates were eluted in 40 µl Lämmli sample buffer, separated by SDS-PAGE and analyzed by Western blot as indicated. Lysate equivalent to 20% of input was loaded as reference.

For immunoprecipitation from native cells, lysates from two confluent 15-cm plates per cell line (wildtype and *LRRC8A*$^{-/-}$) were prepared as described above. 1.9 ml lysate were mixed with equal volumes of IP buffer and 30 µl of Protein A Dynabeads® (Life Technologies) previously coupled to 15 µg of the LRRC8A antibody using dimethyl pimelimidate. After incubation and washing as described above, precipitates were eluted from the beads in 50 µl of 0.2 M glycine (pH 2.5), mixed with Lämmli sample buffer, separated by SDS-PAGE and analyzed by Western blot as indicated.

To assess protein expression, cells were lysed as described above. Protein concentrations were determined by BCA and equal amounts were separated by SDS-PAGE and analyzed by Western blot as indicated.

SDS-Page was usually performed on 8% SDS-polyarcylamide gels using the Mini-PROTEAN 3 gel chamber system (Bio-Rad) and the PageRuler™ Plus Protein Ladder (fermentas) as molecular weight marker. For Western blots, the tank blotting system Mini Trans-Blot Electrophoretic Transfer Cell (Bio-Rad) and transfer buffer with methanol (25 mM Tris-HCl pH 8.2, 20% methanol, 200 mM glycine) was used. Protein samples were blotted onto polyvinylidene difluoride (PVDF) membrane for 2-3 h at 4°C at 84 mV. Membranes were stained with Ponceau S (0.2% Ponceau S, 3% acetic acid) to check for equal protein loading and transfer and subsequently blocked using TBS supplemented with 0.1% Tween 20 and 5% non-fat dried milk power as blocking buffer for at least 30 min. Primary antibodies were incubated overnight at 4°C in blocking buffer. Subsequently, membranes were washed 3 times for 10 min with TBS supplemented with 0.1% Tween. Secondary antibodies coupled to horseradish peroxidase were applied in blocking buffer for 45 min. Afterwards, the washing steps were repeated and signals were visualized by chemiluminescence using SuperSignal West Pico/Femto, (Pierce). Signal documentation was done with a Chemi-Smart 5000 CCD camera system using the ChemiCapt 5000 (PeqLab) software.

3.2.10 Immunocytochemistry

For immunocytochemistry, cells were transfected (if indicated) with plasmids encoding the respective construct(s) using Fugene HD (Promega). 24-36 h after transfection, cells were fixed in pre-cooled methanol at -20°C for 10 min (immunostaining with LRRC8A antibody), or in 2% (topology assay) or 4% PFA in PBS for 15 min followed by a 5-min incubation with 30 mM glycine in PBS at room temperature. Cells were incubated sequentially for 1 h each with primary and secondary antibodies (where applicable) in PBS containing 0.1% Triton X (or without Triton X, for non-permeabilized cells) supplemented with 3% BSA. Images were acquired with an LSM510 confocal microscope with a 63x, 1.4 NA oil-immersion lens (Zeiss). The topology assay was performed by Tobias Stauber.

3.2.11 Quantitative RT-PCR

Total RNA was isolated from cell pellets using the RNeasy Mini Kit (Qiagen). Approx. 1 µg of RNA was subjected to DNase I (amplification grade, Invitrogen) digestion and subsequently transcribed into cDNA using random primers and the Superscript II reverse transcriptase (Invitrogen). A qRT-PCR reaction with a total volume of 20 µl was set up using the Power SYBR Green PCR Master Mix (Applied Biosystems) and 0.5 µM of specific primers. Reactions were run in triplicates with a 60-s elongation time at 60°C. Amplification and melting curves were monitored using a StepOnePlus Real-Time PCR System and the StepOne Software (Applied Biosystems). GAPDH was used as internal control and for ΔΔCt calculations. Primers were designed using the QuantPrime selection tool (Arvidsson et al., 2008) to preferentially span exon-exon boundaries and to give products of 60–150 bp. The primer pairs are listed in Table 4.

Table 4: qRT PCR primers

Gene	no.*	primer pair sequences (5'-3')	product size [bp]
GAPDH	8076	ACAGTCAGCCGCATCTTCT	127
	8077	GTTAAAAGCAGCCCTGGTGA	
LRRC8A	11012	GGGTTGAACCATGATTCCGGTGAC	133
	11013	GAAGACGGCAATCATCAGCATGAC	
LRRC8B	11284	ACCTGGATGGCCCACAGGTAATAG	126
	11285	ATGCTGGTCAACTGGAACCTCTGC	
LRRC8C	11288	ACAAGCCATGAGCAGCGAC	132
	11289	GGAATCATGTTTCTCCGGGC	
LRRC8D	11036	ATGGAGGAGTGAAGTCTCCTGTCG	126
	11037	CTTCCGCAAGGGTAAACATTCCTG	
LRRC8E	11038	ACCGTGGCCATGCTCATGATTG	62
	11039	ATCTTGTCCTGTGTCACCTGGAG	

*Number of primer in internal oligo database of the Jentsch laboratory

3.2.12 Generation of monoclonal knockout cell lines using the CRISPR/Cas and zinc finger nuclease Technologies

For the disruption of *LRRC8* genes by the CRISPR/Cas system in cell culture, we used the px330 single plasmid system as described (Cong et al., 2013). The targeting sgRNA sequences were chosen using both the UCSC Genome Browser tool at www.genome-engineering.org and the sequence collection from Mali et al. (2013) (for sequences see Table 5). Target sgRNAs were cloned into the px330 vector and transfected into the described YFP-expressing HEK293 clone or WT HCT116 cells in a 6-well format using 3 µl of the Fugene HD transfection reagent and 900 ng targeting vector(s) (up to 4) plus 100 ng pEGFP-C1-vector. In HCT116 cells, the *LRRC8A* gene was additionally disrupted using a custom-designed CompoZr® Knockout Zinc-Finger Nuclease (Sigma). The zinc finger nuclease (ZFN) pair encoded on two separate plasmids was transfected as described above, using 500 ng of each ZFN-plasmid and 100 ng of the pEGFP-C1 vector. 2-5 days post-transfection, single GFP-positive cells were FACS-sorted into 96-well plates containing preconditioned DMEM (for HEK cells) or McCoy's 5A (for HCT116 cells) medium. In some cases, transfected cells were enriched by G418 selection before FACS sorting.

Table 5: Guide sequences used for the CRISPR/Cas-based generation of knockout cell lines

Target gene	Construct	Guide sequence (5'→3')	Targeting strand	Target location in protein
LRRC8A	1A	GGCTGATGTAGAAGGACGCCAGG	-	aa 320-328 (beginning of TMD4)
	3A	TGATGATTGCCGTCTTCGGGGGG	+	aa 36-43 (in TMD2)
	4A	TCCTGCAATGATTCGTTCCGGGG	+	aa 64-71 (between TMD1 and TMD2)
LRRC8B	1B	TTTTTCTCTTAACGCCTCAAAGG	-	aa 346-353 (after TMD4)
	2B	GGCCACAAAATGCTCGAGCCTGG	-	aa 147-354 (between TMD2 and TMD3)
LRRC8C	1C	ATGCTCATGATCGGCGTGTTTGG	+	aa 35-42 (in TMD1)
LRRC8D	1D	GTGGCTCTGAGAGGTATGTCAGG	-	aa 107-114 (between TMD1 and TMD2)
LRRC8E	1E	GCTGGCCGAGTACCTCACCGTGG	+	aa 27-34 (inTMD1)

aa, amino acid; TMD, transmembrane domain; PAM sequences are underlined

Monoclonal cell lines were raised and tested for sequence alterations using target-site-specific PCR on genomic DNA followed by Sanger-sequencing and/or Western blot analysis to confirm the absence of the protein when specific antibodies were available. Genomic DNA was isolated from cell pellets using the Invisorb Spin Tissue Minikit (Invitek). PCRs were performed with the primer pairs indicated in Table 6 and the PCR product was sequenced with one or both of the PCR primers.

To generate multiple KOs of several genes, the respective plasmids were transfected together, or cell lines already carrying *LRRC8* gene disruptions were targeted again for other *LRRC8* genes.

Table 6: PCR primer pairs for genotyping of knockout cell lines

Construct	no.*	PCR primers	Product size [bp]
	10998	AGGTGATCAAGTTCATCC	
1A	11200	GAAGGCGAAGTCGTTCTTGACGTCGG	311
	10995	GCAGAATTCCATGATTCCGGTGACAGAGC	
3A	11344	CTCGATCCGTGCCTTGGTCCGCTGCAGC	672
	10998	AGGTGATCAAGTTCATCC	
4A	11041	CAGCTTCTGCAGGTGCACG	905
	11130	CAAAGTCATTTTGTTTGTGC	
1B	11625	GTCCTGGGCATTTTTCACA	470
	12153	AGTACTCCTATATTGATGCC	
2B	12155	TGACTCCAAACCTGGCTGTG	545
	11004	TCGAGCGGCCGCCATGATTCCCGTGACAGAATTCC	
1C	11627	GTATCAATGGTGCTGGAC	469
	11006	GCAGAATTCCATGTTTACCCTTGCGG	
1D	11628	TTAGAATACCACGGAAGG	489
	10838	GCAGAATTCCATGATCCCAGTGGCCGAG	
1E	11629	AGTGGGGCTCTGTCTTCA	255
	10997	GGCCTGCAGCAACTTCTG	
ZFN	11040	CAATGTCCACGGTGCAGTCC	488

*Number of primer in internal oligo database of the Jentsch laboratory

3.2.13 RVD Measurements

Cell volume was measured semi-quantitatively using the calcein fluorescence method (Capo-Aponte et al., 2005). HEK cells were plated two days before measurements at a density of 6.000 cells/well in a 384-well plate. For the RVD assay, 10 µM calcein-AM (Affymetrix eBioscience) in DMEM were loaded for 1 h at 37°C and then washed 3 times with 80 µl isotonic solution (in mM: 145 NaCl, 5 KCl, 1 $MgCl_2$, 2 $CaCl_2$, 10 glucose, 10 HEPES pH 7.4, 329 mOsm) using a Tecan Freedom EVO 200 workstation. Finally, 10 µl of the isotonic solution were added to each well. After a 5-min incubation period the plate was transferred into the FLIPR^{TM} (Molecular Devices) and fluorescence measurements at λ=515-575 nm were initiated using the FLIPR^{TM} Fluo4 LED/filter set. After recording a baseline for 25 s, 25 µl aqua dest. were added to the wells resulting in a final osmolarity of 94 mOsm. Calcein fluorescence was monitored for ~65 min. Wells containing cells of the respective cell line not loaded with calcein-AM (but otherwise treated equally) were used for background subtraction, and fluorescence values were normalized to t=30 s (after the pipetting procedure).

4. Results

4.1 Assay set-up and up-scaling to high-throughput format

In order to perform a genome-wide siRNA screen, a robust read-out assay was needed that could be easily applied to a high-throughput format. To this end, we made use of one characteristic feature of the volume-regulated anion channel, its high permeability for iodide. Since Galietta et al. (2010) had already published the generation of YFP variants that were especially sensitive to halides such as iodide, we opted to use the YFP(H148Q/I152L) variant in a stably-transfected HEK293 cell line. During RVD, VRAC opens upon cell swelling to release chloride from the cell, which is then followed by water and thus counteracts the swelling process (Fig. 5). For the assay, the cells were exposed to hypotonic medium to induce swelling, but additionally a high concentration of iodide (50 mM) was added to this extracellular solution. This would then, due to the steep concentration gradient, lead to an iodide influx into the cell, thereby quenching the fluorescence signal of the halide-sensitive YFP. During the genome-wide siRNA screen we would hopefully find siRNAs leading to a knockdown of VRAC activity and thus reducing or slowing-down the quenching process (Fig. 5).

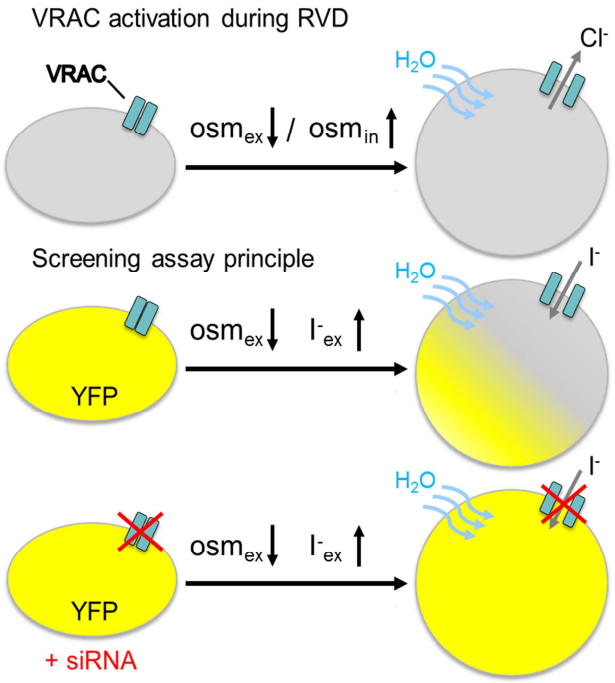

Figure 5: Principle of the YFP assay read-out.
Top: During regulatory volume decrease (RVD), VRAC releases Cl^- upon a swelling stimulus that could occur from a drop in the extracellular osmolarity (osm_{ex} ↓) or a rise in the intracellular osmolarity (osm_{in} ↑). Bottom: Quenching of YFP fluorescence by I^- entering through VRAC upon hypotonic stimulation used as readout in the genome-wide siRNA screening.

The YFP signal could be monitored by different imaging methods. As a first proof of principle, we tested the read-out system in small-scale live-cell imaging experiments using 3.5 cm glass-bottom dishes on a Zeiss Axiovert 200 microscope where we could detect a robust difference between cells that were exposed to isotonic (iso + I^-) or hypotonic (hypo + I^-) medium containing iodide (Fig. 6A). Nevertheless, it has to be noted that there is also a difference between isotonic medium containing iodide (iso + I^-) and iodide-free isotonic medium (iso w/o) (Fig. 6A). This is indicative of an iodide conductor that is open under non-swollen conditions and is thus not likely to be identical to VRAC. Although this conductance may also contribute to the swelling-induced iodide influx, the difference between the hypo + I^- and the iso + I^- is sufficient to provide a robust read-out for a screening approach. Live-cell imaging experiments in a 3.5 cm dish format as used for these preliminary measurements are, however, not suitable for a high-throughput screen. For this reason the read-out assay had to be transferred to an imaging system that would be able to record the fluorescence in a 384-well plate format, since the genome-wide siRNA library at the FMP Screening Unit is distributed in this format. We first tested this using a Safire II plate reader with a 96-well plate to see if detection thresholds would be sufficient to resolve the difference between iso and hypo curves. As shown in Fig. 6B the three conditions are very well separated, when measuring only a few wells for each condition. Although the tested plate reader can also be used in a 384-well format, it measures all wells of a plate consecutively (like all available photomultiplier plate readers), which results in a substantial delay from the first to the last well on a single plate. Furthermore, this delay increases the interval between time points that can be measured for each well. These two disadvantages of the plate reader system would lead to a loss of crucial kinetics data that is needed in order to access subtle changes in VRAC activity. Since siRNA knockdown does not always suppress the expression of a protein completely, it can be expected that the iodide influx would only be slowed down and not fully abolished by a specific siRNA treatment. Additionally, we were hoping to also identify proteins involved in the signal transduction leading to VRAC activation, which would also rather affect the kinetics than the absolute YFP quenching. We therefore went on to test yet another imaging system, called fluoremetic imaging plate reader (FLIPR^{TM}). This apparatus uses a CCD camera to monitor all wells of a 384-well plate simultaneously. Besides this, it is equipped with a pipetting head allowing for a pipetting step adding the hypotonic solution in parallel to the fluorescence measurements. As shown in Fig. 6C, the curves for the different conditions (hypotonic and isotonic solution

with and without iodide) are nicely seperated even when measuring many wells for the same condition and the absolute response over the whole 384-well plate displays little variance when applying just one condition (Fig. 6D). With this uniformity test of the quenching response over the whole plate we could also exclude so called “edge effects” than can occur on the boundary wells of a multi-well plate.

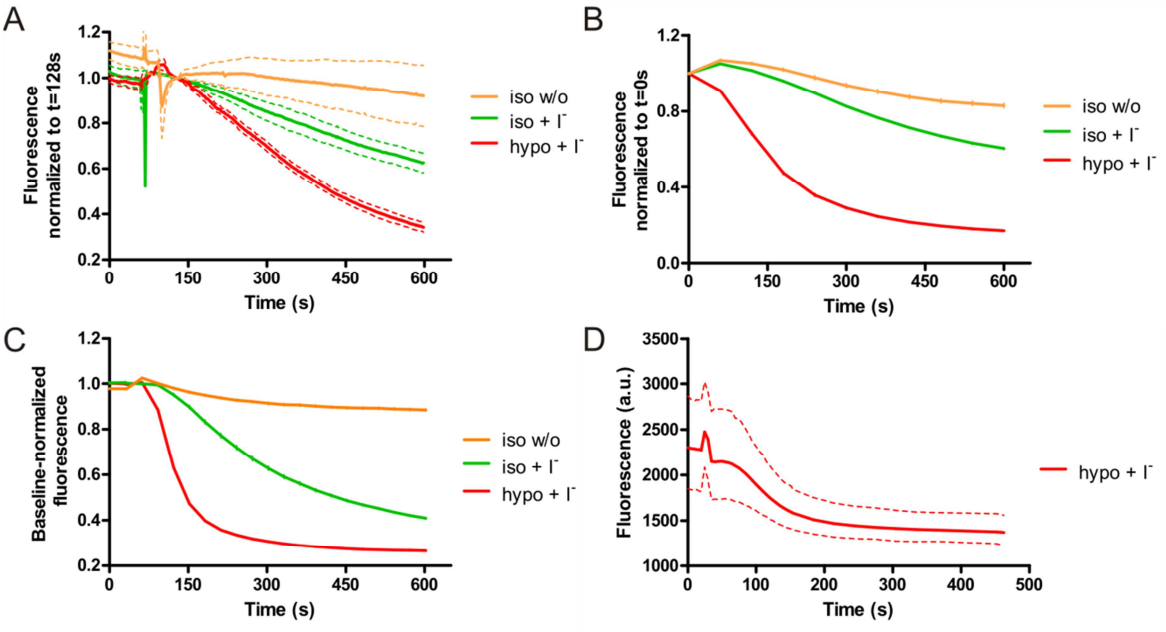

Figure 6: Example fluorescence traces of different imaging methods used for the assay set-up
A: Example traces from a live-cell imaging experiment, traces averaged from separate experiments, n=2 for each condition. **B**: Example traces from a plate reader experiment, traces averaged from single wells of a 96-well plate, n=12 for each condition. **C**: Example traces from a FLIPR^{TM} experiment, normalized to fluorescence at ~30 to 50 s, traces averaged from single wells of a 384-well plate, treated with iodide-containing isotonic saline (n=26), hypotonic saline (n=30) or iodide-free isotonic saline (n=25). **A-C**: Error bars, SEM. **D**: Homogeneity test for all wells of the 384-well plate with hypotonic saline. Average absolute fluorescence over all wells, dotted line indicates minimal and maximal values.

As an additional proof of principle experiment, we tested the effect of carbenoxolone in our YFP assay. Carbenoxolone had been shown previously to inhibit VRAC activity (Benfenati et al., 2009). As shown in Fig. 7A the curve for hypotonic saline is shifted to the level of isotonic treatment when 100 µM carbenoxolone are added to the solution. This shows that VRAC inhibition indeed influences the iodide-influx under hypotonic conditions. The isotonic curve on the other hand is not shifted, indicating that the protein(s) mediating the iodide influx under non-swollen conditions is/are not sensitive to carbenoxolone. In previous experiments on the Safire II Plate Reader we had already observed that two other known inhibitors of VRAC, the rather unspecific chloride channel inhibitor DIDS and the most selective available VRAC inhibitor DCPIB, had similar effects on the hypotonicity-induced iodide influx (Fig. 7B and C). However, they both

also affected the iodide influx under isotonic conditions. While DIDS also inhibited the iodide-influx under non-swelling conditions (Fig. 7B), DCPIB seemed had a rather unexpected, activating effect, shifting the curve to the left, thus representing an increased iodide influx (Fig. 7C). Taken together, these results show that the assay is sensitive to VRAC inhibition and thus will reflect reliably the effects of siRNAs that would lead to a reduction in overall iodide flux through VRAC. Besides this, the results highlight once more the difficulties resulting from the lack of specific VRAC inhibitors and the need of the molecular identification of this channel, since pharmacological experiments will always be limited by the "side-effects" many of these compounds exert on other channels and transporters.

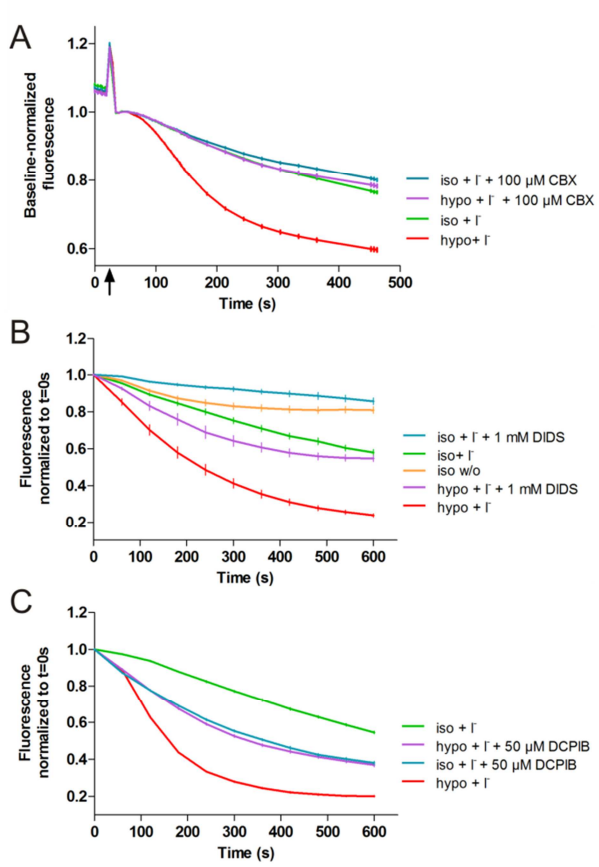

Figure 7: VRAC pharmacology in the YFP quenching assay
A: FLIPR^{TM} experiment using the VRAC and gap-junction inhibitor carbenoxolone (CBX). Carbenoxolone was included in the iodide-containing solution and added at the time point indicated by arrow. Signals were normalized to the fluorescence at ~30 to 50 s, traces averaged from n=24 wells per condition. **B**: Plate reader experiment using the chloride channel inhibitor DIDS. Traces were averaged from n=35 wells for hypotonic, n=23 for each isotonic condition and n=19 for hypotonic saline containing DIDS and n=11 for isotonic saline containing DIDS. **C**: Plate reader experiment using the VRAC inhibitor DCPIB. Traces were averaged from n=12 wells for each condition. Error bars, SEM.

Besides the read-out assay, other elements of the screening procedure also needed to be optimized and adapted to the high-throughput format. A critical step was the preparation of the cells for the fluorescence measurement in the FLIPR^{TM}. For this, the cell culture medium had to be removed and replaced by an isotonic imaging solution in a manner that would not lead to cell loss. Since HEK cells are not very tightly adherent and can easily be detached from culture plate surfaces, numerous experiments were necessary to optimize the pipetting protocol at the Tecan Freedom EVO 200 workstation (data not

shown). Both the pipetting speed as well as the pipetting height had to be adapted, resulting in a protocol that provided minimal to no cell loss during medium exchange. The integrity of the cell layer can be observed in the photographs taken by the FLIPR^{TM} during measurements (Fig. 9C).

Another important parameter was the initial plating cell number, which needed to be optimized in order to meet two essential criteria: maximal transfection efficiency and optimal density for measurement of the iodide-dependent quenching of YFP at t=72 h after transfection. Several experiments performed by Katina Lazarow of the FMP Screening Unit and myself resulted in the optimal plating cell number of 6000 cells/well (data not shown).

4.2. Prescreen

Before starting the genome-wide siRNA screen we tested some of the previous candidate proteins in our assay. We also included some other channels and transporters, among them members of the rather recently identified protein family of anoctamins. Furthermore, we tested whether other anion exchangers and potassium/chloride cotransporters contributed to the iodide influx, either under swollen or non-swollen conditions. To this end, we transfected smartpool siRNAs against the genes listed in Table 7 into the HEK YFP cell line and performed the YFP assay at the FLIPR^{TM}. As shown in Fig. 8 only the siRNA against the anion exchanger AE2 showed a significant effect. Interestingly, treatment with this smartpool siRNA strongly reduced the slope of the quenching curve, not only under hypotonic, but also under isotonic conditions. This indicates that AE2 contributes to the swelling-independent iodide influx observed previously (see section 4.1). Since the AE2 siRNA showed this robust and clearly distinguishable effect we decided to use this as an assay-specific positive control for transfection efficiency in the genome-wide siRNA screen.

Table 7: List of anion transporters tested in the FLIPR™ prescreen.

Gene name	Alternative name(s)	Proposed function
ANO1	Anoctamin1, TMEM16A	Ca^{2+}-activated Cl^- channel
ANO3	Anoctamin3, TMEM16C	Ca^{2+}-activated Cl^- channel (?)
ANO4	Anoctamin4, TMEM16D	Ca^{2+}-activated Cl^- channel (?)
ANO5	Anoctamin5, TMEM16E	Ca^{2+}-activated Cl^- channel (?)
ANO6	Anoctamin6, TMEM16F	Ca^{2+}-activated Cl^- or cation channel, scramblase
ANO7	Anoctamin7, TMEM16G	Ca^{2+}-activated Cl^- channel (?)
ANO8	Anoctamin8, TMEM16H	Ca^{2+}-activated Cl^- channel (?)
ANO9	Anoctamin9, TMEM16J	Ca^{2+}-activated Cl^- channel (?)
ANO10	Anoctamin10, TMEM16K	Ca^{2+}-activated Cl^- channel (?)
CLCN3	ClC-3	Cl^-/H^+-exchanger, wrongly claimed to be VRAC
BEST1	Bestrophin 1	Ca^{2+}-activated Cl^- channel
BEST2	Bestrophin 2	Ca^{2+}-activated Cl^- channel
SLC4A2	AE2, anion exchanger 2	Cl^-/HCO_3^- exchanger
SLC4A3	AE3, anion exchanger 3	Cl^-/HCO_3^- exchanger
SLC12A2	NKCC1	NaK2Cl cotransporter
SLC12A4	KCC1	KCl cotransporter
SLC12A6	KCC3	KCl cotransporter
SLC12A7	KCC4	KCl cotransporter
SLC26A1	SAT1	anion exchanger, sulfate transporter
SLC26A9		anion transporter
SLC26A11	KBAT	Na^+-dependent sulfate transporter, Cl^- channel (?)

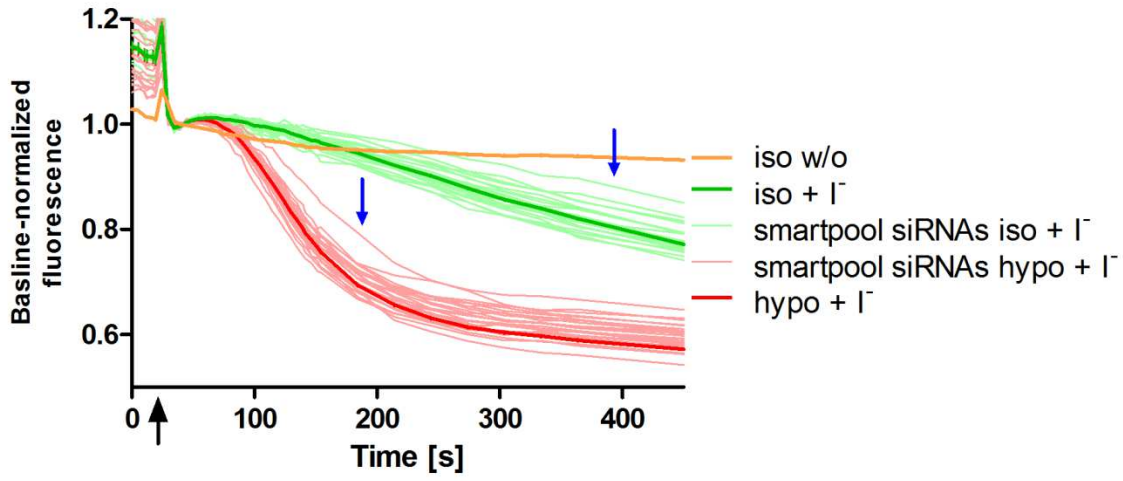

Figure 8: Prescreen FLIPR ™ data
Fluorescence trace from a FLIPR™ experiment including individual traces for wells transfected with the smartpool siRNAs against the prescreen candidate genes and averaged traces for wells, where hypotonic (hypo; 229 mOsm) or isotonic (iso; 329 mOsm) saline with ($+I^-$) or without (w/o) iodide (each condition n=32; error bars, SEM) was added. Blue arrows indicate the traces for the smartpool siRNA against the anion exchanger AE2. The black arrow indicates the timepoint of saline addition.

4.3 Genome-wide siRNA screen

The primary genome-wide siRNA screen was performed by testing the complete Ambion Silencer® Human Genome siRNA Library V3 (Life Technologies) in the FLIPR^{TM}-based YFP assay. To this end, we performed two consecutive screening rounds, with each round containing 189 384-well plates and each gene being targeted by three independently placed siRNAs. As described in section 3.2.2 we included several control siRNAs on each screening plate to assess the quality and consistency of the transfection efficiency and assay performance. As illustrated in Fig. 8 and Fig. 9A the siRNA against AE2 served as a good assay-specific control for both the hypotonic and the isotonic condition. The traces for the scrambled siRNA control show that the siRNA transfection itself does not influence VRAC activity or disturb the read-out assay (Fig. 9A and B). In Fig 9B, the unnormalized fluorescence traces show the effect of the siRNA against YFP, which reduced the fluorescence signal of the cells to background levels. Likewise, the curves for the wells treated with cell death-inducing siRNA also showed only a background fluorescence signal. For these wells the difference between hypotonic and isotonic treatment were not detectable anymore. These two controls were mainly used to assess transfection efficiency on every individual screening plate. The results confirmed that none of the 384-well plates had to be discarded because of low transfection efficiency.

Furthermore, in Fig 9B the Triton X addition leads to a complete quenching of the YFP fluorescence after the pipetting step. This background fluorescence of the Triton X-treated wells was used in the subsequent analysis for background subtraction. The different controls are also clearly visualized in the FLIPR^{TM} photographs (shown inverted in Fig. 9C), where the wells for the siRNA against YFP and the cell death- inducing siRNA show very low signals at the beginning of the measurement (Fig. 9C, column 23 and 24, wells G-H), while the isotonic controls in general have a stronger remaining signal at the end of the measurement due to less iodide influx (Fig 9C, row 24).

When displaying the control wells in a heatmap for the Z-score of the maximal quenching slope S_{max} (Fig. 10D) they can also be clearly distinguished by their color pattern.

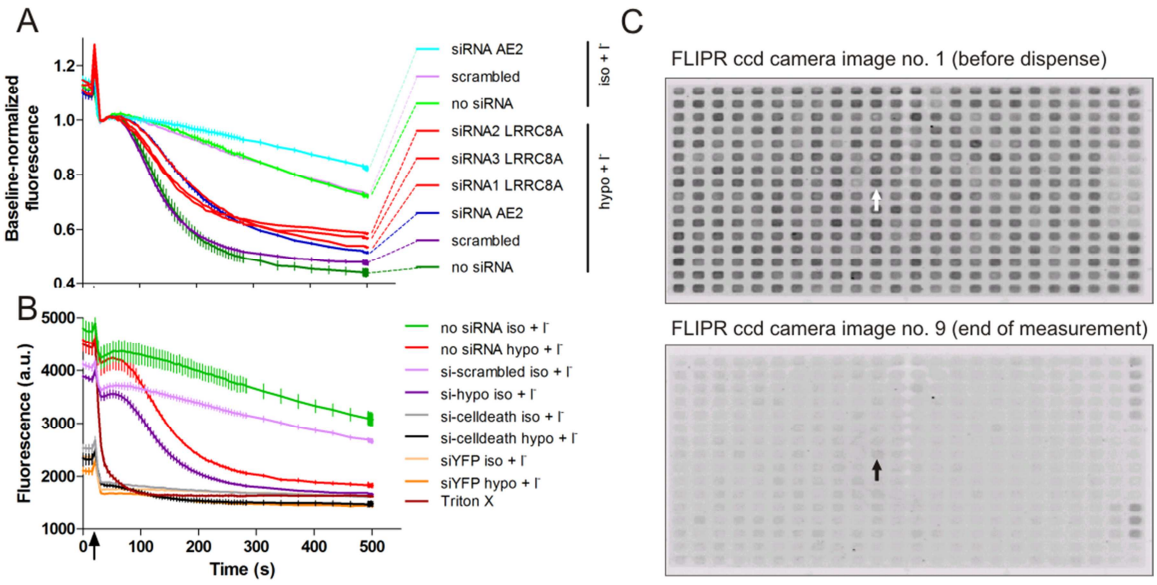

Figure 9: Example fluorescence traces and assay plate from the genome-wide siRNA screen
A: Example traces, normalized to fluorescence at ~30 to 50 s. Traces averaged from wells treated with control siRNAs (scrambled, AE2, both n=3) and no siRNA (n=2) (error bars, SEM), and individual traces from wells singly transfected with the three siRNAs against LRRC8A. Except for LRRC8A siRNA2 and 3, all traces are from the same plate. **B**: Example traces, unnormalized fluorescence signal as recorded by the FLIPR^{TM}. Traces averaged from wells treated with control siRNAs (YFP, cell death-inducing, scrambled, both n=3) and no siRNA (n=2) and Triton X- treated wells (n=4) (error bars, SEM). Arrows indicate addition of I^--containing hypotonic (hypo; 229 mOsm) or isotonic (iso; 329 mOsm) saline. **C**: Photograph (inverted) of YFP fluorescence of an entire plate before the pipetting step (top) and at the end of the experiment (below). Note that fluorescence of cells treated with siRNA against YFP and cell death-inducing siRNA is strongly reduced at the beginning of the experiment (top), (transfection control). At the end of the experiment (bottom), fluorescence has remained strong in wells remaining in isotonic solution throughout. Arrows indicate well H11 containing cells transfected with the most efficient siRNA against LRRC8A.

When comparing the two replicate screens, the effects of individual siRNAs on the respective Z-scores of S_{max} correlate reasonably well. A comparison between Fig. 10A and Fig. 10B shows the efficiency of our warning flag for low starting fluorescence, since many of the outliers disappear when we correct for wells that were marked for low cell number.

As explained in section 3.2.5 our primary criterion for hit definition was the Z-score of the maximal slope of YFP quenching S_{max}. By calculating the mean over the two replicate screens of the mean Z-score for the two best siRNAs for this value, we created a hitlist that was sorted by this parameter and was subsequently submitted to further examination. As expected, many of the hits could be ruled out by one or more criteria. For instance, siRNAs against several ribosomal proteins led to large Z-scores that were caused by poor cell growth or cell death as indicated by the 'low cell' flag. When large Z-scores were not reproduced in the replicate screen, these hits could sometimes be discarded by examining

the photographs of the plates, which showed dirt at the respective well that had caused high background fluorescence.

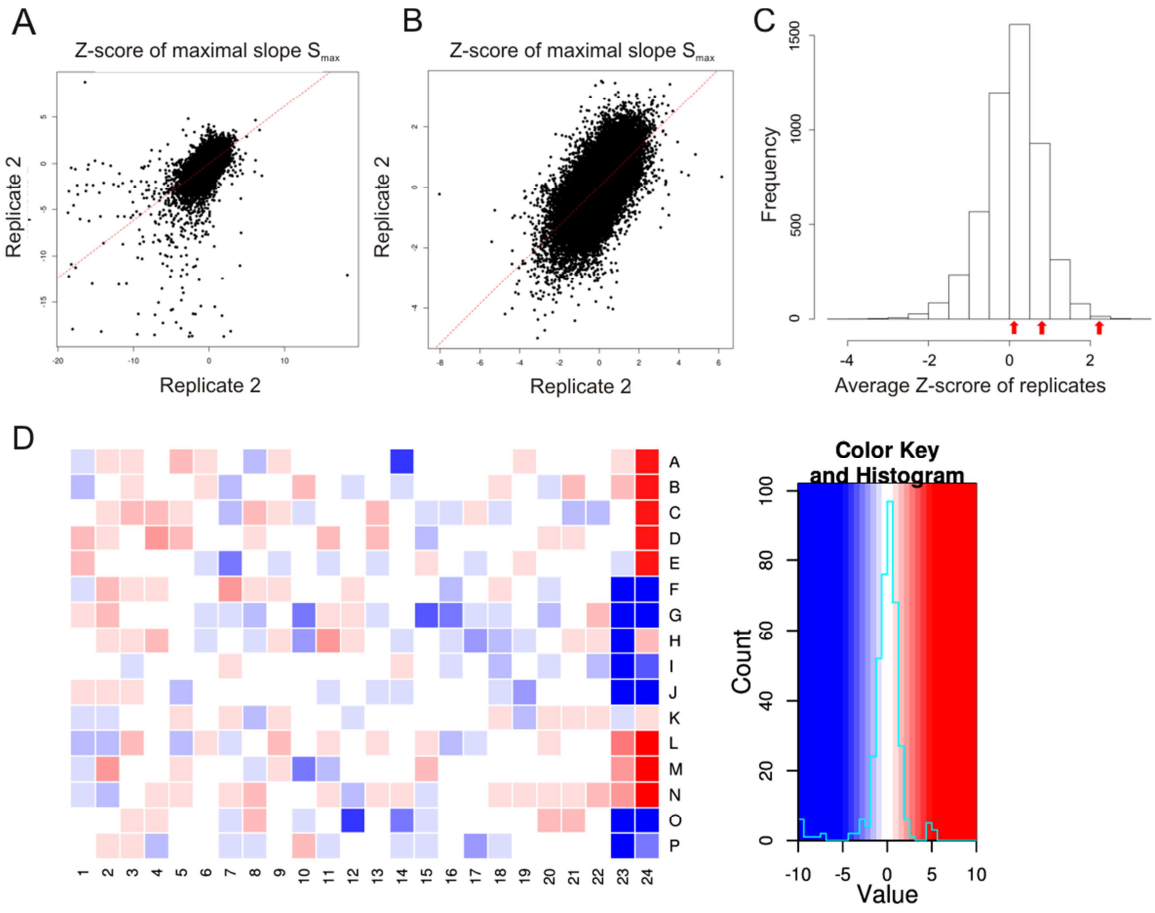

Figure 10: Bioinformatics analysis of the genome-wide siRNA screen performance
A and **B**: Fidelity of replicate screens. Correlation of Z-scores of maximal slope S_{max} between the original and the replicate screen observed with all 65,061 siRNAs (**A**) and after filtering out those measurements that were flagged for low cell number or did not reach near-steady-state fluorescence by the end of the measurement (**B**). Z-scores from screen 1 and screen 2 are plotted on the x- and y-axis, respectively. The Pearson correlation coefficient (r=0.62 and r=0.65, respectively) indicates positive correlation between replicate screens. The regression line from simple linear regression is shown as a dashed red line. The elimination of outliers demonstrated the usefulness of the warning flags. **C**: Histogram of Z-scores for maximal slope (S_{max}) from the genome-wide siRNA screen. Measurements which were flagged for low cell number or did not reach steady state fluorescence by the end of measurement were filtered out, resulting in values for 50258 siRNAs. The averaged Z-scores from screen 1 and screen 2 are plotted. Arrows indicate the Z-scores of three individual siRNAs against *LRRC8A* (0.125, 0.809 and 2.217). **D**: Heat map of a screening plate containing the most effective siRNA1 against *LRRC8A* on position H11. Z-scores for S_{max} are displayed using the color scale shown at right.

The *LRRC8A* gene, that subsequently became the prime candidate after the secondary screen (see section 4.4) was located at position 222 of our genome-wide S_{max} hitlist. Interestingly, only one of the three independent siRNAs for *LRRC8A* gave a Z-score of ~2 and is therefore in the top group, when looking at the overall distribution of Z-scores (Fig. 10C). Accordingly, when looking at the single traces for the three siRNAs against LRRC8A, siRNA1 shows the most prominent shift in the quenching curve, similar to the

effect of the AE2 control siRNA (Fig. 9A). This siRNA is also clearly visible by a strong red color in the heatmap of the respective screening plate at position H11 (Fig.10D).

4.4 Secondary screen

From the S_{max} hitlist that resulted from the data of the primary screen we defined 87 candidate genes for a secondary screen (Table 8), in order to examine them again in the YFP FLIPR^{TM} assay using independent smartpool siRNAs (pools of 4 siRNAs against one target gene). For the selection of these candidate genes, different criteria were applied. As we were primarily looking for the channel itself instead of proteins involved in the signal transduction leading to activation of VRAC, we limited our search to proteins having at least one predicted transmembrane domain. Many candidates could also be discarded due to their well-established function or their inclusion in well-known gene families like olfactory receptors or other G-protein coupled receptors. However, we also included some candidates that had already been connected to a certain function and thus appeared to be incompatible with VRAC, since annotations are not always reliable and proteins may serve more than one function. As VRAC currents have been observed in every mammalian tissue that has been investigated, we excluded candidates that showed a narrow tissue distribution or very low expression levels as indicated by NCBI EST profile databases or the scientific literature, except when they belonged to a gene family whose overlapping expression pattern covered many tissues.

Among the 87 genes tested, only *LRRC8A* could be confirmed as very prominent candidate, since the siRNA pool against it showed a strong effect on the VRAC mediated YFP quenching (Fig.11). With this siRNA pool, the elicited effect was even stronger than the best siRNA from the primary genome-wide screen and shifted the slope of the curve more than the AE2 positive control. We also tested the effect of the 87 candidate siRNA pools under isoosmolar conditions, but the curves did not differ significantly from the isotonic controls (data only shown for LRRC8A, Fig.11).

Table 8: List of candidate genes for the secondary screen

	Gene ID	Gene symbol	TMDs*	Z-score†		Gene ID	Gene symbol	TMDs*	Z-score†
1	3371	TNC	1	2.6931	45	51338	MS4A4A	4	1.3255
2	79652	TMEM204	4	2.3119	46	92255	DKFZp434H2226	9	1.3153
3	253558	ALCAT1	3	2.1069	47	79762	FLJ14146	1	1.3139
4	54879	ST7L	2	1.9163	48	159371	TMEM20	10	1.3091
5	5793	PTPRG	1	1.8685	49	79683	ZDHHC14	4	1.3016
6	28959	LR8 / TMEM176B	4	1.8351	50	65062	ALS2CR4	4	1.2954
7	51234	EMC4	2	1.7410	51	79844	ZDHHC11	5	1.2780
8	10098	TM4SF9/TSPAN5	4	1.7358	52	10100	TSPAN-2	4	1.2743
9	125111	GJC1/GJD3	4	1.7326	53	123606	NIPA1	8	1.2581
10	29940	SART2	3	1.6643	54	55362	TMEM63B	11	1.2448
11	284723	SLC25A34	2	1.6399	55	124491	TMEM170A	3	1.2369
12	130814	PQLC3	4	1.6306	56	56674	TMEM9B	2	1.2335
13	23505	RW1/TMEM131	2	1.6096	57	94015	TTYH2	6	1.2300
14	199953	TMEM201	6	1.5948	58	203562	TMEM31	2	1.2116
15	80759	KHDC1	2	1.5846	59	27069	GHITM	6	1.2099
16	9415	FADS2	4	1.5817	60	26526	TM4-B	3	1.1928
17	57484	RNF150	2	1.5569	61	81671	VMP1	6	1.1703
18	54741	OBRGRP	4	1.5488	62	374882	TMEM205	4	1.1329
19	5348	FXYD1	1	1.5477	63	10712	Fam189B	4	1.1222
20	56172	ANKH	8	1.5316	64	85414	Prostein/SLC45A3	11	1.1208
21	4034	LRCH4	1	1.5303	65	91147	TMEM67	4	1.1122
22	57198	ATP8B2	9	1.5268	66	57348	TTYH1	5	1.0725
23	53346	TM6SF1	9	1.5216	67	128506	OCSTAMP	6	1.0707
24	120224	TMEM45B	5	1.5205	68	55852	TEX2	2	1.0702
25	**56262**	**LRRC8A**	**4**	**1.5129**	69	93109	TMEM44	4	1.0630
26	10959	RNP24	2	1.4911	70	11161	C14orf1	4	1.0598
27	79022	TMEM106C	2	1.4885	71	64137	ABCG4	7	1.0392
28	349149	GJE1/GJC3	3	1.4769	72	29097	HSPC163	3	1.0315
29	746	TMEM258	2	1.4751	73	55625	ZDHHC7	4	1.0268
30	53827	FXYD5	1	1.4684	74	64429	ZDHHC6	4	1.0165
31	55009	C19orf24	2	1.4654	75	54860	MS4A12	4	1.0130
32	29058	C20orf30	2	1.4566	76	162427	FAM134C	3	1.0120
33	10099	TM4SF8/ TSPAN3	4	1.4361	77	23460	ABCA6	13	1.0099
34	54929	TMEM161A	8	1.4268	78	9906	SLC35E2	3	0.9891
35	84561	SLC12A8	10	1.4140	79	64645	HIAT1	12	0.9848
36	113829	SLC35A4	9	1.4016	80	345274	SOAT/SLC10A6	8	0.9758
37	29956	LASS2	5	1.3728	81	347735	TDE2L/SERINC2	11	0.9695
38	145407	C14orf37	2	1.3710	82	55002	TMCO3	10	0.9674
39	51522	TMEM14C	4	1.3670	83	202915	TMEM184A	7	0.9488
40	55739	FLJ10769	1	1.3656	84	8082	SSPN	4	0.9236
41	284099	C17orf78	1	1.3551	85	84548	FAM11A/TMEM185A	8	0.9025
42	81555	SMAP-5	4	1.3487	86	135656	DPCR1	2	0.8911
43	57181	SLC39A10	7	1.3480	87	85013	TMEM128	4	0.7763
44	7355	SLC35A2	8	1.3401					

*predicted number of transmembrane domains

†mean Z-score for S_{max} of the two 'best' siRNAs from 2 replicate primary screens

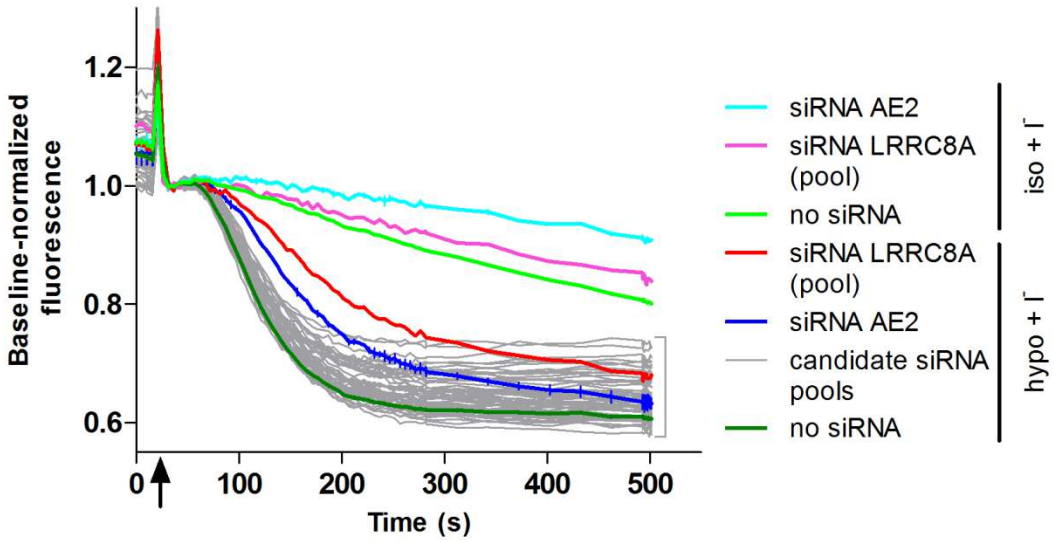

Figure 11: Fluorescence traces from secondary screen using independent smartpool siRNAs
All candidate traces are shown in grey, only the trace from the well transfected with the smartpool siRNAs against LRRC8A is shown separately in red. Averaged control traces from wells treated with control siRNAs against AE2 (n=3) and no siRNA (n=2). Arrow indicates addition of iodide-containing hypotonic (hypo; 229 mOsm) or isotonic (iso; 329 mOsm) saline. Error bars, SEM.

4.5 Electrophysiological measurements of LRRC8A knockdown and overexpression

After the encouraging results of the YFP quenching assay in the secondary screen we wanted to test whether the siRNA treatment would have similar effects on VRAC currents measured in whole-cell patch-clamp experiments. So far we had only measured VRAC activity indirectly by examining the iodide-mediated YFP quenching upon hypotonic stimulation. The effect of the siRNA against *LRRC8A* could theoretically have been the result of a decrease in VRAC-independent iodide influx. In order to verify that the decreased iodide influx we observed in the FLIPR experiments reflects a decrease in VRAC currents it was necessary to electrophysiologically monitor $I_{Cl(swell)}$ in siRNA-transfected cells. As shown in Fig. 12 the siRNA mediated knockdown of LRRC8A in HEK cells abolishes the swelling-activated chloride current almost completely.

As a next step to verify a role of LRRC8A in VRAC activity, we cloned the cDNA for *LRRC8A* from HEK cDNA and expressed a GFP-tagged version of the gene in wildtype HEK cells. The cells were again measured in the whole-cell configuration and stimulated with hypotonicity to induce cell swelling. Surprisingly the overexpression of LRRC8A did not result in larger VRAC currents, but did actually decrease the current in a similar manner as the siRNA knockdown (Fig.12). Although unexpected, these results suggested an important role of LRRC8A in VRAC activation. Due to the fact that LRRC8A is a

member of a protein family that is related to pannexins, which have been shown to form hexameric heteromers, we hypothesized that also LRRC8 proteins might be able to heteromerize. In this case the overexpression of just one subunit could lead to a stoichiometry that is incompatible with channel activity, which might explain the suppressive effect observed upon overexpression of LRRC8A. We tested this hypothesis first by expressing LRRC8A together with one of the other members of the protein family, LRR8C. This combination indeed did not show the suppression effect observed previously and yielded wildtype-like currents (Fig.12). Nevertheless, we could not observe larger currents than in the wildtype situation indicating that another factor, such as a regulatory element or an additional subunit, is limiting the current amplitude.

(The electrophysiological measurements were performed by Florian Ullrich and Jonas Münch.)

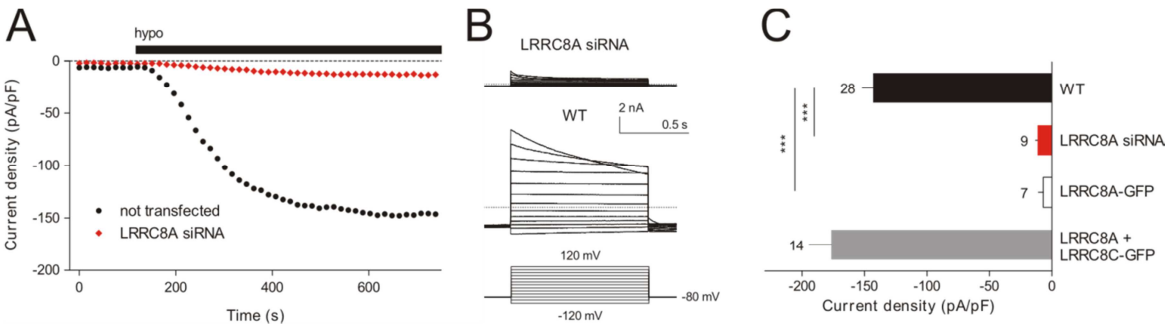

Figure 12: $I_{Cl(swell)}$ of HEK293 cells with siRNA mediated knockdown or overexpression of LRRC8A
A: Typical time course of VRAC activation in WT or LRRC8A siRNA-treated HEK cells. Current densities at -80 mV are shown. The black bar indicates application of hypotonic (hypo) saline (240 mOsm). **B**: Current traces of fully activated $I_{Cl(swell)}$ measured with the voltage protocol shown below. Dotted lines indicate zero current. **C**: $I_{Cl(swell)}$ amplitudes (at -80 mV) of WT HEK cells or cells treated with LRRC8A siRNA, or transfected with indicated LRRC8 cDNAs. Error bars, SEM; number of experiments is indicated; ***P < 0.001

4.6 Subcellular localization and trafficking of LRRC8 proteins

Since the localization to the plasma membrane is a prerequisite for the protein(s) constituting VRAC we tested LRRC8A and the other members of the LRRC8 protein family for their subcellular localization. We found that LRRC8A localized to the plasma membrane when heterologously expressed in HeLa cells (Fig. 13A) as well as under endogenous conditions, when probed with a specific LRRC8A antibody (Fig. 13B). The other family members, however, mainly localized to the ER when expressed individually (Fig. 13E-H). However, when expressing LRRC8B-E together with LRRC8A they are co-trafficked to the plasma membrane (Fig. 13I-L). This supports the hypothesis that LRRC8 proteins interact and may form heteromeric channel complexes in the plasma membrane.

We also tested the subcellular localization of a truncated version of LRRC8A, which corresponds to the protein present in a patient with agammaglobulinemia (Sawada et al., 2003). The truncation of the protein at position R719 leads to cytoplasmic retention (Fig.13D).

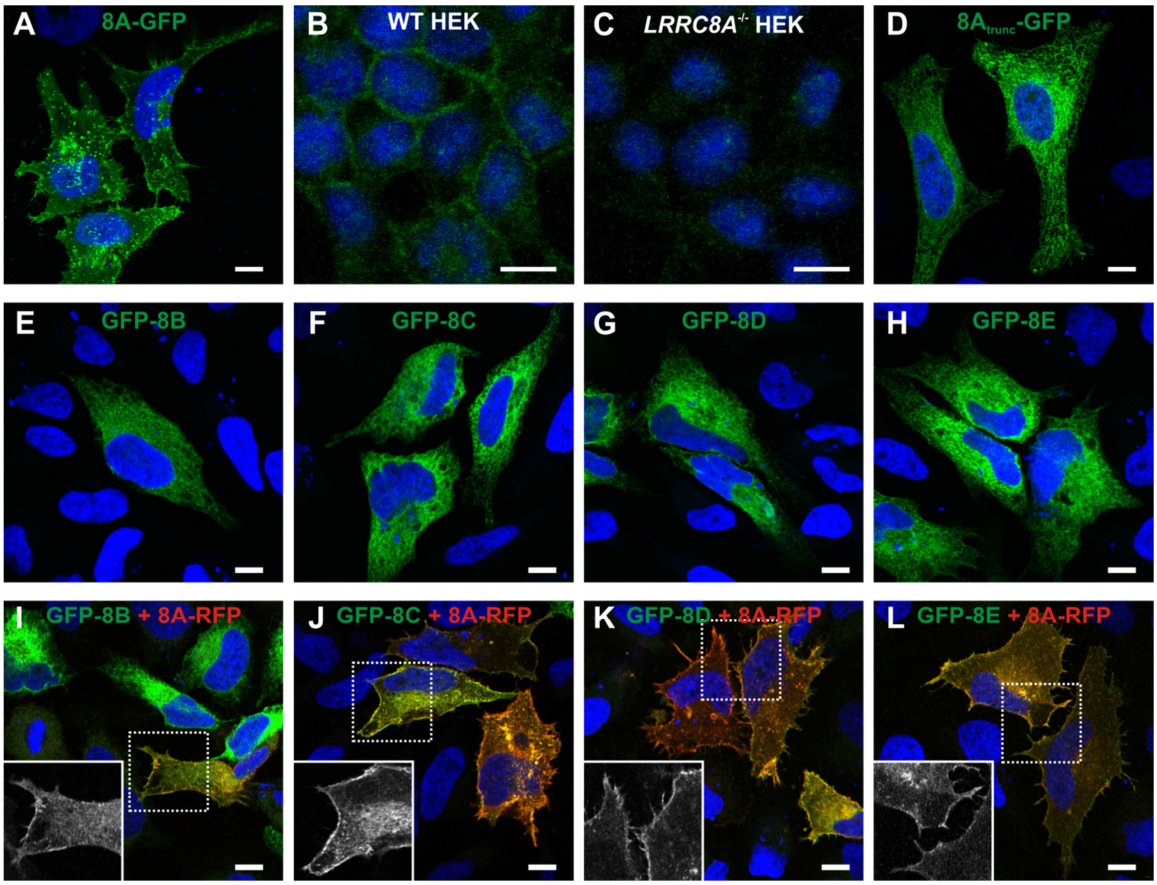

Figure 13: Subcellular localization of LRRC8 proteins
A: Plasma membrane localization of LRRC8A-GFP transfected into HeLa cells detected by GFP fluorescence. **B**: Endogenous LRRC8A detected at the plasma membrane of wildtype HEK cells by immunostaining with LRRC8A antibody. **C:** No LRRC8A signal in *LRRC8A*$^{-/-}$ HEK cells (clone 3E7). **D:** Truncated LRRC8A fused at R719 to GFP failed to reach the plasma membrane. **E-H:** Intracellular localization of LRRC8B-E when transfected alone. **I-L:** LRRC8B-E localize to the plasma membrane when co-transfected with LRRC8A. Insets, magnification of boxed areas exclusively show the GFP fluorescence signal. Scale bar, 10 µm for all panels.

4.7 Verification of the transmembrane topology of LRRC8A

As described in section 1.6, there had been controversial suggestions concerning the orientation of the LRRC8A protein in the plasma membrane. While one group proposed that the LRR-containing C-terminus of the protein is oriented towards the extracellular medium and may function as a receptor for ligand-binding (Sawada et al., 2003), Abascal and Zardoya (2012) suggested an opposing topology with the C-terminus protruding into the cytosol. We wanted to check these hypotheses by two different methods. First, we mutated two putative N-glycosylation sites (N66A, N83A) located in the loop between

the first two transmembrane domains of the protein to alanines (Fig. 14A). These sites can only be glycosylated if this loop is extracytosolic. Accordingly, one would expect a size shift of the protein upon degylcosylation by PNGase F treatment only if these sites are indeed glycosylated; and absence of the shift in the mutated version of the protein. As shown in Fig. 14B, a size shift is visible in the wildtype version of the protein (endogenously or transfected) that is not present in the mutant (N66A, N83A). The changed banding pattern of the mutant version of the protein suggests that there might be additional post-translational modifications that are disturbed or changed in the mutant.

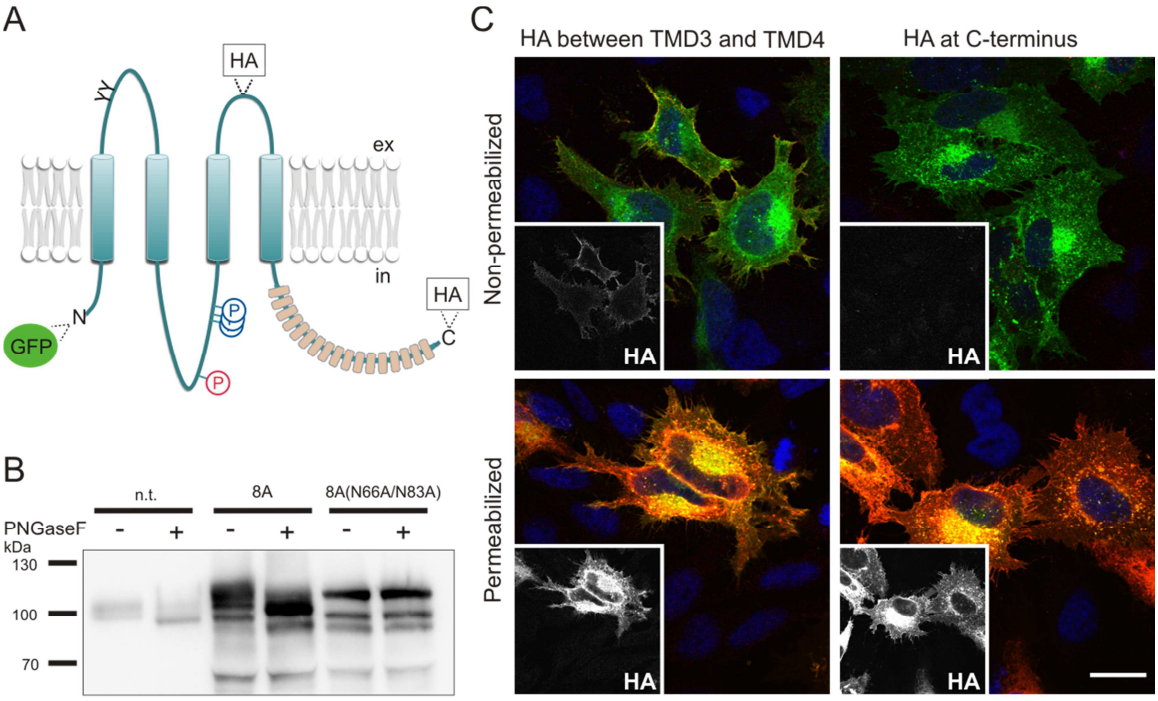

Figure 14: Transmembrane topology of LRRC8A
A: LRRC8 model (modified from Abascal and Zardoya, 2012). Four transmembrane domains precede a C-terminus with up to 17 leucine-rich repeats (orange). Phosphoserines in LRRC8A (red P) and LRRC8D (blue P), according to Uniprot (Magrane and Consortium, 2011), predicted N-linked glycosylation sites (Y), and added epitopes are indicated. B: PNGaseF treatment of endogenous LRRC8A and transfected LRRC8A decreased LRRC8A size in Western blots. This is not the case for lysate from cells transfected with LRRC8A$^{(N66A,N83A)}$ with disrupted glycosylation sites. The changed banding pattern of LRRC8A$^{(N66A,N83A)}$ suggests altered posttranslational modifications. n.t, not transfected. C: Immunofluorescence of non-permeabilized and permeabilized HeLa cells transfected with HA-tagged GFP-LRRC8A. Overlays of GFP (green) and HA (red) labeling. Insets show exclusively HA staining. Scale bar, 20 mm.

In a second approach, we inserted hemagglutinin (HA) tags either in the loop between transmembrane domains 3 and 4 or at the C-terminus in an N-terminally GFP-tagged version of the protein (Fig. 14A). We expressed these constructs in HeLa cells and immunostained for the HA tag, either under permeabilizing or non-permeabilizing conditions. As shown in Fig. 14C, the HA tag at the C-terminus is only accessible for the antibody after cell permeabilization, while the HA tag in the loop is clearly recognized

under both conditions, verifying that this loop is located at the extracellular side of the membrane. (The immunocytochemistry experiment was performed by Dr. Tobias Stauber.)

Taken together, these results confirm the topology suggested by Abascal and Zardoya (2012) with the LRR-containing C-terminus and also the N-terminus located towards the cytosol.

4.8 Heteromerization of LRRC8A with the other members of the LRRC8 protein family

In order to further investigate the hypothesis that LRRC8A might form heteromers with other members of the LRRC8 protein family we performed several co-immunoprecipitation experiments.

In a first approach we expressed a tagged version of LRRC8A together with a differently tagged version of each of the other family members and precipitated either with an antibody against the tag on LRRC8A or the tag of the other LRRC8 protein. As shown in Fig. 15 we could co-precipitate the different family members with LRRC8A and vice-versa. As a negative control we used vectors expressing the tag alone. Additionally, we tested the plasma membrane chloride channel ClC-1, which does not co-precipitate with LRRC8A (Fig. 15B). In general, we noted that LRRC8B and LRRC8D were poorly expressible both during these experiments as well as in transfections for electrophysiological measurements in HCT116 cells (see section 4.11).

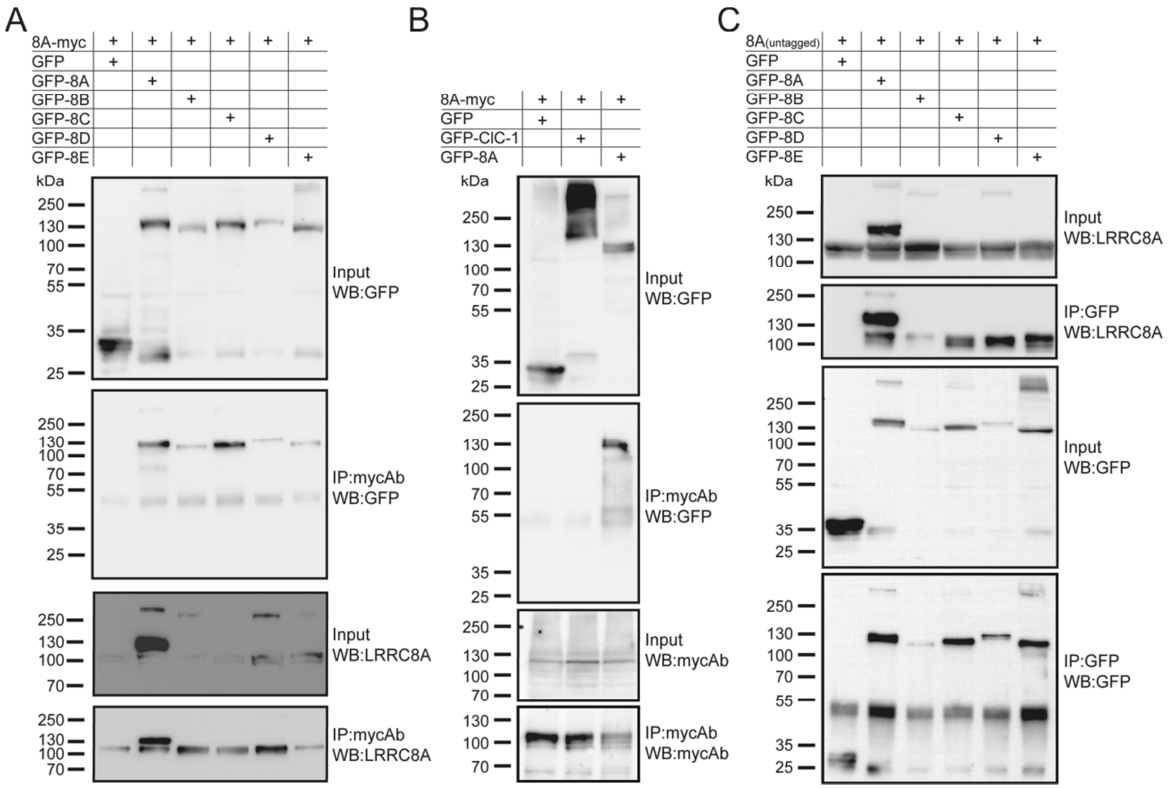

Figure 15: Co-immunoprecipitation with differentially tagged versions of LRRC8A and LRRC8B-E
A: Myc-tagged LRRC8A co-precipitated GFP-tagged LRRC8B-E in double-transfected HEK cells. LRRC8B and LRRC8D were poorly expressed. B: LRRC8A did not co-precipitate the ClC-1 Cl-channel. C: GFP-tagged LRRC8B through LRRC8E co-precipitated LRRC8A (untagged). Lysate equivalent to 20% of input was loaded as reference.

Secondly we precipitated LRRC8A from native HEK cells using our lab-generated antibody (see section 3.1.7). We then probed the precipitate for the other family members using specific antibodies. The same experiment was performed in parallel with a knockout cell line for LRRC8A. As shown in Fig. 16 all family members co-precipitate with LRRC8A in the wildtype but not in the knockout situation. We also included KCC1 as a negative control, which does not co-precipitate with LRRC8A. Besides the confirmation of the interaction by Western blot we also subjected the eluates from this experiment to analysis by mass spectrometry. Here we could also find peptides from all 5 family members strongly enriched in the wildtype sample (data not shown).

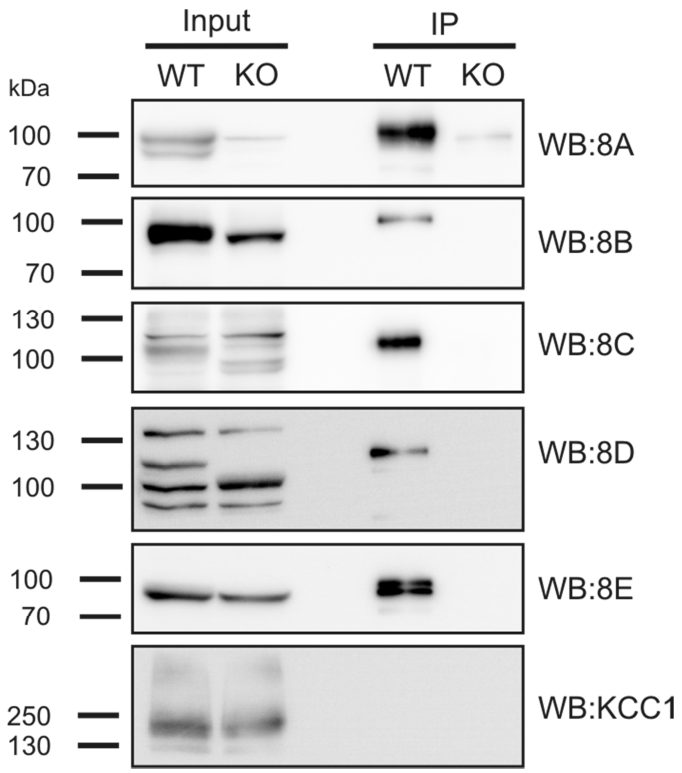

Figure 16: Co-immunoprecipitation experiment on native HEK cell lysate
LRRC8A was precipitated from native HEK cell lysate using the LRRC8A antibody. LRRC8B-E could be detected in the wildtype precipitate by Western blot using specific antibodies. As control the experiment was performed in parallel using the LRRC8A knockout HEK cell line 3E7. The plasma membrane ion transporter KCC1 (negative control) did not co-precipitate with LRRC8A. Lysate equivalent to 25% of input was loaded as reference.

4.9 Generation of LRRC8 knockout cell lines

In order to further investigate the role of LRRC8 heteromers in VRAC activity we aimed to generate knockout cell lines for the different LRRC8 proteins.

We did this first for LRRC8A using the zinc finger nuclease technology and in parallel used the newly developed CRISPR/Cas technology for genome-editing. In both cases we obtained knockout clones that were confirmed by sequencing and Western blot (Fig. 17 and Table 9). We used several targeting constructs directed against different genomic sites for the CRISPR/Cas approach to exclude off-target effect. We obtained knockout clones from 3 different CRISPR/Cas constructs and from the zinc finger nuclease that we further investigated by electrophysiological measurements (see section 4.10). For the generation of the knockout cell lines for LRRC8A, we used two different parent cell lines: The HEK YFP cell line used for the genome-wide siRNA screen and the human colon cancer cell line HCT116 that has the advantage of being stably diploid in contrast to the polyploid HEK cells.

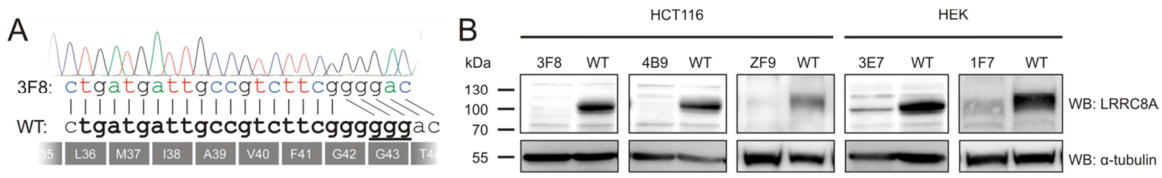

Figure 17: Confirmation of LRRC8A knockout clones
A: Example trace for the confirmation by genomic sequencing, site specific PCR followed by genomic sequencing of *LRRC8A*$^{-/-}$ HCT116 cell line 3F8 reveals a frameshift at G43 on both alleles. Guide sequence in bold, PAM sequence underlined. B: Western blots confirm LRRC8A disruption in mutant cell lines. First number in the knockout clone name indicates construct number (see Table 9). ZF9 is the zinc finger nuclease clone. α-tubulin was probed as loading control.

We then also aimed to generate knockout cell lines for the other LRRC8 family members LRRC8B-E. To this end, we again used several targeting constructs per gene. For these targetings we now exclusively used HCT116 cells, since a stable number of 2 alleles per genomic locus reduced the sequencing complexity. The clones used for further analysis in electrophysiology and other experimental procedures are summarized in Table 9.

For the generation of multiple knockout cell lines we used targeting constructs for different sites in parallel, but also did multiple targeting rounds when necessary.

In general, the cutting by the Cas9 nuclease and the following non-homologous repair mechanisms can lead to various different alterations in the genomic sequence. These alterations also occur independently on both (or all) alleles and thus different mutations for one genomic locus might occur per clone. Accordingly, we could also observe these variances in our knockout cell lines like duplications of nucleotides, deletion of a single nucleotide or larger regions and insertions of larger regions. All genomic alterations of our knockout cell lines are given in Table 9.

We identified all clones by genomic sequencing and confirmed them by Western blot using specific antibodies that we generated against all LRRC8 proteins. As shown in Fig. 18 some of these lab-generated antibodies give additional unspecific bands. Especially the antibodies for LRRC8C and LRRC8D show many unspecific bands at a similar height as the LRRC8 protein. The respective knockout cell line and the quintuple knockout (*LRRC8*$^{-/-}$) are however missing the specific band in both cases. Interestingly, the LRRC8A knockout leads to an alteration in the banding pattern of all the other LRRC8 proteins. For instance, LRRC8E appears as a double band in the wildtype probably representing an ER version and a post-ER (probably glycosylated) version of the protein. In the LRRC8A knockout, however, the upper band for LRRC8E is missing, indicating

that the protein might be retained in the ER. This agrees with our observations from the co-trafficking experiments with heterologously expressed proteins (Fig.13).

Similar alterations in the banding pattern are observed for all LRR8B-E proteins in the LRRC8A knockout.

The several different single and multiple knockout cell lines were then further examined using mainly electrophysiological methods. In this regard, the quintuple knockout cell line *LRRC8*$^{-/-}$ was of great use, since it served as an expression system where no remaining endogenous expression of the LRRC8 proteins could interfere with the channel composition.

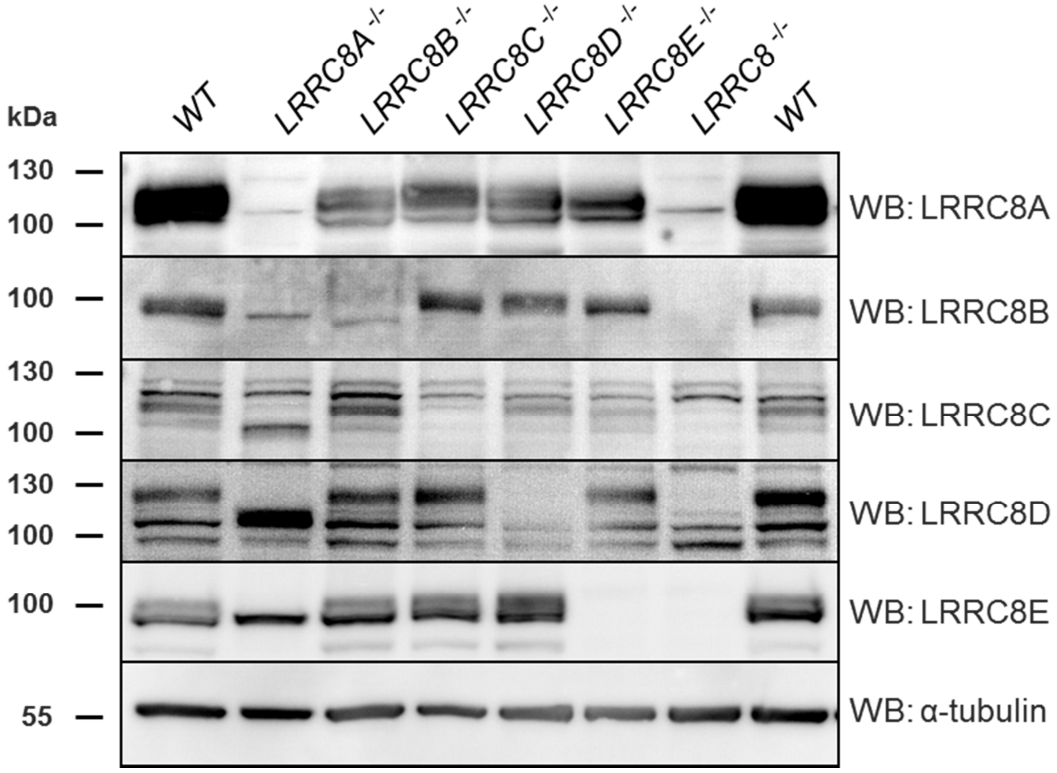

Figure 18: Western blot analysis of LRRC8 knockout cell lines
Western blot analysis of several LRRC8 knockout cell lines using the specific antibodies listed in Table 3. α-tubulin was probed as loading control.

Table 9: LRRC8 knockout cell lines

Cell line	Clone name	Construct *	Genetic modification	Protein modification
LRRC8A$^{-/-}$ (HEK)	3E7	3A	a1: Δ21nt (t110-a130) a2: insertion of 1 nt (t after c123)	**A1**: ΔM37-G43 in TMD1 (non- functional) **A2**: G42W-fs in TMD1
	1F7	1A	a1: Δ9nt (a958-g966) a2: Δ2nt (c965-g966) a3: Δ23nt (a958-g980)	**A1**: ΔI320-A322 at start of TMD4(non-functional) **A2**: A322V-fs at start of TMD4 **A3**: I320P-fs at start of TMD4
LRRC8A$^{-/-}$ (HCT116)	3F8	3A	Δ2g out of 6g (g124-g129)	G43D-fs in TMD1
	4B9	4A	a1: Δ32nt (c195-g226) a2: duplication of t206	**A1**: C65W-fs between TMD1 and TMD2 **A2**: R70P-fs between TMD1 and TMD2
	ZF9	ZFN	a1: Δ2nt (a508-c509) a2: insertion of 5nt (cacga after a511)	**A1**: T170E-fs between TMD2 and TMD3 **A2**: R171T-fs between TMD2 and TMD3
LRRC8B$^{-/-}$ (HCT116)	n2B-D3	2B	duplication of t446	E150R-fs after TMD2
LRRC8C$^{-/-}$ (HCT116)	n1C-C2	1C	duplication of t119	F41V-fs in TMD1
LRRC8D$^{-/-}$ (HCT116)	n1D-F11	1D	a1: Δ19nt (a325-t343) a2: duplication of a325	**D1**: P110L-fs between TMD1 and TMD2 **D2**: I109N-fs between TMD1 and TMD2
	n1D-B2	1D	duplication of a325	I109N-fs between TMD1 and TMD2
LRRC8E$^{-/-}$ (HCT116)	BCDE(WT)-F5	1E	duplication of a94	T32N-fs in TMD1
	CE(WT)-B6	1E	duplication of a94	T32N-fs in TMD1
LRRC8(D/E)$^{-/-}$ (HCT116)	nBCDE (WT)-G9	1D, 1E	D: duplication of a325	**D**: I109N-fs between TMD1 and TMD2
			E: duplication of a94	**E**: T32N-fs in TMD1
	nBCDE (WT)-B3	1D, 1E	D: duplication of a325	**D**: I109N-fs between TMD1 and TMD2
			E: duplication of a94	**E**: T32N-fs in TMD1
LRRC8(C/E)$^{-/-}$ (HCT116)	BCDE(WT)-F5+1C-D5	1C, 1E	C: a1: duplication of t119 a2: Δ5nt (c114-g118) and duplication of t119	**C1**: F41V-fs in TMD1 **C2**: G39C-fs in TMD1
			E: duplication of a94	**E**: T32N-fs in TMD1
LRRC8(C/D/E)$^{-/-}$ (HCT116)	nBCDE(WT)-H8	1C, 1D, 1E	C: 78nt (from a66 onwards) incl. splice acceptor site replaced by 13 nt (net Δ65nt)	**C**: W23R-fs at start of TMD1, before missing splice site
			D: a1: duplication of a325 a2: Δ11nt (g322-t332)	**D1**: I109N-fs between TMD1 and TMD2 **D2**: D108Q-fs between TMD1 and TMD2
			E: a1: duplication of a94 a2: Δ10nt (g87-c96)	**E1**: T32N-fs in TMD1 **E2**: Y30W-fs in TMD1
LRRC8(B/C/D/E)$^{-/-}$ (HCT116)	BCDE (WT2)-D2+2B-E8	2B,1C, 1D, 1E	B: a1: duplication of t446 a2: Δ2nt (c447-g448)	**B1**: E150R-fs after TMD2 **B2**: E150A-fs after TMD2
			C: duplication of t119	**C**: F41V-fs in TMD1
			D: duplication of a325	**D**: I109N-fs between TMD1 and TMD2
			E: Δ2nt (t92-c93)	**E**: L31H-fs in TMD1
LRRC8$^{-/-}$ (HCT116)	BC+DE (KO)D5+ 2B-G4	3A, 2B, 1B[§], 1C, 1D, 1E	A: Δ2g out of 6g (g124-g129)	**A**: G43D-fs in TMD1
			B: a1: duplication of t446 a2: Δ4nt (c447-g450)	**B1**: E150R-fs after TMD2 **B2**: E150I-fs after TMD2
			C: duplication of t119	**C**: F41V-fs in TMD1
			D: duplication of a325	**D**: I109N-fs between TMD1 and TMD2
			E: duplication of a94	**E**: T32N-fs in TMD1

a, allele (only given if alleles differed in modifications); fs, frameshift; nt, nucleotide; TMD, transmembrane domain; ZFN, zinc finger nuclease; Δ, deletion;
Indicated nucleotide numbers give nucleotide position within the ORF.
* For targeted guide sequences, see Table 5.
[§] Targeting with construct 1B in *LRRC8*$^{-/-}$ cell line resulted in a duplication of a1043 which would lead to A349G-fs after TMD4. However, the mutations by the 2B targeting truncate LRRC8B already after TMD2.

4.10 Electrophysiological measurements of LRRC8 knockout cell lines

In order to characterize the LRRC8A knockout cell lines that we generated from our HEK YFP cell line and HCT116 cells, we performed whole-cell patch clamp experiments. We quantified current amplitudes of $I_{Cl(swell)}$ (Fig. 19) and could show that the current is gone in all our LRRC8A knockout clones generated with different CRISPR/Cas constructs and a zinc finger nuclease (also see Table 9). We also tested whether we could rescue the knockout by heterologous expression of a GFP-tagged version of LRRC8A and indeed the current regained wildtype-like amplitudes in these experiments (Fig. 19).

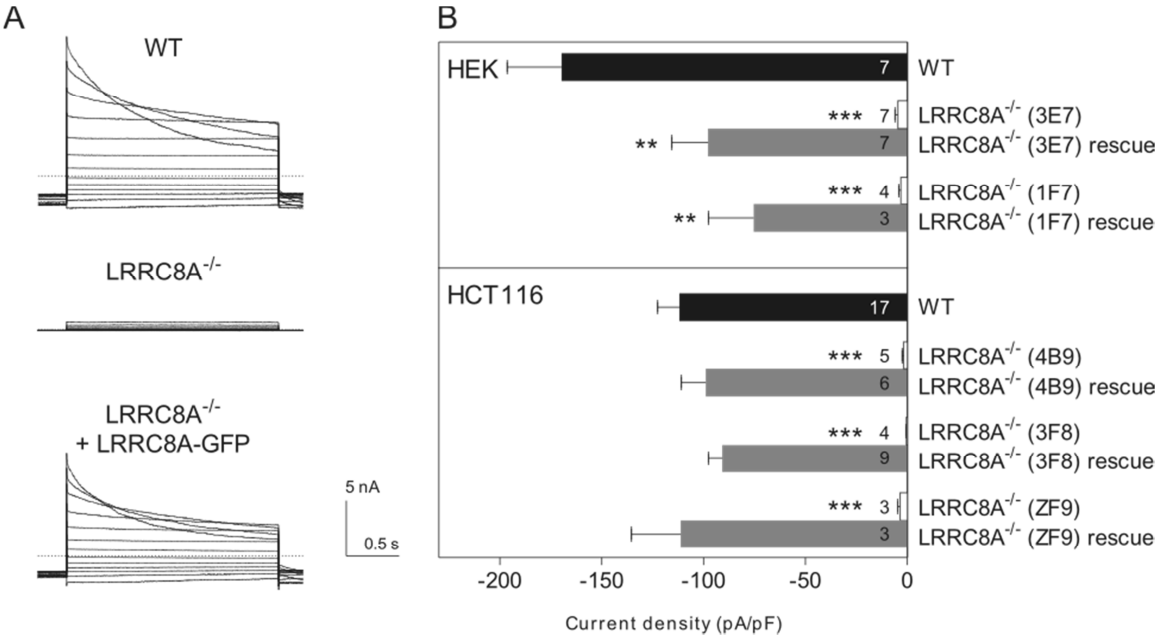

Figure 19: Electrophysiological characterization of LRRC8A knockout cell lines
A: Example $I_{Cl(swell)}$ traces (as in Fig. 12B, but 2-s pulses) of WT and mutant HEK cells (clone 3E7). When transfected into HEK *LRRC8A*$^{-/-}$ cells, LRRC8A rescues $I_{Cl(swell)}$. **B**: Amplitudes of maximally activated $I_{Cl(swell)}$ (at -80 mV) of WT HEK, WT HCT116 and different *LRRC8A*$^{-/-}$ cell lines, rescued by transfection of LRRC8A-GFP cDNA. Note that the amplitude of $I_{Cl(swell)}$ current was not fully rescued in HEK cells by LRRC8-GFP transfection, an observation that fits to the suppression of $I_{Cl(swell)}$ in native HEK cells by LRRC8A transfection (Fig. 12C). Mean currents ± SEM, number of measurements is indicated. **, $p<0.01$ and ***, $p<0.001$ compared to WT HEK or WT HCT116, respectively. For a description of the different knockout cell lines see Table 9.

In a next step we investigated $I_{Cl(swell)}$ in the other LRRC8 knockout cell lines we generated. It has to be noted that none of the other single knockouts of LRRC8B-E completely abolishes $I_{Cl(swell)}$ (Fig. 20). Hence, none of the LRRC8B-E proteins seems to be indispensable for VRAC activity. Nevertheless, the currents do not resemble the wildtype situation since inactivation kinetics are drastically changed in some of these mutant cell lines (Fig. 20 A and C). Especially the LRRC8C knockout leads to a considerably accelerated inactivation at positive potentials. The double knockout for LRRC8D and LRRC8E however decelerates the inactivation kinetics compared to

wildtype. This strongly points to an involvement of LRRC8 heteromers in the composition of the pore region of the channel, since regulatory elements are not likely to influence an intrinsic channel property such as the inactivation kinetics.

We also investigated a cell line where all LRRC8B-E proteins are missing. Interestingly, in this mutant $I_{Cl(swell)}$ is abolished completely, demonstrating that VRAC activity is dependent on the presence of LRRC8A and at least one of the other LRRC8 family members (Fig. 20A and B). In the quintuple knockout cell line *LRRC8*$^{-/-}$ VRAC activity is also lost. (These electrophysiological measurements were performed by Florian Ullrich and Jonas Münch.)

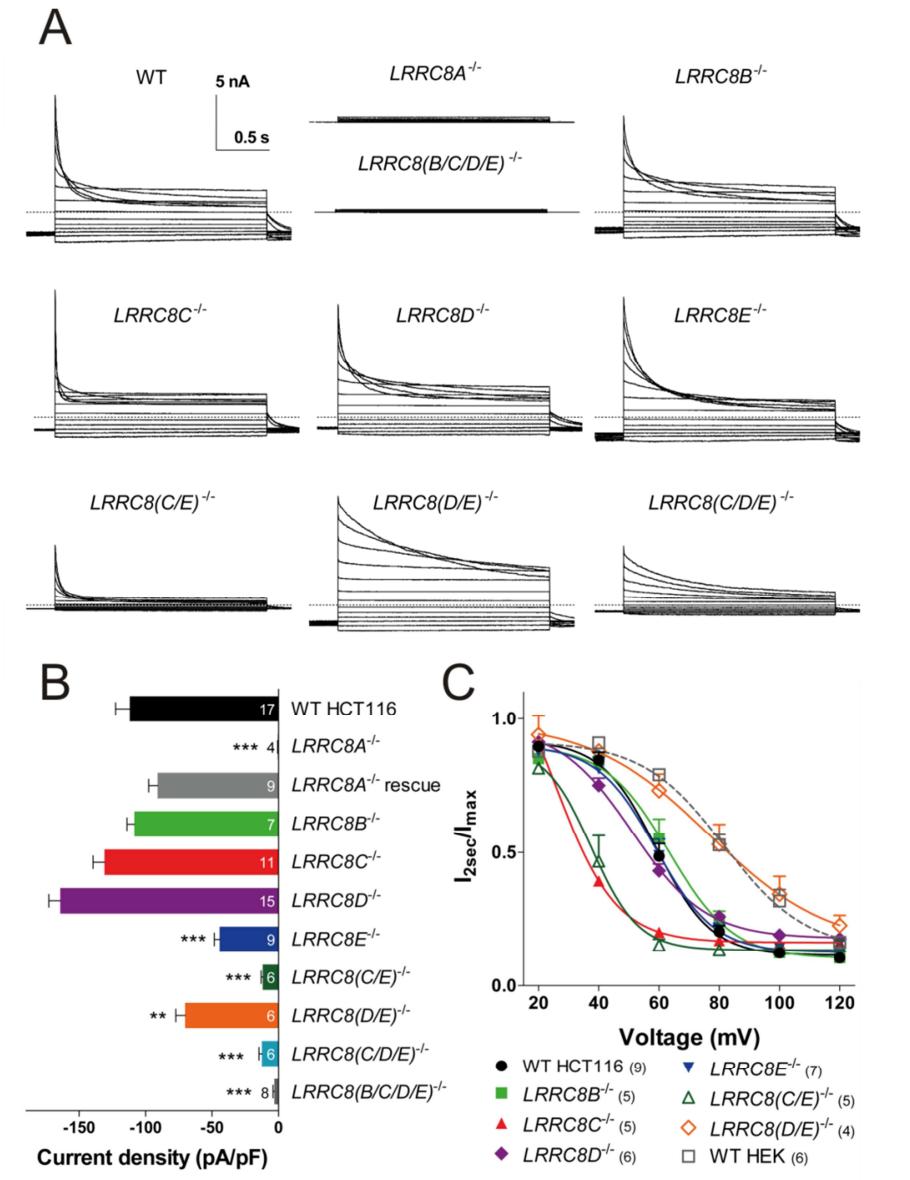

Figure 20: Electrophysiological characterization of LRRC8 knockout cell lines
A: Example $I_{Cl(swell)}$ traces (as in Fig. 19) of WT and mutant HCT116 cells. **B**: Current densities (at -80 mV) of maximally activated $I_{Cl(swell)}$ of WT and mutant HCT116 cells. **C**: $I_{Cl(swell)}$ inactivation assessed by ratio of current at end/beginning of pulse.

4.11 Inactivation kinetics in the reconstituted LRRC8 quintuple knockout

Through the generation of the quintuple knockout cell line we gained an important tool to further investigate the role of the different LRRC8 subunits on $I_{Cl(swell)}$ current characteristics. We could now specifically express combinations of subunits to test them for current properties, especially the inactivation kinetics, since these had already shown to be dependent to some extent on the presence of certain subunits in the single knockout cell lines. Accordingly, the reconstitution of $I_{Cl(swell)}$ in the *LRRC8*$^{-/-}$ cell line by heterologous expression of LRRC8A together with either LRRC8C, LRRC8D, or LRRC8E resulted in a current that presented changed inactivation kinetics at positive potentials (Fig. 21A and C). While co-expression with LRRC8E strongly accelerated inactivation, co-expression with LRRC8D mildly and LRRC8C strongly decelerated inactivation kinetics. It has to be noted also that the combination with LRRC8D diminished current amplitudes significantly (Fig. 21B). This is probably due to the very low expression efficiency of LRRC8D that we observed throughout several experiments and can also be observed in the Western blots in Fig 15. The same is true for LRRC8B, which was expressed even less and thus could not be used for the reconstitution of $I_{Cl(swell)}$ in the quintuple knockout. We know, however, that the combination of LRRC8A and LRRC8B yields $I_{Cl(swell)}$ currents from the measurements of the LRRC8(C/D/E)$^{-/-}$ knockout cell line (Fig. 20).

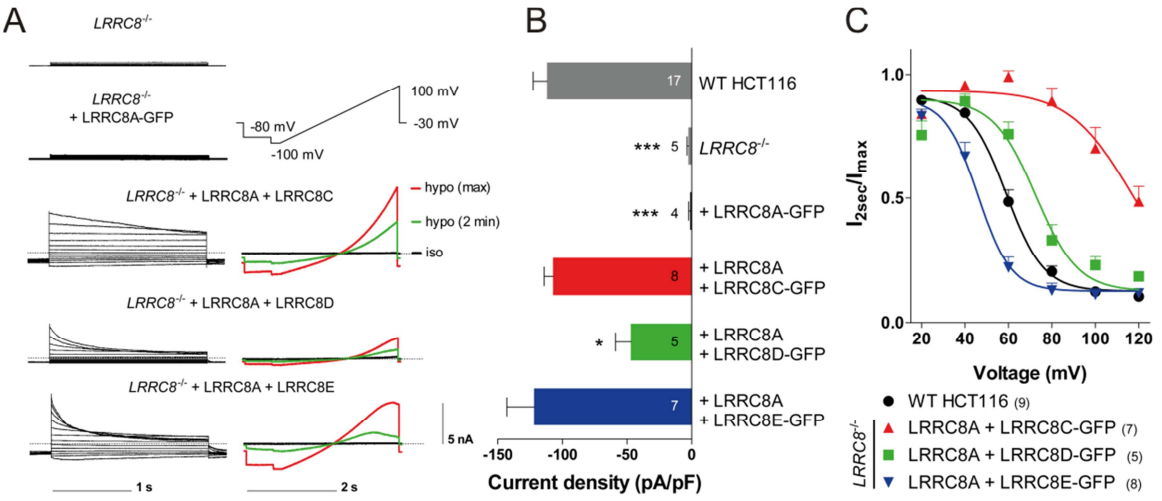

Figure 21: $I_{Cl(swell)}$ in the reconstituted LRRC8 quintuple knockout cell line
A:When transfected into HCT116 *LRRC8*$^{-/-}$ cells (with all *LRRC8* genes disrupted), LRRC8A rescues $I_{Cl(swell)}$ only when co-expressed with LRRC8C, D or E. *Left*, example ramp current traces from reconstituted $I_{Cl(swell)}$ at isotonicity (black), 2 minutes after switching to hypotonicity (green) and at maximal activation (red). **B**: $I_{Cl(swell)}$ current densities at -80 mV for indicated combinations. **C**: Voltage-dependent inactivation of $I_{Cl(swell)}$. Error bars, SEM. Number of cells in brackets. *, p<0.05 **, p<0.01 and ***, p<0.001 vs. WT.

In agreement with the previous results from single and multiple knockout cell lines, a reconstitution of VRAC with transfection of only LRRC8A was not possible. Minimally one other subunit needs to be co-expressed to restore $I_{Cl(swell)}$.
(These electrophysiological measurements were performed by Florian Ullrich and Jonas Münch.)

4.12 Differences in inactivation kinetics coincide with endogenous subunit expression

Differences in the inactivation kinetics of $I_{Cl(swell)}$ had also been observed previously in cell lines from different tissue origin. In the blood cell line HL-60, for example, almost no inactivation at positive potentials can be observed and also neurons show only very little inactivation (Hernandez-Carballo et al., 2010; Leaney et al., 1997). HEK and HCT116 cells, however, show prominent inactivation with HCT116 cells displaying rather fast inactivation kinetics. Since our previous results indicated that the subunit composition has an influence on the inactivation kinetics, we wanted to investigate whether the expression profile of different cell lines reflects their inactivation profile. To this end, we performed quantitative real time PCR analysis for all five LRRC8 members on HEK, HCT116 and HL-60 cells. As shown in Fig. 22, in agreement with the absence of inactivation at positive potentials, HL-60 cells do not or only to a very small extent express LRRC8E which had an accelerating effect on the inactivation kinetics in our reconstitution experiments. HCT116 cells however, that show a rather fast inactivation, express relatively little LRRC8C which led to a slow inactivation profile when co-expressed in the quintuple knockout.

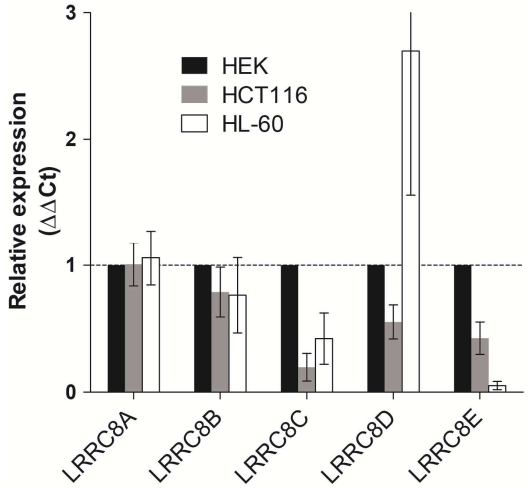

Figure 22: Relative LRRC8 mRNA expression.
LRRC8A-E mRNA expression in HEK, HCT116 and HL60 cells determined by quantitative RT-PCR. Values were normalized to the respective value of HEK cells. Values represent the means from 4 experiments. Error bars indicate SEM.

Taken together, these results support the notion that the endogenous subunit composition of VRAC differs among tissues which explains the variation in inactivation kinetics that had been an unsolved mystery in the VRAC field.

4.13 LRRC8A as an essential component of regulatory volume decrease (RVD)

In order to investigate the physiological relevance of LRRC8A mediated VRAC activity we performed a fluorescence-based assay to monitor cell volume changes over time using calcein-AM (Fig. 23). We used our HEK *LRRC8A*$^{-/-}$ cell line 3E7 in comparison to the wildtype, loaded the cell cells with calcein-AM on 384-well plates and then monitored the fluorescence over time in the FLIPR^{TM}. The calcein fluorescence increases with the cell volume due to a reduction in the concentration of intracellular quenching components. At t=30 s we diluted the isotonic imaging solution to a final osmolarity of 96 mOsm. The cell volume then increased rapidly due to the osmotic pressure. Under wildtype conditions the cells are able to perform regulatory volume decrease and thereby slowly shrink towards their original volume. In *LRRC8A*$^{-/-}$ cells this process is dramatically impaired. The cells continuously swell without being able to counteract this process. This illustrates that VRAC activity via LRRC8A is essential for the process of regulatory volume decrease in HEK cells.

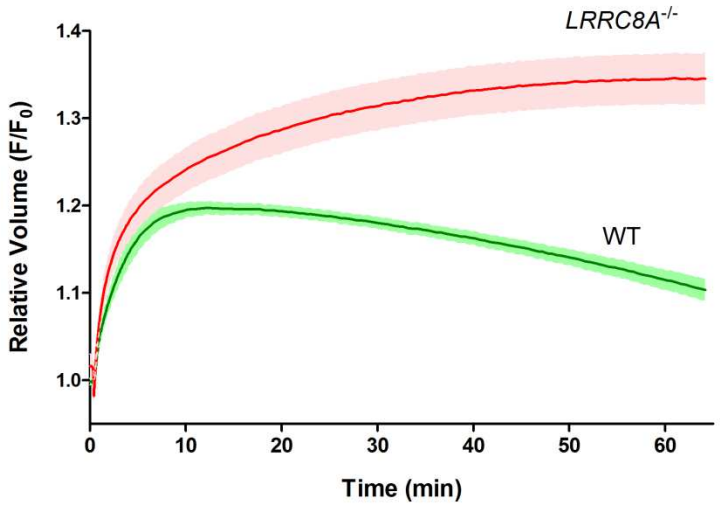

Figure 23: RVD measurements using calcein-AM
WT and *LRRC8A*$^{-/-}$ HEK cells were shifted to hypotonic saline (96 mOsm) at t=30 s, and cell volume was monitored by calcein fluorescence. Mean of six measurements; error range, SEM. Similar results were obtained in three independent experiments.

5. Discussion

5.1 The genome-wide siRNA screen as superior approach for the identification of VRAC

The many failed attempts to identify the molecular constituents of VRAC in the past clearly demonstrate the difficulty of this task. This is mostly due to the fact that many of the classical approaches for the molecular identification of an ion channel were, in retrospect, not suitable for VRAC. Although mentioned already briefly in section 2, this issue should be discussed here in further detail, in order to illustrate the importance of a more innovative screening strategy.

A widely used method to uncover the molecular identity of ion channels that has been proven to be successful in several cases (Canessa et al., 1993; Frech et al., 1989) is expression-cloning, where a cDNA library is expressed in *Xenopus laevis* oocytes and subsequently subdivided into smaller pools until ending up with a single cDNA coding for the sought-after channel. For VRAC this approach could not be applied for two reasons. First of all, *Xenopus laevis* oocytes display endogenous volume-activated chloride currents and are therefore not a suitable expression system. Second of all, there are a number of technical obstacles for the measurement of $I_{Cl(swell)}$ (endogenous or heterologously expressed) in frog oocytes. It has been observed that when using the regularly applied protocol for oocyte preparation, where the follicle membrane is removed by collagenase treatment, $I_{Cl(swell)}$ cannot be induced by hypotonic treatment (Ackerman et al., 1994). It seems like either the sensor or the channel itself depends on a component that is removed together with the follicle membrane when applying collagenase. Interestingly, we also observed in our experiments that HEK cells that had very recently been trypsinized did not display $I_{Cl(swell)}$ upon hypoosmotic stimulation (unpublished data). It is therefore likely that the heterologously expressed channel would also depend on the presence of the follicle membrane. However, with the intact membrane in place the injection of the oocytes with mRNA is very difficult and the electrophysiological measurements are hindered. Interestingly, in the case of another ion channel that had remained unidentified on the molecular level for decades, the calcium-activated chloride channel, this method could also not be used due to the presence of endogenous currents. Fortunately, oocytes of another amphibian, the axolotl salamander (*Ambystoma mexicanum*) do not display these currents and could successfully be used as

expression system. This approach led to the identification of Ano1 as *bona fide* calcium-activated chloride channel (Schroeder et al., 2008). For VRAC one could also have used such an alternative expression system, but so far nobody could show the absence of the current in a certain cell type that would be suitable for this approach. It has to be noted, however, that insect cells like S2 cells from *Drosophila melanogaster* display volume-sensitive chloride currents, mediated by dbest1, with properties distinct from $I_{Cl(swell)}$ (Stotz and Clapham, 2012). In theory, it would therefore be possible to distinguish the endogenous current from a current present only when expressing the respective protein of interest. It is, however, possible if not likely that insect cells lack essential elements of the signal transduction leading to VRAC activation, especially since in these organisms a different class of chloride channels has taken over the task of volume regulation.

Another argument against an expression cloning approach, besides the lack of a suitable expression system, is that it could not be used to identify a multimeric channel complex. In retrospect, the fact that $I_{Cl(swell)}$ requires the expression of LRRC8A together with at least one other LRRC8 family member would have made it nearly impossible to identify the channel proteins via this approach. The suppression effect we observed upon overexpression of LRRC8A in HEK cells furthermore corroborates this point.

Another commonly used method is the identification by affinity purification using a specific ligand or inhibitor (Beneski and Catterall, 1980). As discussed before (section 1.2), poor inhibitor specificity is a general problem in the chloride channel field. Therefore, this approach could also not be used in the case of VRAC.

A different strategy is a large scale genomics approach. In case of the calcium-activated chloride channel, a second group successfully identified Ano1 using a functional genomics approach. They had noticed that calcium-activated chloride currents are upregulated in bronchial epithelial cells upon interleukin-4 treatment and thus used this finding to perform a microarray analysis on interleukin-4-treated cells and found Ano1 to be among the upregulated genes (Caputo et al., 2008). A similar approach would also have been feasible for the identification of VRAC. In fact, we performed a preliminary experiment with HEK cells that were osmotically challenged by repetitive medium exchanges from isotonic to hypotonic medium in 30 min intervals for 24 h. We measured VRAC currents in these cells before and after the treatment with the hypothesis that the cells would upregulate VRAC expression in order to cope with the osmotic challenge. Unfortunately, current densities were unchanged (data not shown). Although

disappointing, this finding fits to the fact that in the literature only quite small variances in current density are reported between different cell types, culture conditions or drug treatments (Nilius et al., 1997a; Nilius et al., 1994b). Hence, this type of functional genomics approach was also hampered by the lack of knowledge about possible modulators of VRAC expression or activation.

With the discovery of small interfering RNAs that can be used to specifically silence genes simply by transfecting them into a cultured cell, new possibilities for genomic analyses emerged. The synthesis and commercial availability of genome-wide siRNA libraries allows for screenings that can be performed in high-throughput formats and thus enables a rapid scan for possible players in complex physiological processes. Accordingly, the majority of genome-wide siRNA screenings that have been performed so far aimed at the identification of novel factors influencing specific cellular pathways or processes such as cell migration, cancer drug resistance, viral infection or signal transduction (Prusty et al., 2011; Warner et al., 2013; Whitehurst et al., 2007; Yang et al., 2013). In case of the molecular identity of an electrophysiologically known ion channel like VRAC, a genome-wide siRNA screening is still a needle-in-a-haystack approach. Even if performed in a very sophisticated manner, there is a high risk of missing the gene(s) encoding for the channel itself. For the identification of the mechanically activated cation channels piezo1 and piezo2, a previously defined candidate list from expression profiling was used in a subsequent siRNA screen (Coste et al., 2010). Other studies used bioinformatics analyses to select a list of candidate genes for their siRNA screen (Yang et al., 2008). In case of the Ca^{2+} release–activated Ca^{2+} (CRAC) channel, however, the authors opted for a genome-wide siRNA screen and successfully identified essential components of this ion channel in S2 cells (Vig et al., 2006).

During the planning phase of our siRNA screen for VRAC, we also discussed the possibility of preselecting a subset of siRNAs encoding for transmembrane proteins, but subsequently discarded this option for several reasons. On the one hand this would have limited us to finding VRAC without being able to identify possible regulators or members of the signaling cascade, which we still hope to extract from the data we gained during the genome-wide siRNA screen. On the other hand, a smaller set of siRNAs would not have eliminated the most prominent risk factor of the screen, which would be false-negatives due to non-functional siRNAs. We therefore opted to perform the genome-wide siRNA screen and sought to minimize the possibility of false-negatives by very carefully

optimizing the transfection protocol and including a large number of controls (see section 3.2.2). Through these measures, we could successfully monitor the transfection efficiency on every single plate. This minimized the risk of missing the sought-after gene due to a technical problem like low transfection efficiency, washed-off cells or obliterating artifacts caused by dirt particles on the plate. To exclude the latter, we examined the photographs taken by the FLIPR^{TM} during the measurements. We also accounted for possible dropout siRNAs in our bioinformatics screening analysis, by calculating the mean value of the best 2 out of 3 siRNAs for each gene. Thereby, we could clearly identify the hit for LRRC8A although only one of the three siRNAs gave a very high value for the slope shift in the YFP quenching assay (Fig. 10C).

The assay set-up was also very carefully planned in order to obtain a robust and reproducible quenching response, which was clearly distinguishable from the response under isotonic conditions. We performed numerous experiments to determine the perfect assay conditions and to find the right equipment for the performance of the read-out assay in a high-throughput manner. With the FLIPR^{TM} we could then monitor the time course of the quenching response very precisely with a high number of measurements per plate. Therefore, even small changes in the kinetics of the response could be detected, which is crucial since siRNA knockdown is rarely complete and thus a residual iodide influx through remaining VRAC channels was likely to occur even with high transfection efficiency and well-performing siRNAs.

Despite the careful planning of the assay set-up and screening controls, which could minimize technical shortcomings, there was still the risk that the molecular identification of VRAC via an siRNA screen would not be possible due to redundant expression of different proteins underlying VRAC. Especially in case of heteromeric protein complexes functional redundancy or at least compensatory effects between subunits are frequently observed and would have impeded the identification via single-gene knockdown experiments.

Shortly before the start of our primary screen, the lab of David Clapham at the Howard Hughes Medical Institute in Boston published a genome-wide siRNA screen performed for the volume-regulated anion channel in *Drosophila* S2 cells, also using a YFP-based assay similar to the one we used in our screen (Stotz and Clapham, 2012). They successfully confirmed dbest1 as the volume-regulated anion channel of insect cells with this method, showing that the assay is a suitable tool for indirectly monitoring volume-

regulated anion currents. In contrast to our read-out assay, however, they measured the fluorescence just before and after the hypotonic stimulation using a plate reader. In retrospect, it is doubtable that we would have successfully identified LRRC8A if we had performed a similar end-point measurement since the slope of the quenching curve is more strongly affected by a reduction in channel density due to siRNA knockdown than the finally reached steady-state.

In parallel to our publication of the main findings of this study (Voss et al., 2014), the lab of Ardem Patapoutian at the Scripps Research Institute in San Diego also reported the identification of LRRC8A as a component of the VRAC channel by a genome-wide siRNA screen that was performed in a surprisingly similar manner to our own screen (Qiu et al., 2014). They also used the FLIPR^{TM} to monitor the quenching of the halide-sensitive YFP variant upon hypotonic stimulation. In contrast to our assay, they stimulated VRAC opening by adding a hypotonic solution before adding iodide to the solution and thereby inducing the quenching process. Furthermore, they performed their screen using a different siRNA library. The independent identification of LRRC8A as an essential component of VRAC by this approach strongly supports the validity of the result and illustrates the effectiveness of the applied method.

5.2 LRRC8A is essential for VRAC activity

After having identified LRRC8A as a hit in our primary screen and confirmed during our secondary screen, we could verify its importance for VRAC activity by several electrophysiological experiments. Treatment with the siRNA smartpool against LRRC8A almost completely abolished $I_{Cl(swell)}$ showing that LRRC8A is indispensable for channel function. This is also evident from the several knockout cell lines we generated for LRRC8A in HEK and HCT116 cells, that all lost their ability to produce volume-activated anion currents upon hypotonic stimulation. This is of course no definite proof that the LRRC8A protein is part of the channel pore. However, the fact that it localizes to the plasma membrane and its confirmed topology of 4 transmembrane domains with an intracellular N- and C-terminus support this hypothesis. Furthermore, the phylogenetic relation of LRRC8 proteins to pannexins and thus also the structural similarity to connexins (Abascal and Zardoya, 2012) suggest that LRRC8A might be able to form heteromeric complexes that could function as channels in the plasma membrane.

A usual approach to investigate whether a certain protein might constitute an ion channel is to overexpress the protein in order to check for an increase in current due to the

increased number of ion channels incorporated into the membrane. An increase in current amplitude can be observed for the overexpression of many well-known ion channel proteins, such as voltage-gated potassium channels (Brevnova et al., 2004), calcium-activated chloride channels (Schroeder et al., 2008) or chloride channels of the ClC family (Jordt and Jentsch, 1997). Surprisingly, overexpression of LRRC8A in HEK cells did not result in an increase of current amplitude, but suppressed the current in a similar way as siRNA treatment. Thus, the increased production of the protein, which also correctly localized to the plasma membrane, did have a strong impact on the activity of the endogenous channel. A possible explanation for this suppression effect would be the involvement of LRRC8A in a heteromeric complex in which the stoichiometry could be severely disturbed by the asymmetrical overexpression of one subunit. A similar effect has been shown previously for the correct assembly of heteromeric acetylcholine receptors, which were shown to strongly depend on the correct expression ratio of the different subunits (Eertmoed et al., 1998).

In summary, our results show that LRRC8A is essential for VRAC function and suggest that it might be part of a heteromeric complex that could form the channel pore. We therefore further explored this possibility by investigating the role of the other members of the LRRC8 family for VRAC activity and looked for possible interactions among the family members.

5.3 Heteromerization of LRRC8 proteins

Upon the initial hint from the suppression effect of the overexpression of LRRC8A, we performed several experiments that could successfully show an interaction between LRRC8A and the other members of the LRRC8 family. First of all, LRRC8B-E can only be targeted to the plasma membrane when they are co-expressed together with LRRC8A and are otherwise stuck in the ER. This already indicates that these proteins interact at least during protein trafficking, but likely also at their final destination where they show strong co-localization. A similar trafficking dependence can be observed for several other interaction partners. For example, the beta subunit of ClC-7 Ostm1, which is needed for transport activity, only localizes correctly to the lysosomal membrane when ClC-7 is present. In its absence, Ostm1 is retained in the ER (Lange et al., 2006). Also KCNEs, tissue-specific beta subunits of voltage-gated potassium channels, require the co-expression of their respective alpha subunit for correct trafficking and surface expression (Chandrasekhar et al., 2006; Schroeder et al., 2000). Not only beta subunits, that often

play regulatory roles, but also proteins that heteromerize to form the pore of a channel or transporter can co-depend on mutual expression during protein targeting. Examples for this are the subunits of heterodimeric ABC-transporters (Graf et al., 2003) and multimeric TRPC channel complexes (Hofmann et al., 2002). Thus, the interdependence of LRRC8B-E with LRRC8A according to their localization to the plasma membrane is a strong indicator of functional interaction and possible multimeric channel formation.

We furthermore showed by co-immunoprecipitation that LRRC8A interacts with all other LRRC8 family members. This underlines the physical connection formed between the respective proteins, also pointing towards a functional interplay.

We tried to overcome the dominant-negative effect of LRRC8A overexpression by co-expressing LRRC8A with LRRC8C and could successfully restore wildtype-like currents with this combination. Expression studies in our knockout cell lines confirmed that LRRC8A alone is not sufficient to reconstitute proper VRAC currents. This is also evident from the absence of $I_{Cl(swell)}$ in the quadruple knockout cell line *LRRC8B-E*$^{-/-}$. Concordantly, the quintuple knockout *LRRC8*$^{-/-}$ could only be rescued by co-expression of LRRC8A and one of the other family members, but not by the expression of one subunit alone. This strongly suggests that VRAC channel function depends on the presence of LRRC8 heteromers that obligatorily consist of at least one copy of LRRC8A and one other LRRC8 protein. The suppression effect of LRRC8A overexpression furthermore indicates that the multimeric complex consists of at least 3 subunits, since the stoichiometry of a dimeric complex would not be affected by uneven expression.

Oligomerization of LRRC8 proteins had also been suggested previously by Abascal and Zardoya, who performed a bioinformatics analysis and found a phylogenetic relation of LRRC8 proteins to pannexins which are known to form hexameric channel complexes (Abascal and Zardoya, 2012). They even proposed a structural model explaining how the leucine-rich repeat C-termini of the LRRC8 proteins could be arranged into a hexamer, based on the structural similarity to connexins.

It has to be noted, however, that although pannexins have been shown to oligomerize and form hexameric complexes, these complexes seem to be composed of only one pannexin subtype. Nevertheless, interactions between different pannexin isoforms have also been shown by immunoprecipitation, but so far no connection between possible heteromerization and channel activity could be verified. Co-expression experiments showed a decrease in current amplitude compared to the expression of only one pannexin

isoform and thus pannexins rather seem to form homomeric than heteromeric channels (Bond and Naus, 2014).

5.4 Evidence for a heteromeric LRRC8 channel complex

Despite convincing evidence for the dependence of $I_{Cl(swell)}$ on the presence of LRRC8 heteromers (see section 5.3), these data could not yet sufficiently prove the involvement of LRRC8 proteins in the formation of the channel pore. So far, these findings would also be in agreement with an obligate regulatory role of LRRC8 proteins for VRAC activity. In order to show that a certain protein constitutes part of the channel pore, different strategies could be used. In general, this can be done by showing that a change in the primary sequence or structure of the protein(s) reflects in a change of channel-intrinsic properties such as activation or inactivation kinetics, ion selectivity, single channel conductance or sensitivity to specific pharmacological compounds. We could successfully influence the composition of the channel complex by knocking out single subunits in our CRISPR/Cas cell lines and also by heterologous expression of specific subunit combinations in the *LRRC8*$^{-/-}$ cell line. These alterations in the quaternary structure of the channel then indeed reflected in a change in the inactivation kinetics. For example, *LRRC8C*$^{-/-}$ cells showed accelerated inactivation kinetics compared to the wildtype, while *LRRC8D/E*$^{-/-}$ displayed rather slow inactivation kinetics. Reconstitution experiments in the *LRRC8*$^{-/-}$ cell line with different subunit combinations confirmed this dependence of inactivation kinetics on the subunit composition. While the co-expression of LRRC8A together with LRRC8C leads to a rather slow inactivation at positive potentials, the combination of LRRC8A with LRRC8E results in a prominent acceleration of the inactivation kinetics. Furthermore, we could correlate naturally occurring differences in inactivation kinetics of different cell types with their expression profile of different LRRC8 isoforms. This physically connects a structural property of LRRC8 heteromers with a characteristic feature of $I_{Cl(swell)}$ and thereby strongly supports the notion that the VRAC channel complex is constituted by these proteins.

We also tried to further prove this point by inserting many different point mutations into the cDNA of LRRC8A and also LRRC8C in order to find an amino acid or identify a region in the primary sequence that is responsible for the ion selectivity of VRAC (data not shown). Unfortunately, we could not find any amino acid change that resulted in a change of the known ion selectivity. In parallel to our publication of the main results of this work, another group also published their findings about LRRC8A being a part of

VRAC (Qiu et al., 2014). This group mutated several residues in a cysteine-scanning approach and found that the mutation of the threonine at position 44 to cysteine or glutamate resulted in a shift of the reversal potential for iodide, indicating a changed anion selectivity (Qiu et al., 2014). These findings further support our results that LRRC8A is indeed part of the channel pore and not a mere regulatory element of VRAC. It has to be noted, however, that the reported ion-selectivity change could not be reproduced by expressing the respective mutants in our HEK and HCT116 knockout cell lines (unpublished data).

An additional approach to further fortify the connection to LRRC8 protein expression, could be the measurement of single channel currents in the different knockout cell lines in order to find possible differences in the unitary current amplitude. These types of measurements of $I_{Cl(swell)}$ are, however, technically very demanding since VRAC needs to be activated by swelling for single channel openings to be detectable. Cells either have to be pre-swollen and subsequently a stable high-resistance on-cell patch has to be established, or cells have to be patched with two pipettes at once in the whole-cell and on-cell mode, in order to record single channel currents (Akita and Okada, 2014).

5.5 The molecular identity of VRAC from an evolutionary perspective

From an evolutionary point of view it is interesting to note that the LRRC8 protein family originated from an ancestral pannexin protein at the phylogenetic time point of the emergence of chordate animals. Volume-regulated anion currents are, as stated previously, known to exist in all vertebrate cell lines tested, but they also exist in cells from non-chordate organisms like S2 cells from the arthropoda *Drosophila melanogaster*. In arthropoda, innexins, which are related to the mammalian pannexins, but no LRRC8 homologs are present (Abascal and Zardoya, 2012). In agreement with this, it could repeatedly be shown in the past that the main volume-regulated anion channel in *Drosophila melanogaster* cells is dbest1 (Chien and Hartzell, 2007; Stotz and Clapham, 2012). This protein is a homolog to the mammalian family of bestrophins and not related to innexins or pannexins. In mammals, however, bestrophins do not constitute VRAC as shown in bestrophin knockout mice with unchanged VRAC currents compared to wildtype (Chien and Hartzell, 2008). It could therefore be concluded that ancestral forms of pannexin proteins that exist today in both arthropoda and chordates, evolved separately in the two different phyla. While LRRC8 proteins evolved to form the volume-regulated

anion channel in chordates like vertebrates, in arthropoda a different class of proteins had to take over this task.

Furthermore, sequence comparison revealed that the LRRC8 protein family is less diverse compared to pannexins. This could be caused by a strong selective restraint connected to protein function (Abascal and Zardoya, 2012). Since VRAC has been implicated in a large number of essential biological processes such as cell division, apoptosis and general cell integrity, it seems likely that alterations in VRAC functionality might hardly be tolerable. Strikingly, LRRC8A seems to have been under an even stronger purifying selection pressure than the other LRRC8 family members, which is indicated by a high sequence similarity to orthologues from rather distant chordates like actinopterygians (Abascal and Zardoya, 2012). This is in agreement with the fact that we found LRRC8A to be the only subunit that is absolutely essential for the formation of a functional channel, whereas the other subunits could substitute for one another in our reconstitution experiments and knockout cell lines. Our data also suggest that the evolutionary evolvement of LRRC8B-E might have caused differences in current properties of $I_{Cl(swell)}$, like in the inactivation kinetics. Other characteristics of VRAC could also be influenced by the subunit composition, which will be a subject of further investigations.

Another interesting fact is the conservation of certain amino acids or amino acid stretches among the different LRRC8 proteins or even between the members of the LRRC8 family and pannexins. Particularly remarkable is the conservation of several opposing cysteine residues in the two extracellular loops that are also present in all members of the pannexin family, where they can be considered a homologous structural trait (Abascal and Zardoya, 2012). Even in the merely structurally related connexin protein family, these cysteine residues are present. Here they were shown to be important for the formation of disulfide bonds between adjacent loops (Birkenhager et al., 2014; Foote et al., 1998). The latter concordance could thus be considered an analogous structural feature and implies that these cysteine residues play an equally important role in stabilizing intra- or even intermolecular bonds in LRRC8 heteromers. This hypothesis and the question whether the presence of several other conserved stretches in the primary structure of LRRC8 proteins are somehow indicative of important sites for VRAC regulation and structure-function relations will be the subject of future investigations.

5.6 Transport of other osmolytes and substances through VRAC

Cell volume regulation does not only comprise ion transport in response to swelling. The movement of organic osmolytes is also an important feature of regulatory volume decrease and has a strong protective effect during osmotic perturbations, especially of the extracellular space. Since the intracellular amino acid concentration significantly contributes to the intracellular osmolarity, the transport of these organic osmolytes can have a strong impact on volume regulation. The β-amino acid taurine has been the focus of many investigations, since it is one of the most abundant intracellular organic osmolytes and thus its transport might be involved in several pathological conditions connected to volume regulation. However, the question by which pathway or channel taurine is released from the cell upon swelling could not be answered conclusively so far (Shennan, 2008). A major contentious point is whether taurine is released through VRAC, or a separate transport pathway. A number of characteristics of the volume-regulated taurine efflux are in accordance with features of volume-regulated anion currents. For instance, the pharmacological profile of both processes is in agreement in many tested cell types (Jackson and Strange, 1993; Kirk and Kirk, 1993), but as mentioned before, most VRAC and taurine efflux inhibitors are very unspecific. Furthermore, some differences in the pharmacological profile of specific cell types were reported (Culliford et al., 2004; Tomassen et al., 2004a). A similar controversy exists about evidence for common and distinct regulatory mechanisms of volume-regulated anion and taurine efflux (Galietta et al., 1997; Tomassen et al., 2004b). A rather strong argument in favor of a common pathway comes from two studies that found evidence for taurine permeation through volume-activated anion channels in electrophysiological recordings, claiming taurine to chloride permeability ratios of 0.75 and 0.2, respectively (Banderali and Roy, 1992; Jackson and Strange, 1993), but since taurine is not charged at physiological pH, these measurements had to be performed at pH=~8, which could possibly influence channel properties.

With the identification of LRRC8 heteromers as essential component of the volume-regulated anion channel, we now had the tool to elucidate this long-debated contention. To this end, Darius Lutter performed efflux studies with radioactively labeled taurine in our HCT116 and HEK LRRC8A knockout cell lines and could show that swelling-induced taurine efflux was reduced to background levels. In *LRRC8B-E*$^{-/-}$ cells, the swelling-activated taurine efflux was also abolished, demonstrating its dependence on the presence of at least LRRC8A and one of the other LRRC8 proteins (Voss et al., 2014). In

accordance with these results, the lab of Ardem Patapoutian could also show a strong reduction in hypotonicity-induced taurine efflux in HeLa cells treated with siRNA against LRRC8A (Qiu et al., 2014). Taken together, these studies prove that both, volume-regulated anion current and swelling-activated taurine release, depend on the presence of LRRC8 heteromers. It has to be noted, however, that unlike for $I_{Cl(swell)}$ there is so far no direct evidence (like changes in permeability ratios or subunit specific efflux kinetics) that LRRC8 heteromers form the pore for the permeation of taurine. It is also possible that the taurine release pathway is downstream of VRAC activation and is thus abolished together with $I_{Cl(swell).}$ To unambiguously show that both halide anions and the organic osmolyte taurine are released through the same channel, further investigations are needed. This work provides a valuable tool set for this task in form of the numerous single and multiple knockout cell lines.

Besides taurine, a variety of other organic osmolytes might also contribute to the process of regulatory volume decrease in several cell types. Among these are the α-amino acids alanin and glycine, the anionic amino acids aspartate and glutamate as well as other organic osmolytes, such as inositol, betaine, choline, uridine, creatine, sorbitol and glucose (Burg and Ferraris, 2008; Shennan, 2008). Most of these compounds have previously been suggested to share a common volume-regulated release pathway with taurine, but no unambiguous data exists on this so far (Shennan, 2008). Of special interest is the glutamate and aspartate release from neuronal and glial cells upon ischemic brain edema, which is at least in part causative for the neurotoxic consequences of this pathological state (Kimelberg, 2005). There is already some experimental evidence that glutamate might permeate through VRAC (Inoue et al., 2007; Roy, 1995; Schlichter et al., 2011). A prerequisite for the permeation of these rather large anionic molecules through an ion channel is a sufficiently large pore. Assuming the permeation of taurine and inositol, the pore size of VRAC has been estimated to be between 5.4 and 8 Å (Nilius et al., 1997a). In this regard, it is slightly puzzling that VRAC shows selectivity between the halide anions, depending on their size, while it should at the same time (and possibly through the same pore) be permeable for much larger molecules as well.

The lack of knowledge about the molecular identity of VRAC has precluded further investigation of the actual role of VRAC in glutamate release, and most of the existing data is based on rather unspecific pharmacology. With the identification of LRRC8 heteromers as an essential component of VRAC it will now be possible to test whether the

observed swelling-induced glutamate and aspartate release from neurons and glial cells is equally dependent on these proteins. If a role of LRRC8 in glutamate efflux can be confirmed, the generation of knockout mice for LRRC8A and/or the other family members will be of interest to study the contribution of swelling-activated amino acid efflux to stroke pathology. Interestingly, it was noticed recently that carbenoxolone, which is a known inhibitor of gap junction proteins, also blocks $I_{Cl(swell)}$ and that carbenoxolone treatment has a neuroprotective effect in a mouse model of brain ischemia (Benfenati et al., 2009; Vakili et al., 2009). The effect of the drug might be based on an inhibitory effect on VRAC, although gap junction-mediated effluxes could also be a factor in this pathology. Besides this, the drug riluzole, which is used to treat amyotrophic lateral sclerosis by inhibiting Na^+ channels and glutamate receptors, was shown to inhibit VRAC (Bausch and Roy, 1996; Schlichter et al., 2011). This might be another hint that the inhibition of glutamate release via VRAC could contribute to the alleviating effect of drugs used for conditions connected to excitatory neuronal injury.

Another substrate that has been discussed to be transported via VRAC is ATP. Mainly based on pharmacological data, it was reported that ATP is released from aortic endothelial cells through VRAC in a swelling-activated manner (Hisadome et al., 2002). This finding is in agreement with previous reports of comparable time courses of VRAC activation and ATP release during hypotonic stress (Koyama et al., 2001). In this regard, it is interesting to note that intracellular as well as extracellular ATP seems to have an effect on VRAC activity. While intracellular ATP is required for VRAC opening (Oiki et al., 1994), extracellular ATP seems to block $I_{Cl(swell)}$ in a voltage-dependent manner at least in some cell types (Jackson and Strange, 1995; Tsumura et al., 1996). These findings might be explained by a permeation block model. The voltage-dependence of the inhibition by intracellular ATP has also been discussed as the mechanistic basis of the outward rectification of $I_{Cl(swell)}$ (Hisadome et al., 2002). Interestingly, another study showed a connection of ATP and volume-regulated amino acid release from astrocytes. The authors suggest that extracellular ATP activates VRAC-mediated amino acid release with the involvement of P2X receptors upon cell-swelling (Mongin and Kimelberg, 2002). They interpret their results as evidence for ATP being a cooperative signal for volume-regulated amino acid release. However, their results could also be indicative of ATP directly regulating VRAC function or even permeation of ATP through VRAC. Furthermore, it is important to mention that pannexin channels have also been proposed to mediate ATP release and/or being regulated by ATP both via P2Y receptors as well as

through a permeation block mechanism as proposed for VRAC (Qiu et al., 2012). The homologous structure of LRRC8 proteins and pannexins could therefore be responsible for similar ATP permeation and/or ATP sensitivity of the two protein families. While LRRC8 heteromers could function as swelling-activated ATP release channels, pannexins might mediate ATP release upon other intra- or extracellular cues. The physiological role of volume-regulated ATP release could on one hand rely on a form of signal-amplification to activate osmolyte release from neighboring cells during hypotonic stress or a completely opposite role as feedback-inhibition to block the VRAC pore and stop further osmolyte efflux. This would explain why $I_{Cl(swell)}$ deactivates after a few minutes even if the hypoosmotic stimulus persists, as observed in whole-cell patch clamp experiments, where the intracellular osmolarity is fixed by the pipette solution. Besides these possibilities, it has been suggested that volume-activated ATP release through VRAC might serve non-synaptic communication between neuronal axons and glial cells during action potential firing (Fields and Ni, 2010).

Recently, another possible substrate for VRAC has been suggested by a study about LRRC8D and the import of blasticidin S. This study confirmed the topology of LRRC8 proteins with N- and C-terminus located in the cytosol and showed that LRRC8D-deficient cells are resistant to blasticidin S treatment. Furthermore, the interaction between LRRC8D and A (and also B and C) could be confirmed in co-immunoprecipitation and mass spectrometry analysis (Lee et al., 2014). At the time when the authors performed their experiments, LRRC8 proteins were not yet known to be involved in VRAC activity and therefore they did not include experiments with hypotonic stimulation of the cells and likewise did not propose a connection to volume regulation. Considering the molecular size of blasticidin S, the idea of a common channel pore, which is furthermore selectively permeable for halide anions and shows a distinct selectivity sequence among them, seems rather surprising if not unlikely. Nevertheless, these findings have to be taken into consideration for future experiments. Especially in connection to the proposed role of VRAC in apoptosis and multidrug resistance, it is crucial to determine or possibly exclude the option that apoptosis-inducing agents might enter the cell through VRAC, since this would shed a different light on the interconnection of the processes of apoptosis and volume regulation.

5.7 Possible regulatory sites in LRRC8 proteins

With the molecular identification of the VRAC-forming LRRC8 protein family, it is now feasible to look for possible regulatory mechanisms of $I_{Cl(swell)}$ based on structural motifs present in the primary sequence. In case of LRRC8A there is evidence, both from bioinformatics sequence analysis and experimental mass spectrometry data for several sites of posttranslational modification. There are at least two putative glycosylation sites, which were confirmed by our topology experiments. Besides this, several putative phosphorylation sites in the N- and C-terminus and in the intracellular loop have been assigned, of which one was experimentally confirmed by mass spectrometry. Besides this there are two predicted acetylation sites which are also located in the intracellular loop (Abascal and Zardoya, 2012; Olsen et al., 2006; Rigbolt et al., 2011).

Interestingly, LRRC8 proteins contain a putative sterile-20-related proline-alanine-rich kinase (SPAK) recognition motif with the consensus sequence (R/K)FX(V/I) shortly before the C-terminal leucine-rich-repeat region. The SPAK kinase and the oxidative stress response 1 kinase (OSR1) are known to be involved in osmoregulation, but so far mainly as activators of NKCC transporters during hyperosmotic stress (Hoffmann et al., 2007). It has been suggested that SPAK functions as a link from the cytoskeleton to the channel proteins during cell shrinkage, thereby conferring the signal from a mechanical stimulus to a chemical cue in form of protein phosphorylation. It was shown that SPAK can bind to F-actin but not to G-actin (Tsutsumi et al., 2000), indicating that actin assembly or disassembly might regulate the kinase activity. This would also be a conceivable mechanism to translate cell swelling into chemical activation of VRAC activity. Indeed, there already have been a number of studies suggesting a stimulatory effect of F-actin disruption on $I_{Cl(swell),}$ even under isotonic conditions, indicating that F-actin integrity could have a silencing effect under non-swollen conditions (Klausen et al., 2006; Levitan et al., 1995; Schwiebert et al., 1994).

Other kinases like Src family kinases, serine/threonine kinases, tyrosine kinases, rho kinases and myosin light chain kinase have also been described to have an effect on $I_{Cl(swell)}$ (Hoffmann and Pedersen, 2006). Thus, the putative phosphorylation sites in the intracellular loop of LRRC8 proteins fit the hypothesis that VRAC activity or activation is linked to phosphorylation events. This can now be investigated in more detail by biochemical approaches that had not been feasible so far. For example, it is now possible

to look for an increase in phosphorylated LRRC8A-E upon hypoosmotic treatment of native cells using the knockout cell lines as an essential negative control.

Calmodulin binding has also been suggested to play a role in VRAC activation since the calmodulin blocker primozide was shown to inhibit $I_{Cl(swell)}$ in Ehrlich ascites tumor cells (Hoffmann et al., 1986). Similar results were obtained for VRAC activation in HeLa cells. It is also known that VRAC activity requires an intracellular Ca^{2+} concentration of at least 50 nM (Kirk and Kirk, 1994; Szucs et al., 1996b). Furthermore, there exists some evidence for the involvement of calmodulin in swelling-mediated taurine efflux in a few cell types (Lang et al., 2000; Vitarella et al., 1994). This might indicate a cell type-specific regulatory role of Ca^{2+}/calmodulin binding in the activation cascade of volume-regulated osmolyte efflux. LRRC8 proteins do however not exhibit the IQ-calmodulin-binding motif [FILV]Qxxx[RK]Gxxx[RK]xx[FILVWY] (Rhoads and Friedberg, 1997). A direct binding of calmodulin to any of the subunits is thus unlikely. Calmodulin binding might still be involved in the signaling cascade leading to VRAC activation. This remains to be addressed by future investigations on the mechanisms underlying VRAC activation.

5.8 Are we missing something? - The possibility of a limiting auxiliary subunit

While this work clearly shows the dependence of $I_{Cl(swell)}$ on the presence of LRRC8A and at least one other LRRC8 subunit, one point has remained enigmatic throughout our investigation: Why is it not possible to increase current densities of $I_{Cl(swell)}$ upon overexpression of LRRC8A or any tested combination of subunits? As mentioned in section 5.3, the suppression effect of the overexpression of LRRC8A can be explained by the obligatory heteromerization of LRRC8A with the other subunits that depends on a stoichiometry that is altered upon LRRC8A overexpression. Co-expression of LRRC8A with, for example, LRRC8C does not yield this suppression effect and can rescue currents in the *LRRC8*$^{-/-}$ cell line. However, it is not clear why co-overexpression of two subunits that are capable of forming a functional channel does not increase amplitudes above wildtype levels as one would expect when the protein amount at the plasma membrane is drastically increased, as we can see from immunofluorescence experiments. One possible explanation would be that there is another essential accessory subunit or beta subunit that is not part of the LRRC8 protein family and limits the activation or the formation of functional VRAC complexes. So far, we have no conclusive evidence for other interaction partners of LRRC8 proteins that could constitute this assumed beta subunit. With the large amount of data from the genome-wide siRNA screen we do, however,

possess a valuable treasure of data that could hint at a secondary subunit. So far the analysis of this data has been focused on transmembrane proteins that could constitute the channel pore, but has left out candidate proteins with cytosolic localization. These could well be members of the signaling cascade or regulatory subunits needed for VRAC activation. The future evaluation of this dataset will most likely yield a number of possible interaction partners of LRRC8 proteins that can be further analyzed by biochemical interaction assays. Furthermore, additional assays could be performed to look for potential interacting proteins, for example yeast two-hybrid assays or co-immunoprecipitation experiments followed by mass spectrometry. Even before the molecular identification of VRAC, a number of proteins were suggested to play a regulatory or accessory role in volume-regulated anion transport. It has been proposed that caveolin might constitute such an accessory protein essential for VRAC activation, since caveolin-1-α-deficient cells display extremely small $I_{Cl(swell)}$, which could be rescued by transient expression (Trouet et al., 1999). Caveolin may constitute a link between VRAC and the cytoskeleton providing a mechanical means to sense the volume expansion of the cell during swelling. In line with this model, one could argue that either caveolin expression or parts of the cytoskeleton and their distribution might limit $I_{Cl(swell)}$ amplitudes. Other putative elements of the signal transduction cascade like kinases or small GTPases are not very likely to play such a limiting role, since they can quickly process a high number of substrate molecules consecutively. The limiting effect is therefore more likely conveyed via a direct physical interaction with the LRRC8 proteins. A possible site of interaction is the leucine-rich-repeat (LRR)-containing C-terminus. LRRs have been shown to mediate protein-protein interactions (Kobe and Kajava, 2001). For LRRC8 proteins, however, no such interaction partners have been identified thus far. Therefore, it will be interesting to perform mutagenesis studies and other structure-function experiments in the C-terminus of LRRC8A and the other subunits to see whether it is possible to identify specific binding sites for a putative limiting beta subunit, which could in turn be identified via “fishing” approaches using the respective part of the C-terminus as bait.

Besides caveolin, the cAMP activated CFTR has also been suggested as interaction partner of VRAC, based on several findings: Intestinal epithelial cells from CFTR knockout mice display a defective volume regulation (Valverde et al., 1995). Furthermore, expression of the cystic fibrosis-causing mutant version of CFTR (ΔF508) significantly reduced $I_{Cl(swell)}$ in C127 epithelial cells (Xia et al., 1996). This is in

agreement with results from experiments with a CFTR antibody in T84 cells, that also show an inhibitory effect on $I_{Cl(swell)}$ (Chan et al., 1992). The CFTR hypothesis can now be tested by co-expression of CFTR (both wildytpe and mutant) and LRRC8 proteins, to see whether this modulates $I_{Cl(swell).}$ Furthermore, it will be of interest to test whether CFTR currents are changed in the LRRC8 knockout cell lines. Nevertheless, it is unlikely that CFTR is a general obligatory interaction partner of VRAC in all cell types, since its expression is mostly restricted to epithelial cells. In these cells, however, it is possible, that it has a modulatory effect on $I_{Cl(swell).}$

In summary, it cannot be excluded at this point that there is an essential beta subunit needed for proper channel function and thus limiting $I_{Cl(swell)}$ amplitudes even upon overexpression of LRRC8 heteromers. It is however also possible that the channel itself is exclusively formed by LRRC8 heteromers, while it is activated by a mechanism that involves, for example, elements of the cytoskeleton that somehow limit the number of channels that can be activated and thus determine $I_{Cl(swell)}$ amplitudes. In order to investigate these possibilities, further studies will be necessary to look for both, possible interaction partners, as well as the signal transduction cascade leading to VRAC activation.

5.9 Possible physiological significance of LRRC8 proteins

Shortly after the publication of the results of this work, two studies became available that give new insights into possible physiological roles of LRRC8 proteins.

First, a LRRC8A knockout mouse has been published by a group mainly interested in the suggested immunological function of the protein (Kumar et al., 2014). This interest is based on a reported patient mutation in LRRC8A that leads to B-cell deficiency (Sawada et al., 2003). Concerning the immunological phenotype, the authors found a modest block in B-cell development but intact B-cell function and a rather severe defect in thymus development caused by decreased proliferation and increased apoptosis of thymocytes (Kumar et al., 2014). However, their further results on the possible link between thymocyte development and LRRC8A are largely based on the assumption that the C-terminal LRRs are located on the extracellular site and function as a ligand-binding domain. Since the opposite topology of LRRC8 proteins has now been confirmed by three independent labs and methods, it is very unlikely that this hypothesis is true (Lee et al., 2014; Qiu et al., 2014; Voss et al., 2014). Besides their immunological phenotype, the *Lrrc8a*$^{-/-}$ mice displayed other very severe symptoms. They showed increased pre- and

postnatal mortality, growth retardation and abnormal morphology of several tissues. For example, they displayed vacuolation of the renal tubular cells and thinned skeletal muscle bundles. Furthermore, the few surviving mice exhibited curly hair, hind limb weakness, progressive hydronephrosis and epidermal hyperkeratosis. *Lrrc8a*$^{-/-}$ mice were also sterile. So far it is not clear how one or all of these symptoms are related to VRAC function. The very high mortality rate, already during early stages of embryogenesis but also after complete embryonic development, however, points to a pivotal role for volume-regulated chloride and/or amino acid release in survival and development. The pathology of the kidney might be a result of a strong dependence on functioning volume regulation of this organ, since it is constantly facing osmolarity changes during secretion and absorption processes at the kidney epithelium. Also, a general dependence of proliferation on volume regulation is likely since changes in cell volume are a known feature of mitosis and it has been shown that VRAC activity also varies during different cell cycle stages (Klausen et al., 2007). However, our own LRRC8 knockout cell lines did not display an apparent proliferation defect, although quantitative studies on this matter have not been performed so far. It is however possible that the proliferation of certain cell types and tissues shows a stronger dependence on VRAC activity than others, which could explain the skeletal muscle and thymus phenotype of the mice.

During development, apoptotic cell death is a crucial feature for correct organ and tissue formation. Therefore, an impairment of apoptosis through the lack of apoptotic volume decrease, that has been suggested to be mediated by VRAC, could lead to severe developmental pathologies. Besides the high embryonic lethality, the observed epidermal hyperkeratosis in surviving mice might also be the result of dysfunctional apoptosis of keratinocytes in the skin that show especially high rates of proliferation and apoptosis in newborn animals (Raj et al., 2006).

The second publication that suggests another physiological role of LRRC8 proteins deals with the protein synthesis inhibitor blasticidin S and its uptake into cells (Lee et al., 2014). In this study the authors were aiming at identifying new players in the NF-κB pathway by performing a gene trapping approach that used blasticidin S resistance as read-out (Lee et al., 2013). As a bycatch of this screen, they discovered that LRRC8D-deficient cells were resistant to blasticidin S due to a strongly reduced uptake of the drug. Based on the homology to pannexins, the authors propose that LRRC8 proteins might form complexes that mediate the uptake of solutes like blasticidin S. As already

mentioned in section 5.6 blasticidin S is a much larger molecule than halide anions or organic osmolytes like taurine and glutamate. It remains enigmatic how a channel can concomitantly show a strict anion selectivity sequence and still be permeable for such large compounds. Of course it has not yet been shown directly that amino acids or blasticidin S really permeate through a pore formed by LRRC8 heteromers. Accordingly, this question remains to be addressed in further studies.

Besides these functional studies on LRRC8A and LRRC8D, there have been a number of genetic studies in which one or several members of the *LRRC8* gene family came up, suggesting further physiological functions of the protein family.

A group interested in congenital heart disease and left-right body axis patterning found *LRRC8A* as one of the genes that showed abnormal copy number variations in patients. However, subsequently generated *Xenopus* morpholinos for *LRRC8A* did not show the expected left-right looping phenotype (Fakhro et al., 2011).

Another study focused on gene expression profiles of a specific inner ear cell line and found *LRRC8E* among the genes that were differentially higher expressed in this specific cell line (Fujimoto et al., 2010). This could suggest that LRRC8E might be the dominant LRRC8 subunit in this cell type, which would maybe alter the heteromeric composition of VRAC. This could in turn influence functional channel properties.

Another expression profiling study focused on the opposing effect of serotonin transporter (HTT) inhibition on the neonatal brain and during the depression treatment in the adult brain. The authors found that LRRC8A expression is downregulated in brain tissue from $HTT^{-/-}$ mice and upregulated in tissue from mice treated with the serotonin transporter inhibitor fluoxetine (Ichikawa et al., 2008). Interestingly, it has been shown previously that fluoxetine also inhibits VRAC at concentrations close to plasma concentrations during depression treatment with this drug (Maertens et al., 1999). Accordingly, it might be possible that a modulatory effect on $I_{Cl(swell)}$ contributes to the mode of action of this psychotherapeutic drug.

A very interesting link comes from a study that compared expression profiles of pancreatic β-cells from wildtype and transgenic mice overexpressing the serine/threonine protein kinase Akt, which is a known effector of the insulin/IGF-I signaling pathway. The authors found LRRC8C to be differentially expressed in these cells, but did not further investigate this (Gleason et al., 2010). However, with the suggested role of VRAC activity in insulin secretion (see section 1.4) this data could be an important hint towards

an involvement of LRRC8 heteromers in this process. It has to be noted, however, that the authors found that genes linked to growth, suppression of apoptosis, RNA processing, and metabolism were in general differentially expressed in the transgenic islet cells. In this context the connection to VRAC might also be via an involvement in apoptotic induction rather than in insulin secretion. Either way, it will be interesting to further investigate the role of LRRC8 heteromers in pancreatic β-cells.

Another group performed a genomics analysis of imatinib-resistant cancer cells and found alterations in the *LRRC8A* gene (Joha et al., 2011). This might point to an involvement of VRAC in proliferation, which is drastically altered in cancer cells. Another possibility is a connection to drug uptake or drug resistance (and thereby to apoptosis induction), as suggested previously (Gollapudi et al., 1992; Lee et al., 2007; Min et al., 2011).

Another connection of an *LRRC8* gene to cancer comes from a study on genetic risk factors for neutropenia and leucopenia, which are known side effects of many chemotherapeutic drugs. The authors identified genetic modifications (single nucleotide polymorphisms) in the *LRRC8B* gene in patients that had been treated with the mitotic inhibitor paclitaxel, also known as taxol, which acts through the stabilization of microtubules (Low et al., 2013). Furthermore, another study has explicitly investigated the expression of leucine-rich-repeat-containing gene families in colorectal cancer and found *LRRC8A* and *LRRC8E* to be upregulated in their cancer specimens (Piepoli et al., 2012).

Another link to apoptosis can be found in a study dealing with a model for vascular atrophy that found *LRRC8A* among the differentially expressed genes in a microarray analysis and furthermore showed that *LRRC8A* expression gets upregulated upon treatment with the apoptotic inducer Fas ligand (Kenagy et al., 2011).

A possible connection to spontaneous brain hemorrhage comes from a microarray analysis performed on patients that suffered from stroke induced by spontaneous brain bleed. The authors sought to identify genes that are up- or downregulated in the brain following this pathological event. Interestingly, they found *LRRC8B* among the strongest upregulated genes (Rosell et al., 2011). This finding is intriguing in the context of the discussed swelling-activated glutamate release during brain ischemia, which might be mediated by VRAC and could contribute immensely to the severity of this pathological state.

Finally, a recently published genomics study has aimed at investigating genes that might be regulated by vitamin D via the transcription factor vitamin D receptor (VDR). The authors found a VDR binding site in the *LRRC8A* gene and showed it to be an early response gene in monocytic cells (Wilfinger et al., 2014). The physiological role of this observation was however not further investigated in this study.

5.10 Expression pattern of LRRC8 proteins – a key to functional diversity?

A crucial point in the discussion about the molecular identity of VRAC during the past two decades has been the question whether there is actually just one type of VRAC channel or if the task of volume-regulated anion release is mediated by different channels or proteins in different tissues. The reason for this controversy are the different characteristics of $I_{Cl(swell)}$ in different tissues. For example, the pharmacological profile as well as the inactivation kinetics differs significantly between cell types. Similar discrepancies are also known for volume-regulated amino acid release as well as volume-stimulated ATP release, which both also have been discussed to be mediated by VRAC (Hisadome et al., 2002; Shennan, 2008). Furthermore, by now there have been quite a number of different substrates suggested to permeate through VRAC, from monovalent anions to amino acids and larger compounds like blasticidin S. This broad range of putative substrates also points to a high variability in channel characteristics that might even be reflected in structural diversity of the channel pore. A diversity of this kind could be provided by the many different possible heteromeric channel compositions formed by complexes of LRRC8A with LRRC8B-E. So far, it is not known whether the interaction of the LRRC8 proteins leads to the formation of a hexameric complex -as suggested by their homology to pannexins- or if it forms oligomers of more or less subunits. Depending on this, there might be a huge number of possible variations of subunit arrangements that could form an oligomeric channel. This structural diversity could then be the key to the functional variability that has been observed in many electrophysiological studies on the properties of $I_{Cl(swell)}$. For one of the variable characteristics, the inactivation kinetics, we already showed in this work that the subunit composition is the underlying cause by examining the different LRRC8 knockout cell lines and through reconstitution experiments in the *LRRC8*$^{-/-}$ cell line. We further plan to generate all combinations of triple knockout cell lines that would then just express LRRC8A and one of the other LRRC8 proteins, to investigate these effects at endogenous expression levels, since overexpression in the quintuple knockout could lead to aberrant subunit stoichiometry. In all of these cell lines it will then be possible to investigate further on the differences in

pharmacological profile, osmolyte transport and even the suggested permeation of other substances such as ATP, antibiotics or chemotherapeutic drugs. Together with further biochemical experiments to investigate the parameters of oligomerization, including subunit stoichiometry and complex size, these studies will help to elucidate the enigma of VRAC heterogeneity among different tissues. Furthermore, these findings, together with the analysis of the tissue expression levels of the different LRRC8 proteins, could uncover new physiological roles of VRAC in different cell types. Additionally, it would be of great interest to gain more insight into the structure of LRRC8 proteins and the heteromeric channel complex. However, for approaches to solve the structure of a protein or protein complex like crystallography or cryo-electron microscopy, the possible irregularity of a heteromeric channel complex might be a major obstacle. To this end, it would also be of great value to identify the specific protein domains that contribute to the formation of the pore or other essential parts for channel activity in order to create a chimeric construct that might the be able to form a functional homomeric complex. This chimeric protein could then be produced in a suitable expression system, for instance insect cells, to gain large amounts of correctly assembled heteromers which then could be subjected to crystallography. Structural information on the channel complex would then provide new information on pore size and a possible selectivity filter that might explain how substrates of different size and charge can permeate through VRAC.

In conclusion the identification of LRRC8 heteromers as an essential component of the volume-regulated anion channel provides solid grounds for future investigations of the regulatory mechanisms of VRAC activity on the molecular level. It furthermore enables structure-function studies which will elucidate the molecular basis of the observed channel properties and selectivity. Findings from these studies will provide new insights into the roles of VRAC in essential cell biological processes like cell division and apoptosis. Furthermore, the proposed involvement of the channel in (patho-) physiological processes like insulin secretion, transepithelial transport and ischemic amino acid release in the brain can now be investigated in detail. With the knowledge about the molecular identity of VRAC the search for highly specific inhibitors is also facilitated since it allows the pinpointing of binding sites within the channel protein. In summary the results of this study open up a plethora of possibilities for the investigation of VRAC activity and volume regulation in general that had been beyond the scope of ion channel research so far.

6. References

Abascal, F., and Zardoya, R. (2012). LRRC8 proteins share a common ancestor with pannexins, and may form hexameric channels involved in cell-cell communication. Bioessays *34*, 551-560.

Abascal, F., and Zardoya, R. (2013). Evolutionary analyses of gap junction protein families. Biochim Biophys Acta *1828*, 4-14.

Ackerman, M.J., Wickman, K.D., and Clapham, D.E. (1994). Hypotonicity activates a native chloride current in Xenopus oocytes. J Gen Physiol *103*, 153-179.

Akita, T., and Okada, Y. (2014). Characteristics and roles of the volume-sensitive outwardly rectifying (VSOR) anion channel in the central nervous system. Neuroscience *275C*, 211-231.

Almaca, J., Tian, Y., Aldehni, F., Ousingsawat, J., Kongsuphol, P., Rock, J.R., Harfe, B.D., Schreiber, R., and Kunzelmann, K. (2009). TMEM16 proteins produce volume-regulated chloride currents that are reduced in mice lacking TMEM16A. J Biol Chem *284*, 28571-28578.

Arreola, J., Begenisich, T., Nehrke, K., Nguyen, H.V., Park, K., Richardson, L., Yang, B., Schutte, B.C., Lamb, F.S., and Melvin, J.E. (2002). Secretion and cell volume regulation by salivary acinar cells from mice lacking expression of the Clcn3 Cl- channel gene. J Physiol *545*, 207-216.

Arvidsson, S., Kwasniewski, M., Riano-Pachon, D.M., and Mueller-Roeber, B. (2008). QuantPrime--a flexible tool for reliable high-throughput primer design for quantitative PCR. BMC bioinformatics *9*, 465.

Banderali, U., and Roy, G. (1992). Anion channels for amino acids in MDCK cells. Am J Physiol *263*, C1200-1207.

Bausch, A.R., and Roy, G. (1996). Volume-sensitive chloride channels blocked by neuroprotective drugs in human glial cells (U-138MG). Glia *18*, 73-77.

Beneski, D.A., and Catterall, W.A. (1980). Covalent labeling of protein components of the sodium channel with a photoactivable derivative of scorpion toxin. Proc Natl Acad Sci U S A *77*, 639-643.

Benfenati, V., Caprini, M., Nicchia, G.P., Rossi, A., Dovizio, M., Cervetto, C., Nobile, M., and Ferroni, S. (2009). Carbenoxolone inhibits volume-regulated anion conductance in cultured rat cortical astroglia. Channels (Austin) *3*, 323-336.

Best, L., Brown, P.D., Sener, A., and Malaisse, W.J. (2010). Electrical activity in pancreatic islet cells: The VRAC hypothesis. Islets *2*, 59-64.

Birkenhager, R., Prera, N., Aschendorff, A., Laszig, R., and Arndt, S. (2014). A novel homozygous mutation in the EC1/EC2 interaction domain of the gap junction complex connexon 26 leads to profound hearing impairment. BioMed research international *2014*, 307976.

Bond, S.R., and Naus, C.C. (2014). The pannexins: past and present. Frontiers in physiology *5*, 58.

Bowens, N.H., Dohare, P., Kuo, Y.H., and Mongin, A.A. (2013). DCPIB, the proposed selective blocker of volume-regulated anion channels, inhibits several glutamate transport pathways in glial cells. Molecular pharmacology *83*, 22-32.

Brattain, M.G., Fine, W.D., Khaled, F.M., Thompson, J., and Brattain, D.E. (1981). Heterogeneity of malignant cells from a human colonic carcinoma. Cancer research *41*, 1751-1756.

Brevnova, E.E., Platoshyn, O., Zhang, S., and Yuan, J.X. (2004). Overexpression of human KCNA5 increases IK V and enhances apoptosis. Am J Physiol Cell Physiol *287*, C715-722.

Browe, D.M., and Baumgarten, C.M. (2003). Stretch of beta 1 integrin activates an outwardly rectifying chloride current via FAK and Src in rabbit ventricular myocytes. J Gen Physiol *122*, 689-702.

Browe, D.M., and Baumgarten, C.M. (2004). Angiotensin II (AT1) receptors and NADPH oxidase regulate Cl- current elicited by beta1 integrin stretch in rabbit ventricular myocytes. J Gen Physiol *124*, 273-287.

Browe, D.M., and Baumgarten, C.M. (2006). EGFR kinase regulates volume-sensitive chloride current elicited by integrin stretch via PI-3K and NADPH oxidase in ventricular myocytes. J Gen Physiol *127*, 237-251.

Burg, M.B., and Ferraris, J.D. (2008). Intracellular organic osmolytes: function and regulation. J Biol Chem *283*, 7309-7313.

Canessa, C.M., Horisberger, J.D., and Rossier, B.C. (1993). Epithelial sodium channel related to proteins involved in neurodegeneration. Nature *361*, 467-470.

Cannon, C.L., Basavappa, S., and Strange, K. (1998). Intracellular ionic strength regulates the volume sensitivity of a swelling-activated anion channel. Am J Physiol *275*, C416-422.

Capo-Aponte, J.E., Iserovich, P., and Reinach, P.S. (2005). Characterization of regulatory volume behavior by fluorescence quenching in human corneal epithelial cells. J Membr Biol *207*, 11-22.

Caputo, A., Caci, E., Ferrera, L., Pedemonte, N., Barsanti, C., Sondo, E., Pfeffer, U., Ravazzolo, R., Zegarra-Moran, O., and Galietta, L.J. (2008). TMEM16A, a membrane protein associated with calcium-dependent chloride channel activity. Science *322*, 590-594.

Carton, I., Trouet, D., Hermans, D., Barth, H., Aktories, K., Droogmans, G., Jorgensen, N.K., Hoffmann, E.K., Nilius, B., and Eggermont, J. (2002). RhoA exerts a permissive effect on volume-regulated anion channels in vascular endothelial cells. Am J Physiol Cell Physiol *283*, C115-125.

Chan, H.C., Kaetzel, M.A., Nelson, D.J., Hazarika, P., and Dedman, J.R. (1992). Antibody against a cystic fibrosis transmembrane conductance regulator-derived synthetic peptide inhibits anion currents in human colonic cell line T84. J Biol Chem *267*, 8411-8416.

Chandrasekhar, K.D., Bas, T., and Kobertz, W.R. (2006). KCNE1 subunits require co-assembly with K+ channels for efficient trafficking and cell surface expression. J Biol Chem *281*, 40015-40023.

Chien, L.T., and Hartzell, H.C. (2007). Drosophila bestrophin-1 chloride current is dually regulated by calcium and cell volume. J Gen Physiol *130*, 513-524.

Chien, L.T., and Hartzell, H.C. (2008). Rescue of volume-regulated anion current by bestrophin mutants with altered charge selectivity. J Gen Physiol *132*, 537-546.

Chou, C.Y., Shen, M.R., and Wu, S.N. (1995). Volume-sensitive chloride channels associated with human cervical carcinogenesis. Cancer research *55*, 6077-6083.

Christensen, O., and Hoffmann, E.K. (1992). Cell swelling activates K+ and Cl- channels as well as nonselective, stretch-activated cation channels in Ehrlich ascites tumor cells. J Membr Biol *129*, 13-36.

Collins, S.J., Gallo, R.C., and Gallagher, R.E. (1977). Continuous growth and differentiation of human myeloid leukaemic cells in suspension culture. Nature *270*, 347-349.

Cong, L., Ran, F.A., Cox, D., Lin, S., Barretto, R., Habib, N., Hsu, P.D., Wu, X., Jiang, W., Marraffini, L.A., *et al.* (2013). Multiplex genome engineering using CRISPR/Cas systems. Science *339*, 819-823.

Coste, B., Mathur, J., Schmidt, M., Earley, T.J., Ranade, S., Petrus, M.J., Dubin, A.E., and Patapoutian, A. (2010). Piezo1 and Piezo2 are essential components of distinct mechanically activated cation channels. Science *330*, 55-60.

Culliford, S.J., Borg, J.J., O'Brien, M.J., and Kozlowski, R.Z. (2004). Differential effects of pyrethroids on volume-sensitive anion and organic osmolyte pathways. Clinical and experimental pharmacology & physiology *31*, 134-144.

D'Hondt, C., Ponsaerts, R., De Smedt, H., Bultynck, G., and Himpens, B. (2009). Pannexins, distant relatives of the connexin family with specific cellular functions? Bioessays *31*, 953-974.

Decher, N., Lang, H.J., Nilius, B., Bruggemann, A., Busch, A.E., and Steinmeyer, K. (2001). DCPIB is a novel selective blocker of I(Cl,swell) and prevents swelling-induced shortening of guinea-pig atrial action potential duration. Br J Pharmacol *134*, 1467-1479.

Do, C.W., and Civan, M.M. (2006). Swelling-activated chloride channels in aqueous humour formation: on the one side and the other. Acta Physiol (Oxf) *187*, 345-352.

Doroshenko, P. (1991). Second messengers mediating activation of chloride current by intracellular GTP gamma S in bovine chromaffin cells. J Physiol *436*, 725-738.

Doroshenko, P., Sabanov, V., and Doroshenko, N. (2001). Cell cycle-related changes in regulatory volume decrease and volume-sensitive chloride conductance in mouse fibroblasts. J Cell Physiol *187*, 65-72.

Du, X.L., Gao, Z., Lau, C.P., Chiu, S.W., Tse, H.F., Baumgarten, C.M., and Li, G.R. (2004). Differential effects of tyrosine kinase inhibitors on volume-sensitive chloride current in human atrial myocytes: evidence for dual regulation by Src and EGFR kinases. J Gen Physiol *123*, 427-439.

Duan, D., Cowley, S., Horowitz, B., and Hume, J.R. (1999). A serine residue in ClC-3 links phosphorylation-dephosphorylation to chloride channel regulation by cell volume. J Gen Physiol *113*, 57-70.

Duan, D., Winter, C., Cowley, S., Hume, J.R., and Horowitz, B. (1997). Molecular identification of a volume-regulated chloride channel. Nature *390*, 417-421.

Eertmoed, A.L., Vallejo, Y.F., and Green, W.N. (1998). Transient expression of heteromeric ion channels. Methods in enzymology *293*, 564-585.

Fakhro, K.A., Choi, M., Ware, S.M., Belmont, J.W., Towbin, J.A., Lifton, R.P., Khokha, M.K., and Brueckner, M. (2011). Rare copy number variations in congenital heart disease patients identify unique genes in left-right patterning. Proc Natl Acad Sci U S A *108*, 2915-2920.

Feustel, P.J., Jin, Y., and Kimelberg, H.K. (2004). Volume-regulated anion channels are the predominant contributors to release of excitatory amino acids in the ischemic cortical penumbra. Stroke; a journal of cerebral circulation *35*, 1164-1168.

Fields, R.D., and Ni, Y. (2010). Nonsynaptic communication through ATP release from volume-activated anion channels in axons. Science signaling *3*, ra73.

Fischmeister, R., and Hartzell, H.C. (2005). Volume sensitivity of the bestrophin family of chloride channels. J Physiol *562*, 477-491.

Foote, C.I., Zhou, L., Zhu, X., and Nicholson, B.J. (1998). The pattern of disulfide linkages in the extracellular loop regions of connexin 32 suggests a model for the docking interface of gap junctions. J Cell Biol *140*, 1187-1197.

Frech, G.C., VanDongen, A.M., Schuster, G., Brown, A.M., and Joho, R.H. (1989). A novel potassium channel with delayed rectifier properties isolated from rat brain by expression cloning. Nature *340*, 642-645.

Fujimoto, C., Ozeki, H., Uchijima, Y., Suzukawa, K., Mitani, A., Fukuhara, S., Nishiyama, K., Kurihara, Y., Kondo, K., Aburatani, H., *et al.* (2010). Establishment of mice expressing EGFP in the placode-derived inner ear sensory cell lineage and FACS-array analysis focused on the regional specificity of the otocyst. The Journal of comparative neurology *518*, 4702-4722.

Fürst, J., Bazzini, C., Jakab, M., Meyer, G., Konig, M., Gschwentner, M., Ritter, M., Schmarda, A., Botta, G., Benz, R., *et al.* (2000). Functional reconstitution of ICln in lipid bilayers. Pflügers Arch *440*, 100-115.

Galietta, L.J., Falzoni, S., Di Virgilio, F., Romeo, G., and Zegarra-Moran, O. (1997). Characterization of volume-sensitive taurine- and Cl(-)-permeable channels. Am J Physiol *273*, C57-66.

Galietta, L.J., Haggie, P.M., and Verkman, A.S. (2001). Green fluorescent protein-based halide indicators with improved chloride and iodide affinities. FEBS Lett *499*, 220-224.

Gamba, G. (2005). Molecular physiology and pathophysiology of electroneutral cation-chloride cotransporters. Physiological reviews *85*, 423-493.

Gey, G.O., Coffman, W.D., and Kubicek, M.T. (1952). Tissue culture studies of the prliferative capacity of cervical cacinoma and normal epithelium. Cancer research *12*, 264-265.

Gill, D.R., Hyde, S.C., Higgins, C.F., Valverde, M.A., Mintenig, G.M., and Sepulveda, F.V. (1992). Separation of drug transport and chloride channel functions of the human multidrug resistance P-glycoprotein. Cell *71*, 23-32.

Gleason, C.E., Ning, Y., Cominski, T.P., Gupta, R., Kaestner, K.H., Pintar, J.E., and Birnbaum, M.J. (2010). Role of insulin-like growth factor-binding protein 5 (IGFBP5) in organismal and pancreatic beta-cell growth. Mol Endocrinol *24*, 178-192.

Gollapudi, S., McDonald, T., Gardner, P., Kang, N., and Gupta, S. (1992). Abnormal chloride conductance in multidrug resistant HL60/AR cells. Cancer letters *66*, 83-89.

Gong, W., Xu, H., Shimizu, T., Morishima, S., Tanabe, S., Tachibe, T., Uchida, S., Sasaki, S., and Okada, Y. (2004). ClC-3-independent, PKC-dependent activity of volume-sensitive Cl channel in mouse ventricular cardiomyocytes. Cell Physiol Biochem *14*, 213-224.

Gosling, M., Smith, J.W., and Poyner, D.R. (1995). Characterization of a volume-sensitive chloride current in rat osteoblast-like (ROS 17/2.8) cells. J Physiol *485 (Pt 3)*, 671-682.

Gottesman, M.M., and Pastan, I. (1993). Biochemistry of multidrug resistance mediated by the multidrug transporter. Annual review of biochemistry *62*, 385-427.

Graf, G.A., Yu, L., Li, W.P., Gerard, R., Tuma, P.L., Cohen, J.C., and Hobbs, H.H. (2003). ABCG5 and ABCG8 are obligate heterodimers for protein trafficking and biliary cholesterol excretion. J Biol Chem *278*, 48275-48282.

Graham, F.L., Smiley, J., Russell, W.C., and Nairn, R. (1977). Characteristics of a human cell line transformed by DNA from human adenovirus type 5. The Journal of general virology *36*, 59-74.

Gründer, S., Thiemann, A., Pusch, M., and Jentsch, T.J. (1992). Regions involved in the opening of CIC-2 chloride channel by voltage and cell volume. Nature *360*, 759-762.

Gschwentner, M., Nagl, U.O., Woll, E., Schmarda, A., Ritter, M., and Paulmichl, M. (1995). Antisense oligonucleotides suppress cell-volume-induced activation of chloride channels. Pflügers Arch *430*, 464-470.

Hardy, S.P., Goodfellow, H.R., Valverde, M.A., Gill, D.R., Sepulveda, V., and Higgins, C.F. (1995). Protein kinase C-mediated phosphorylation of the human multidrug resistance P-glycoprotein regulates cell volume-activated chloride channels. EMBO J *14*, 68-75.

Harrigan, T.J., Abdullaev, I.F., Jourd'heuil, D., and Mongin, A.A. (2008). Activation of microglia with zymosan promotes excitatory amino acid release via volume-regulated anion channels: the role of NADPH oxidases. J Neurochem *106*, 2449-2462.

Hayashi, T., Nozaki, Y., Nishizuka, M., Ikawa, M., Osada, S., and Imagawa, M. (2011). Factor for adipocyte differentiation 158 gene disruption prevents the body weight gain and insulin resistance induced by a high-fat diet. Biological & pharmaceutical bulletin *34*, 1257-1263.

Hazama, A., and Okada, Y. (1988). Ca2+ sensitivity of volume-regulatory K+ and Cl- channels in cultured human epithelial cells. J Physiol *402*, 687-702.

Helix, N., Strobaek, D., Dahl, B.H., and Christophersen, P. (2003). Inhibition of the endogenous volume-regulated anion channel (VRAC) in HEK293 cells by acidic di-aryl-ureas. J Membr Biol *196*, 83-94.

Hernandez-Carballo, C.Y., De Santiago-Castillo, J.A., Rosales-Saavedra, T., Perez-Cornejo, P., and Arreola, J. (2010). Control of volume-sensitive chloride channel inactivation by the coupled action of intracellular chloride and extracellular protons. Pflügers Arch *460*, 633-644.

Hisadome, K., Koyama, T., Kimura, C., Droogmans, G., Ito, Y., and Oike, M. (2002). Volume-regulated anion channels serve as an auto/paracrine nucleotide release pathway in aortic endothelial cells. J Gen Physiol *119*, 511-520.

Hoffmann, E.K. (2011). Ion channels involved in cell volume regulation: effects on migration, proliferation, and programmed cell death in non adherent EAT cells and adherent ELA cells. Cell Physiol Biochem *28*, 1061-1078.

Hoffmann, E.K., Lambert, I.H., and Pedersen, S.F. (2009). Physiology of cell volume regulation in vertebrates. Physiological reviews *89*, 193-277.

Hoffmann, E.K., Lambert, I.H., and Simonsen, L.O. (1986). Separate, Ca2+-activated K+ and Cl- transport pathways in Ehrlich ascites tumor cells. J Membr Biol *91*, 227-244.

Hoffmann, E.K., and Pedersen, S.F. (2006). Sensors and signal transduction pathways in vertebrate cell volume regulation. Contrib Nephrol *152*, 54-104.

Hoffmann, E.K., Schettino, T., and Marshall, W.S. (2007). The role of volume-sensitive ion transport systems in regulation of epithelial transport. Comparative biochemistry and physiology Part A, Molecular & integrative physiology *148*, 29-43.

Hoffmann, E.K., and Simonsen, L.O. (1989). Membrane mechanisms in volume and pH regulation in vertebrate cells. Physiological reviews *69*, 315-382.

Hofmann, T., Schaefer, M., Schultz, G., and Gudermann, T. (2002). Subunit composition of mammalian transient receptor potential channels in living cells. Proc Natl Acad Sci U S A *99*, 7461-7466.

Ichikawa, M., Okamura-Oho, Y., Shimokawa, K., Kondo, S., Nakamura, S., Yokota, H., Himeno, R., Lesch, K.P., and Hayashizaki, Y. (2008). Expression analysis for inverted effects of serotonin transporter inactivation. Biochem Biophys Res Commun *368*, 43-49.

Inoue, H., Ohtaki, H., Nakamachi, T., Shioda, S., and Okada, Y. (2007). Anion channel blockers attenuate delayed neuronal cell death induced by transient forebrain ischemia. Journal of neuroscience research *85*, 1427-1435.

Jackson, P.S., and Strange, K. (1993). Volume-sensitive anion channels mediate swelling-activated inositol and taurine efflux. Am J Physiol *265*, C1489-1500.

Jackson, P.S., and Strange, K. (1995). Characterization of the voltage-dependent properties of a volume-sensitive anion conductance. J Gen Physiol *105*, 661-676.

Jakab, M., and Ritter, M. (2006). Cell volume regulatory ion transport in the regulation of cell migration. Contrib Nephrol *152*, 161-180.

Jentsch, T.J., Stein, V., Weinreich, F., and Zdebik, A.A. (2002). Molecular structure and physiological function of chloride channels. Physiological reviews *82*, 503-568.

Jiao, J.D., Xu, C.Q., Yue, P., Dong, D.L., Li, Z., Du, Z.M., and Yang, B.F. (2006). Volume-sensitive outwardly rectifying chloride channels are involved in oxidative stress-induced apoptosis of mesangial cells. Biochem Biophys Res Commun *340*, 277-285.

Joha, S., Dauphin, V., Lepretre, F., Corm, S., Nicolini, F.E., Roumier, C., Nibourel, O., Grardel, N., Maguer-Satta, V., Idziorek, T., *et al.* (2011). Genomic characterization of Imatinib resistance in CD34+ cell populations from chronic myeloid leukaemia patients. Leukemia research *35*, 448-458.

Jordt, S.E., and Jentsch, T.J. (1997). Molecular dissection of gating in the ClC-2 chloride channel. EMBO J *16*, 1582-1592.

Juul, C.A., Grubb, S., Poulsen, K.A., Kyed, T., Hashem, N., Lambert, I.H., Larsen, E.H., and Hoffmann, E.K. (2014). Anoctamin 6 differs from VRAC and VSOAC but is involved in apoptosis and supports volume regulation in the presence of Ca. Pflügers Arch.

Kawasaki, M., Uchida, S., Monkawa, T., Miyawaki, A., Mikoshiba, K., Marumo, F., and Sasaki, S. (1994). Cloning and expression of a protein kinase C-regulated chloride channel abundantly expressed in rat brain neuronal cells. Neuron *12*, 597-604.

Kenagy, R.D., Min, S.K., Mulvihill, E., and Clowes, A.W. (2011). A link between smooth muscle cell death and extracellular matrix degradation during vascular atrophy. Journal of vascular surgery *54*, 182-191 e124.

Kimelberg, H.K. (2005). Astrocytic swelling in cerebral ischemia as a possible cause of injury and target for therapy. Glia *50*, 389-397.

Kirk, J., and Kirk, K. (1994). Inhibition of volume-activated I- and taurine efflux from HeLa cells by P-glycoprotein blockers correlates with calmodulin inhibition. J Biol Chem *269*, 29389-29394.

Kirk, K., Ellory, J.C., and Young, J.D. (1992). Transport of organic substrates via a volume-activated channel. J Biol Chem *267*, 23475-23478.

Kirk, K., and Kirk, J. (1993). Volume-regulatory taurine release from a human lung cancer cell line. Evidence for amino acid transport via a volume-activated chloride channel. FEBS Lett *336*, 153-158.

Klausen, T.K., Bergdahl, A., Hougaard, C., Christophersen, P., Pedersen, S.F., and Hoffmann, E.K. (2007). Cell cycle-dependent activity of the volume- and Ca2+-activated anion currents in Ehrlich lettre ascites cells. J Cell Physiol *210*, 831-842.

Klausen, T.K., Hougaard, C., Hoffmann, E.K., and Pedersen, S.F. (2006). Cholesterol modulates the volume-regulated anion current in Ehrlich-Lettre ascites cells via effects on Rho and F-actin. Am J Physiol Cell Physiol *291*, C757-771.

Kobe, B., and Deisenhofer, J. (1995). A structural basis of the interactions between leucine-rich repeats and protein ligands. Nature *374*, 183-186.

Kobe, B., and Kajava, A.V. (2001). The leucine-rich repeat as a protein recognition motif. Current opinion in structural biology *11*, 725-732.

Koyama, T., Oike, M., and Ito, Y. (2001). Involvement of Rho-kinase and tyrosine kinase in hypotonic stress-induced ATP release in bovine aortic endothelial cells. J Physiol *532*, 759-769.

Krapivinsky, G.B., Ackerman, M.J., Gordon, E.A., Krapivinsky, L.D., and Clapham, D.E. (1994). Molecular characterization of a swelling-induced chloride conductance regulatory protein, pICln. Cell *76*, 439-448.

Krogh, A., Larsson, B., von Heijne, G., and Sonnhammer, E.L. (2001). Predicting transmembrane protein topology with a hidden Markov model: application to complete genomes. Journal of molecular biology *305*, 567-580.

Kubo, M., and Okada, Y. (1992). Volume-regulatory Cl- channel currents in cultured human epithelial cells. J Physiol *456*, 351-371.

Kubota, K., Kim, J.Y., Sawada, A., Tokimasa, S., Fujisaki, H., Matsuda-Hashii, Y., Ozono, K., and Hara, J. (2004). LRRC8 involved in B cell development belongs to a novel family of leucine-rich repeat proteins. FEBS Lett *564*, 147-152.

Kumar, L., Chou, J., Yee, C.S., Borzutzky, A., Vollmann, E.H., von Andrian, U.H., Park, S.Y., Hollander, G., Manis, J.P., Poliani, P.L., *et al.* (2014). Leucine-rich repeat containing 8A (LRRC8A) is essential for T lymphocyte development and function. J Exp Med *211*, 929-942.

Lambert, I.H. (2004). Regulation of the cellular content of the organic osmolyte taurine in mammalian cells. Neurochemical research *29*, 27-63.

Lambert, I.H., Hoffmann, E.K., and Pedersen, S.F. (2008). Cell volume regulation: physiology and pathophysiology. Acta Physiol (Oxf) *194*, 255-282.

Lang, F. (2007). Mechanisms and significance of cell volume regulation. Journal of the American College of Nutrition *26*, 613S-623S.

Lang, F., and Hoffmann, E.K. (2012). Role of ion transport in control of apoptotic cell death. Comprehensive Physiology *2*, 2037-2061.

Lang, F., Madlung, J., Siemen, D., Ellory, C., Lepple-Wienhues, A., and Gulbins, E. (2000). The involvement of caspases in the CD95(Fas/Apo-1)- but not swelling-induced cellular taurine release from Jurkat T-lymphocytes. Pflügers Arch *440*, 93-99.

Lang, F., Shumilina, E., Ritter, M., Gulbins, E., Vereninov, A., and Huber, S.M. (2006). Ion channels and cell volume in regulation of cell proliferation and apoptotic cell death. Contrib Nephrol *152*, 142-160.

Lange, P.F., Wartosch, L., Jentsch, T.J., and Fuhrmann, J.C. (2006). ClC-7 requires Ostm1 as a beta-subunit to support bone resorption and lysosomal function. Nature *440*, 220-223.

Leaney, J.L., Marsh, S.J., and Brown, D.A. (1997). A swelling-activated chloride current in rat sympathetic neurones. J Physiol *501 (Pt 3)*, 555-564.

Lee, C.C., Carette, J.E., Brummelkamp, T.R., and Ploegh, H.L. (2013). A reporter screen in a human haploid cell line identifies CYLD as a constitutive inhibitor of NF-kappaB. PLoS One *8*, e70339.

Lee, C.C., Freinkman, E., Sabatini, D.M., and Ploegh, H.L. (2014). The Protein Synthesis Inhibitor Blasticidin S Enters Mammalian Cells via Leucine-Rich Repeat-Containing Protein 8D. J Biol Chem.

Lee, E.L., Shimizu, T., Ise, T., Numata, T., Kohno, K., and Okada, Y. (2007). Impaired activity of volume-sensitive Cl- channel is involved in cisplatin resistance of cancer cells. J Cell Physiol *211*, 513-521.

Lepple-Wienhues, A., Szabo, I., Laun, T., Kaba, N.K., Gulbins, E., and Lang, F. (1998). The tyrosine kinase p56lck mediates activation of swelling-induced chloride channels in lymphocytes. J Cell Biol *141*, 281-286.

Levitan, I., Almonte, C., Mollard, P., and Garber, S.S. (1995). Modulation of a volume-regulated chloride current by F-actin. J Membr Biol *147*, 283-294.

Levitan, I., Christian, A.E., Tulenko, T.N., and Rothblat, G.H. (2000). Membrane cholesterol content modulates activation of volume-regulated anion current in bovine endothelial cells. J Gen Physiol *115*, 405-416.

Li, C., Breton, S., Morrison, R., Cannon, C.L., Emma, F., Sanchez-Olea, R., Bear, C., and Strange, K. (1998). Recombinant pICln forms highly cation-selective channels when reconstituted into artificial and biological membranes. J Gen Physiol *112*, 727-736.

Liu, H.T., Akita, T., Shimizu, T., Sabirov, R.Z., and Okada, Y. (2009). Bradykinin-induced astrocyte-neuron signalling: glutamate release is mediated by ROS-activated volume-sensitive outwardly rectifying anion channels. J Physiol *587*, 2197-2209.

Liu, H.T., Tashmukhamedov, B.A., Inoue, H., Okada, Y., and Sabirov, R.Z. (2006). Roles of two types of anion channels in glutamate release from mouse astrocytes under ischemic or osmotic stress. Glia *54*, 343-357.

Lopes, T.J., Schaefer, M., Shoemaker, J., Matsuoka, Y., Fontaine, J.F., Neumann, G., Andrade-Navarro, M.A., Kawaoka, Y., and Kitano, H. (2011). Tissue-specific subnetworks and characteristics of publicly available human protein interaction databases. Bioinformatics *27*, 2414-2421.

Low, S.K., Chung, S., Takahashi, A., Zembutsu, H., Mushiroda, T., Kubo, M., and Nakamura, Y. (2013). Genome-wide association study of chemotherapeutic agent-induced severe neutropenia/leucopenia for patients in Biobank Japan. Cancer science *104*, 1074-1082.

Maeno, E., Ishizaki, Y., Kanaseki, T., Hazama, A., and Okada, Y. (2000). Normotonic cell shrinkage because of disordered volume regulation is an early prerequisite to apoptosis. Proc Natl Acad Sci U S A *97*, 9487-9492.

Maertens, C., Droogmans, G., Chakraborty, P., and Nilius, B. (2001). Inhibition of volume-regulated anion channels in cultured endothelial cells by the anti-oestrogens clomiphene and nafoxidine. Br J Pharmacol *132*, 135-142.

Maertens, C., Wei, L., Voets, T., Droogmans, G., and Nilius, B. (1999). Block by fluoxetine of volume-regulated anion channels. Br J Pharmacol *126*, 508-514.

Magrane, M., and Consortium, U. (2011). UniProt Knowledgebase: a hub of integrated protein data. Database : the journal of biological databases and curation *2011*, bar009.

Mali, P., Yang, L., Esvelt, K.M., Aach, J., Guell, M., DiCarlo, J.E., Norville, J.E., and Church, G.M. (2013). RNA-guided human genome engineering via Cas9. Science *339*, 823-826.

Mao, J., Wang, L., Fan, A., Wang, J., Xu, B., Jacob, T.J., and Chen, L. (2007). Blockage of volume-activated chloride channels inhibits migration of nasopharyngeal carcinoma cells. Cell Physiol Biochem *19*, 249-258.

Min, X.J., Li, H., Hou, S.C., He, W., Liu, J., Hu, B., and Wang, J. (2011). Dysfunction of volume-sensitive chloride channels contributes to cisplatin resistance in human lung adenocarcinoma cells. Exp Biol Med (Maywood) *236*, 483-491.

Mitchell, C.H., Wang, L., and Jacob, T.J. (1997). A large-conductance chloride channel in pigmented ciliary epithelial cells activated by GTPgammaS. J Membr Biol *158*, 167-175.

Mongin, A.A., and Kimelberg, H.K. (2002). ATP potently modulates anion channel-mediated excitatory amino acid release from cultured astrocytes. Am J Physiol Cell Physiol *283*, C569-578.

Morin, X.K., Bond, T.D., Loo, T.W., Clarke, D.M., and Bear, C.E. (1995). Failure of P-glycoprotein (MDR1) expressed in Xenopus oocytes to produce swelling-activated chloride channel activity. J Physiol *486 (Pt 3)*, 707-714.

Morishima, S., Shimizu, T., Kida, H., and Okada, Y. (2000). Volume expansion sensitivity of swelling-activated Cl(-) channel in human epithelial cells. The Japanese journal of physiology *50*, 277-280.

Nilius, B., and Droogmans, G. (2003). Amazing chloride channels: an overview. Acta Physiol Scand *177*, 119-147.

Nilius, B., Eggermont, J., Voets, T., Buyse, G., Manolopoulos, V., and Droogmans, G. (1997a). Properties of volume-regulated anion channels in mammalian cells. Prog Biophys Mol Biol *68*, 69-119.

Nilius, B., Gerke, V., Prenen, J., Szucs, G., Heinke, S., Weber, K., and Droogmans, G. (1996). Annexin II modulates volume-activated chloride currents in vascular endothelial cells. The Journal of biological chemistry *271*, 30631-30636.

Nilius, B., Oike, M., Zahradnik, I., and Droogmans, G. (1994a). Activation of a Cl- current by hypotonic volume increase in human endothelial cells. J Gen Physiol *103*, 787-805.

Nilius, B., Prenen, J., and Droogmans, G. (1998). Modulation of volume-regulated anion channels by extra- and intracellular pH. Pflügers Arch *436*, 742-748.

Nilius, B., Prenen, J., Kamouchi, M., Viana, F., Voets, T., and Droogmans, G. (1997b). Inhibition by mibefradil, a novel calcium channel antagonist, of Ca(2+)- and volume-activated Cl- channels in macrovascular endothelial cells. Br J Pharmacol *121*, 547-555.

Nilius, B., Prenen, J., Walsh, M.P., Carton, I., Bollen, M., Droogmans, G., and Eggermont, J. (2000). Myosin light chain phosphorylation-dependent modulation of volume-regulated anion channels in macrovascular endothelium. FEBS Lett *466*, 346-350.

Nilius, B., Sehrer, J., Viana, F., De Greef, C., Raeymaekers, L., Eggermont, J., and Droogmans, G. (1994b). Volume-activated Cl- currents in different mammalian non-excitable cell types. Pflügers Arch *428*, 364-371.

Nilius, B., Voets, T., Prenen, J., Barth, H., Aktories, K., Kaibuchi, K., Droogmans, G., and Eggermont, J. (1999). Role of Rho and Rho kinase in the activation of volume-regulated anion channels in bovine endothelial cells. J Physiol *516 (Pt 1)*, 67-74.

Oiki, S., Kubo, M., and Okada, Y. (1994). Mg2+ and ATP-dependence of volume-sensitive Cl- channels in human epithelial cells. The Japanese journal of physiology *44 Suppl 2*, S77-79.

Okada, Y. (1997). Volume expansion-sensing outward-rectifier Cl- channel: fresh start to the molecular identity and volume sensor. Am J Physiol *273*, C755-789.

Okada, Y. (2006). Cell volume-sensitive chloride channels: phenotypic properties and molecular identity. Contrib Nephrol *152*, 9-24.

Okada, Y., Maeno, E., and Mori, S. (2004). Anion channel involved in induction of apoptosis and necrosis. Advances in experimental medicine and biology *559*, 205-209.

Okada, Y., Sato, K., and Numata, T. (2009). Pathophysiology and puzzles of the volume-sensitive outwardly rectifying anion channel. J Physiol *587*, 2141-2149.

Olsen, J.V., Blagoev, B., Gnad, F., Macek, B., Kumar, C., Mortensen, P., and Mann, M. (2006). Global, in vivo, and site-specific phosphorylation dynamics in signaling networks. Cell *127*, 635-648.

Orlov, S.N., Platonova, A.A., Hamet, P., and Grygorczyk, R. (2013). Cell volume and monovalent ion transporters: their role in cell death machinery triggering and progression. Am J Physiol Cell Physiol *305*, C361-372.

Papageorgiou, A.C., Shapiro, R., and Acharya, K.R. (1997). Molecular recognition of human angiogenin by placental ribonuclease inhibitor--an X-ray crystallographic study at 2.0 A resolution. EMBO J *16*, 5162-5177.

Paulmichl, M., Li, Y., Wickman, K., Ackerman, M., Peralta, E., and Clapham, D. (1992). New mammalian chloride channel identified by expression cloning. Nature *356*, 238-241.

Pedemonte, N., and Galietta, L.J. (2014). Structure and function of TMEM16 proteins (anoctamins). Physiological reviews *94*, 419-459.

Pedersen, S.F., Beisner, K.H., Hougaard, C., Willumsen, B.M., Lambert, I.H., and Hoffmann, E.K. (2002). Rho family GTP binding proteins are involved in the regulatory volume decrease process in NIH3T3 mouse fibroblasts. J Physiol *541*, 779-796.

Pedersen, S.F., Hoffmann, E.K., and Novak, I. (2013). Cell volume regulation in epithelial physiology and cancer. Frontiers in physiology *4*, 233.

Piepoli, A., Palmieri, O., Maglietta, R., Panza, A., Cattaneo, E., Latiano, A., Laczko, E., Gentile, A., Carella, M., Mazzoccoli, G., *et al.* (2012). The expression of leucine-rich repeat gene family members in colorectal cancer. Exp Biol Med (Maywood) *237*, 1123-1128.

Poulsen, K.A., Andersen, E.C., Hansen, C.F., Klausen, T.K., Hougaard, C., Lambert, I.H., and Hoffmann, E.K. (2010). Deregulation of apoptotic volume decrease and ionic movements in multidrug-resistant tumor cells: role of chloride channels. Am J Physiol Cell Physiol *298*, C14-25.

Prusty, B.K., Karlas, A., Meyer, T.F., and Rudel, T. (2011). Genome-wide RNAi screen for viral replication in mammalian cell culture. Methods Mol Biol *721*, 383-395.

Pu, W.T., Krapivinsky, G.B., Krapivinsky, L., and Clapham, D.E. (1999). pICln inhibits snRNP biogenesis by binding core spliceosomal proteins. Molecular and cellular biology *19*, 4113-4120.

Qiu, F., Wang, J., and Dahl, G. (2012). Alanine substitution scanning of pannexin1 reveals amino acid residues mediating ATP sensitivity. Purinergic signalling *8*, 81-90.

Qiu, Z., Dubin, A.E., Mathur, J., Tu, B., Reddy, K., Miraglia, L.J., Reinhardt, J., Orth, A.P., and Patapoutian, A. (2014). SWELL1, a plasma membrane protein, is an essential component of volume-regulated anion channel. Cell *157*, 447-458.

Raj, D., Brash, D.E., and Grossman, D. (2006). Keratinocyte apoptosis in epidermal development and disease. The Journal of investigative dermatology *126*, 243-257.

Rhoads, A.R., and Friedberg, F. (1997). Sequence motifs for calmodulin recognition. FASEB J *11*, 331-340.

Rigbolt, K.T., Prokhorova, T.A., Akimov, V., Henningsen, J., Johansen, P.T., Kratchmarova, I., Kassem, M., Mann, M., Olsen, J.V., and Blagoev, B. (2011). System-wide temporal characterization of the proteome and phosphoproteome of human embryonic stem cell differentiation. Science signaling *4*, rs3.

Romanenko, V.G., Rothblat, G.H., and Levitan, I. (2004). Sensitivity of volume-regulated anion current to cholesterol structural analogues. J Gen Physiol *123*, 77-87.

Rosell, A., Vilalta, A., Garcia-Berrocoso, T., Fernandez-Cadenas, I., Domingues-Montanari, S., Cuadrado, E., Delgado, P., Ribo, M., Martinez-Saez, E., Ortega-Aznar, A., *et al.* (2011). Brain perihematoma genomic profile following spontaneous human intracerebral hemorrhage. PLoS One *6*, e16750.

Roy, G. (1995). Amino acid current through anion channels in cultured human glial cells. J Membr Biol *147*, 35-44.

Rust, M.B., Alper, S.L., Rudhard, Y., Shmukler, B.E., Vicente, R., Brugnara, C., Trudel, M., Jentsch, T.J., and Hübner, C.A. (2007). Disruption of erythroid K-Cl cotransporters alters erythrocyte volume and partially rescues erythrocyte dehydration in SAD mice. The Journal of clinical investigation *117*, 1708-1717.

Sabirov, R.Z., Prenen, J., Tomita, T., Droogmans, G., and Nilius, B. (2000). Reduction of ionic strength activates single volume-regulated anion channels (VRAC) in endothelial cells. Pflügers Arch *439*, 315-320.

Sawada, A., Takihara, Y., Kim, J.Y., Matsuda-Hashii, Y., Tokimasa, S., Fujisaki, H., Kubota, K., Endo, H., Onodera, T., Ohta, H., *et al.* (2003). A congenital mutation of the novel gene LRRC8 causes agammaglobulinemia in humans. The Journal of clinical investigation *112*, 1707-1713.

Schlichter, L.C., Mertens, T., and Liu, B. (2011). Swelling activated Cl- channels in microglia: Biophysics, pharmacology and role in glutamate release. Channels (Austin) *5*, 128-137.

Schlichter, L.C., Sakellaropoulos, G., Ballyk, B., Pennefather, P.S., and Phipps, D.J. (1996). Properties of K+ and Cl- channels and their involvement in proliferation of rat microglial cells. Glia *17*, 225-236.

Schroeder, B.C., Cheng, T., Jan, Y.N., and Jan, L.Y. (2008). Expression cloning of TMEM16A as a calcium-activated chloride channel subunit. Cell *134*, 1019-1029.

Schroeder, B.C., Waldegger, S., Fehr, S., Bleich, M., Warth, R., Greger, R., and Jentsch, T.J. (2000). A constitutively open potassium channel formed by KCNQ1 and KCNE3. Nature *403*, 196-199.

Schumacher, P.A., Sakellaropoulos, G., Phipps, D.J., and Schlichter, L.C. (1995). Small-conductance chloride channels in human peripheral T lymphocytes. J Membr Biol *145*, 217-232.

Schwab, A., Nechyporuk-Zloy, V., Fabian, A., and Stock, C. (2007). Cells move when ions and water flow. Pflügers Arch *453*, 421-432.

Schwiebert, E.M., Mills, J.W., and Stanton, B.A. (1994). Actin-Based Cytoskeleton Regulates a Chloride Channel and Cell-Volume in a Renal Cortical Collecting Duct Cell-Line. The Journal of biological chemistry *269*, 7081-7089.

Shen, M.R., Droogmans, G., Eggermont, J., Voets, T., Ellory, J.C., and Nilius, B. (2000). Differential expression of volume-regulated anion channels during cell cycle progression of human cervical cancer cells. J Physiol *529 Pt 2*, 385-394.

Shennan, D.B. (2008). Swelling-induced taurine transport: relationship with chloride channels, anion-exchangers and other swelling-activated transport pathways. Cell Physiol Biochem *21*, 15-28.

Shimizu, T., Iehara, T., Sato, K., Fujii, T., Sakai, H., and Okada, Y. (2013). TMEM16F is a component of a Ca2+-activated Cl- channel but not a volume-sensitive outwardly rectifying Cl- channel. Am J Physiol Cell Physiol *304*, C748-759.

Shimizu, T., Numata, T., and Okada, Y. (2004). A role of reactive oxygen species in apoptotic activation of volume-sensitive Cl(-) channel. Proc Natl Acad Sci U S A *101*, 6770-6773.

Smits, G., and Kajava, A.V. (2004). LRRC8 extracellular domain is composed of 17 leucine-rich repeats. Molecular immunology *41*, 561-562.

Soroceanu, L., Manning, T.J., Jr., and Sontheimer, H. (1999). Modulation of glioma cell migration and invasion using Cl(-) and K(+) ion channel blockers. J Neurosci *19*, 5942-5954.

Stobrawa, S.M., Breiderhoff, T., Takamori, S., Engel, D., Schweizer, M., Zdebik, A.A., Bosl, M.R., Ruether, K., Jahn, H., Draguhn, A., *et al.* (2001). Disruption of ClC-3, a chloride channel expressed on synaptic vesicles, leads to a loss of the hippocampus. Neuron *29*, 185-196.

Stotz, S.C., and Clapham, D.E. (2012). Anion-sensitive fluorophore identifies the Drosophila swell-activated chloride channel in a genome-wide RNA interference screen. PLoS One *7*, e46865.

Strange, K., Emma, F., and Jackson, P.S. (1996). Cellular and molecular physiology of volume-sensitive anion channels. Am J Physiol *270*, C711-730.

Szucs, G., Heinke, S., De Greef, C., Raeymaekers, L., Eggermont, J., Droogmans, G., and Nilius, B. (1996a). The volume-activated chloride current in endothelial cells from bovine pulmonary artery is not modulated by phosphorylation. Pflügers Arch *431*, 540-548.

Szucs, G., Heinke, S., Droogmans, G., and Nilius, B. (1996b). Activation of the volume-sensitive chloride current in vascular endothelial cells requires a permissive intracellular Ca2+ concentration. Pflügers Arch *431*, 467-469.

Thiemann, A., Gründer, S., Pusch, M., and Jentsch, T.J. (1992). A chloride channel widely expressed in epithelial and non-epithelial cells. Nature *356*, 57-60.

Tomassen, S.F., Fekkes, D., de Jonge, H.R., and Tilly, B.C. (2004a). Osmotic swelling-provoked release of organic osmolytes in human intestinal epithelial cells. Am J Physiol Cell Physiol *286*, C1417-1422.

Tomassen, S.F., van der Wijk, T., de Jonge, H.R., and Tilly, B.C. (2004b). Activation of phospholipase D by osmotic cell swelling. FEBS Lett *566*, 287-290.

Tominaga, K., Kondo, C., Kagata, T., Hishida, T., Nishizuka, M., and Imagawa, M. (2004). The novel gene fad158, having a transmembrane domain and leucine-rich repeat, stimulates adipocyte differentiation. J Biol Chem *279*, 34840-34848.

Tominaga, M., Tominaga, T., Miwa, A., and Okada, Y. (1995). Volume-sensitive chloride channel activity does not depend on endogenous P-glycoprotein. J Biol Chem *270*, 27887-27893.

Trouet, D., Nilius, B., Jacobs, A., Remacle, C., Droogmans, G., and Eggermont, J. (1999). Caveolin-1 modulates the activity of the volume-regulated chloride channel. J Physiol *520 Pt 1*, 113-119.

Tsukada, S., Saffran, D.C., Rawlings, D.J., Parolini, O., Allen, R.C., Klisak, I., Sparkes, R.S., Kubagawa, H., Mohandas, T., Quan, S., *et al.* (1993). Deficient expression of a B cell cytoplasmic tyrosine kinase in human X-linked agammaglobulinemia. Cell *72*, 279-290.

Tsumura, T., Oiki, S., Ueda, S., Okuma, M., and Okada, Y. (1996). Sensitivity of volume-sensitive Cl- conductance in human epithelial cells to extracellular nucleotides. Am J Physiol *271*, C1872-1878.

Tsutsumi, T., Ushiro, H., Kosaka, T., Kayahara, T., and Nakano, K. (2000). Proline- and alanine-rich Ste20-related kinase associates with F-actin and translocates from the cytosol to cytoskeleton upon cellular stresses. J Biol Chem *275*, 9157-9162.

Vakili, A., Hosseinzadeh, S.A., and Khorasani, M.Z. (2009). Peripheral administration of carbenoxolone reduces ischemic reperfusion injury in transient model of cerebral ischemia. Journal of stroke and cerebrovascular diseases : the official journal of National Stroke Association *18*, 81-85.

Valverde, M.A., Diaz, M., Sepulveda, F.V., Gill, D.R., Hyde, S.C., and Higgins, C.F. (1992). Volume-regulated chloride channels associated with the human multidrug-resistance P-glycoprotein. Nature *355*, 830-833.

Valverde, M.A., O'Brien, J.A., Sepulveda, F.V., Ratcliff, R.A., Evans, M.J., and Colledge, W.H. (1995). Impaired cell volume regulation in intestinal crypt epithelia of cystic fibrosis mice. Proc Natl Acad Sci U S A *92*, 9038-9041.

Vandenberg, J.I., Yoshida, A., Kirk, K., and Powell, T. (1994). Swelling-activated and isoprenaline-activated chloride currents in guinea pig cardiac myocytes have distinct electrophysiology and pharmacology. J Gen Physiol *104*, 997-1017.

Varela, D., Simon, F., Riveros, A., Jorgensen, F., and Stutzin, A. (2004). NAD(P)H oxidase-derived H(2)O(2) signals chloride channel activation in cell volume regulation and cell proliferation. J Biol Chem *279*, 13301-13304.

Verdon, B., Winpenny, J.P., Whitfield, K.J., Argent, B.E., and Gray, M.A. (1995). Volume-activated chloride currents in pancreatic duct cells. J Membr Biol *147*, 173-183.

Viana, F., Van Acker, K., De Greef, C., Eggermont, J., Raeymaekers, L., Droogmans, G., and Nilius, B. (1995). Drug-transport and volume-activated chloride channel functions in human erythroleukemia cells: relation to expression level of P-glycoprotein. J Membr Biol *145*, 87-98.

Vig, M., Peinelt, C., Beck, A., Koomoa, D.L., Rabah, D., Koblan-Huberson, M., Kraft, S., Turner, H., Fleig, A., Penner, R., *et al.* (2006). CRACM1 is a plasma membrane protein essential for store-operated Ca2+ entry. Science *312*, 1220-1223.

Vitarella, D., DiRisio, D.J., Kimelberg, H.K., and Aschner, M. (1994). Potassium and taurine release are highly correlated with regulatory volume decrease in neonatal primary rat astrocyte cultures. J Neurochem *63*, 1143-1149.

Voets, T., Buyse, G., Tytgat, J., Droogmans, G., Eggermont, J., and Nilius, B. (1996). The chloride current induced by expression of the protein pICln in Xenopus oocytes differs from the endogenous volume-sensitive chloride current. J Physiol *495 (Pt 2)*, 441-447.

Voets, T., Droogmans, G., Raskin, G., Eggermont, J., and Nilius, B. (1999). Reduced intracellular ionic strength as the initial trigger for activation of endothelial volume-regulated anion channels. Proc Natl Acad Sci U S A *96*, 5298-5303.

Voets, T., Szucs, G., Droogmans, G., and Nilius, B. (1995). Blockers of volume-activated Cl- currents inhibit endothelial cell proliferation. Pflügers Arch *431*, 132-134.

Voss, F.K., Ullrich, F., Münch, J., Lazarow, K., Lutter, D., Mah, N., Andrade-Navarro, M.A., von Kries, J.P., Stauber, T., and Jentsch, T.J. (2014). Identification of LRRC8 heteromers as an essential component of the volume-regulated anion channel VRAC. Science *344*, 634-638.

Warner, N., Burberry, A., Franchi, L., Kim, Y.G., McDonald, C., Sartor, M.A., and Nunez, G. (2013). A genome-wide siRNA screen reveals positive and negative regulators of the NOD2 and NF-kappaB signaling pathways. Science signaling *6*, rs3.

Wehner, F. (2006). Cell volume-regulated cation channels. Contrib Nephrol *152*, 25-53.

Wehner, F., Bondarava, M., ter Veld, F., Endl, E., Nürnberger, H.R., and Li, T. (2006). Hypertonicity-induced cation channels. Acta Physiol (Oxf) *187*, 21-25.

Whitehurst, A.W., Bodemann, B.O., Cardenas, J., Ferguson, D., Girard, L., Peyton, M., Minna, J.D., Michnoff, C., Hao, W., Roth, M.G., *et al.* (2007). Synthetic lethal screen identification of chemosensitizer loci in cancer cells. Nature *446*, 815-819.

Wilfinger, J., Seuter, S., Tuomainen, T.P., Virtanen, J.K., Voutilainen, S., Nurmi, T., de Mello, V.D., Uusitupa, M., and Carlberg, C. (2014). Primary vitamin D receptor target genes as

biomarkers for the vitamin D3 status in the hematopoietic system. The Journal of nutritional biochemistry *25*, 875-884.

Xia, Y., Krouse, M.E., Fang, R.H., and Wine, J.J. (1996). Swelling and Ca2+-activated anion conductances in C127 epithelial cells expressing WT and delta F508-CFTR. J Membr Biol *151*, 269-278.

Yang, J., Fan, J., Li, Y., Li, F., Chen, P., Fan, Y., Xia, X., and Wong, S.T. (2013). Genome-wide RNAi screening identifies genes inhibiting the migration of glioblastoma cells. PLoS One *8*, e61915.

Yang, Y.D., Cho, H., Koo, J.Y., Tak, M.H., Cho, Y., Shim, W.S., Park, S.P., Lee, J., Lee, B., Kim, B.M., *et al.* (2008). TMEM16A confers receptor-activated calcium-dependent chloride conductance. Nature *455*, 1210-1215.

Zhang, J.J., Jacob, T.J., Valverde, M.A., Hardy, S.P., Mintenig, G.M., Sepulveda, F.V., Gill, D.R., Hyde, S.C., Trezise, A.E., and Higgins, C.F. (1994). Tamoxifen blocks chloride channels. A possible mechanism for cataract formation. The Journal of clinical investigation *94*, 1690-1697.

7. Acknowledgements

I would like to thank Thomas Jentsch for the opportunity to prepare my PhD thesis in his laboratory and providing an outstanding work environment concerning professional expertise, technical infrastructure, funds and personnel. I am also grateful for the great support and interest he invested in this project.

I would like to thank Volker Haucke for reviewing my PhD thesis.

I am especially grateful to Tobias Stauber, who let me join the project when I started working in the lab and has supervised me since then. He invested very much time and effort in the success of this project and through this also in the development of my personal academic skills, which is of immense value to me. Thank you for your loyalty, for disagreeing (when necessary) and helping (when needed) and for being my teacher and friend.

I would also like to thank Florian Ullrich and Jonas Münch for joining the "Team X" and devoting their time, technical expertise and creativity to this project. It would have been a lot less fun without you guys. Those endless "submission-nights" will always be on my mind. Thank you and Tobias also for (very patiently) proofreading and proof-formatting my thesis.

To the whole "Team X": I am really amazed by the teamwork that we performed, those endless crazy (and many good) ideas, meetings and discussions about lists, mutants, clones, good and bad cells, frogs and fish. I miss it already…

I would also like to thank Darius Lutter for joining at the last minute and helping us out with an experiment to complete the story. A special thank you also goes to Janet Liebold, Johanna Jedamzick and Karolin Fuchs. Without you I would have been lost somewhere between the cell culture and the PCR machine.

I would also like to acknowledge Katina Lazarow, Martin Neuenschwander and Jens von Kries of the FMP Screening Unit as well as Nancy Mah and Miguel Andrade of the MDC bioinformatics group for a great collaboration on this project.

I would like to thank all current and former members of the Jentsch lab who I had the chance to meet and work with during the past years. A special thank you goes to Kristin Schnuppe, who helped me to get started in the lab and to Karina Oberheide and Sebastian Schütze for sharing the "newbie" worries with me at the beginning. I am also grateful to Kathrin Gödde for revealing the secret of "Headers and Footers" to me.

A big thank you goes to Sonja, Julia and Tine from the "Kuba-Crew" and to Franziska and Jürgen for taking an interest in my work and always listening to my worries and complaints and for cheering me up whenever it was necessary.

I am also very grateful to my parents, who supported me constantly over the past years (despite their worries that I should really "start writing something down"). Thank you for always believing in me and being interested in what I do.